Chapter 3

Update on Global Ozone: Past, Present, and Future

Lead Authors
P. Braesicke
J. Neu

Coauthors
V. Fioletov
S. Godin-Beekmann
D. Hubert
I. Petropavlovskikh
M. Shiotani
B.-M. Sinnhuber

Contributors
W. Ball
K.-L. Chang
R. Damadeo
S. Dhomse
S. Frith
A. Gaudel
B. Hassler
R. Hossaini
S. Kremser
S. Misios
O. Morgenstern
R. Salawitch
V. Sofieva
K. Tourpali
O. Tweedy
D. Zawada

Review Editors
W. Steinbrecht
M. Weber

Cover photo: Image of Earth from space. The ozone layer is a small part of the atmosphere which is a very thin layer surrounding the planet. Photo: Adapted from an Adobe Stock photo.

Chapter 3

Update on Global Ozone: Past, Present, and Future

CONTENTS

SCIENTIFIC SUMMARY 1

3.1. INTRODUCTION 5

3.1.1 Summary of Findings from the Previous Ozone Assessment 5

3.1.2 Major New Developments Since 2014 5

3.1.3 Data Sources 6

3.1.4 Data Quality 6

3.2 NATURAL OZONE VARIATIONS AND TREND DETECTION 9

3.2.1 Natural Variability 9

3.2.1.1 Solar Variability 9

3.2.1.2 Quasi-Biennial Oscillation (QBO) 11

3.2.1.3 El Niño–Southern Oscillation (ENSO) 12

3.2.1.4 Effects of Stratospheric Aerosol Loading 15

Box 3-1. Origin of Stratospheric Aerosols at Mid-latitudes 16

3.2.1.5 Other Dynamical Variations 17

3.2.1.6 Attributing Variability in Regression Analysis 19

3.2.2 Trend Models 19

3.3 PAST OZONE IN OBSERVATIONS 22

3.3.1 Changes in Total Column Ozone 22

3.3.1.1 Interannual Variations 22

3.3.1.2 Total Ozone Trends 22

3.3.2 Trends in Ozone Profiles 27

3.3.2.1 Time Series 27

3.3.2.2 Ozone Trends 2000–2016 29

3.3.2.3 Trend Profiles 30

3.3.2.4 Consistency of Total Column Trends and Integrated Profile Trends 32

3.3.3 Impacts of Changes in Ozone-Depleting Substances and Greenhouse Gases on Ozone Trends 35

3.3.3.1 Effects of Very Short-Lived Substances 38

3.3.3.2 Tropical Ozone Changes 38

Box 3-2. Modelling past and future changes in ozone: Model heritage and application 40

3.4 PROJECTED OZONE CHANGES 40

3.4.1 Expected Return to 1980 Levels and Ozone Recovery 41

3.4.2 Effects of Future Stratospheric Temperature and Circulation Changes 43
Box 3-3. Ozone Return Dates. 44
3.4.3 Sensitivity to the Specification of Different Future Scenarios 46
3.4.3.1 Effects of Different Representative Concentration Pathways 46
3.4.3.2 Influence of Nitrous Oxide and Methane. 47
3.4.3.3 Sensitivity to Geoengineering/Solar Radiation Management 49
3.4.4 Impacts on Tropospheric Ozone 50
REFERENCES 53
APPENDIX 3A: DATA SOURCES. 69
3A.1 Ground-based Measurements 69
3A.2 Space-Based Ozone Profiles 69
3A.3 Space-Based Total Ozone Columns 73

Chapter 3

Update on Global Ozone: Past, Present, and Future

SCIENTIFIC SUMMARY

This chapter deals with the evolution of global ozone outside of the polar regions. The increase of ozone-depleting substance (ODS) concentrations caused the large ozone decline observed from the early satellite era (circa 1980) to the mid-1990s. Since the late 1990s, concentrations of ODSs have been declining due to the successful implementation of the Montreal Protocol. Ozone concentrations show latitudinally dependent increases in the upper stratosphere for the 2000–2016 period; changes in other parts of the stratosphere are not yet statistically significant. A new suite of model simulations confirms previous results for the upper stratosphere that about half of the observed increase is associated with declining ODSs. Ozone column trends are likewise positive but not generally statistically significant. Their overall evolution is, however, compatible with the decline in equivalent effective stratospheric chlorine (EESC).

Over the next decades, we expect increasing global mean stratospheric ozone columns, as ODSs continue to decline. Emissions of greenhouse gases (GHGs), especially carbon dioxide (CO_2), methane (CH_4), and nitrous oxide (N_2O), will also affect the evolution of global stratospheric ozone, particularly in the second half of the 21st century, when ODS concentrations are expected to be low.

PAST CHANGES IN TOTAL COLUMN OZONE

- **Ground- and space-based observations indicate that there is no statistically significant trend in near-global (60°S–60°N) column ozone over the 1997–2016 period.** These datasets show an increase of between 0.3% and 1.2% decade^{-1} since 1997, with uncertainties of about 1% decade^{-1}. These findings are consistent with our understanding of the processes that control ozone:
    - In middle and high latitudes, the increase in total column ozone expected to arise from the 15% decline in EESC since 1997 is small (~1% decade^{-1}) relative to the large, dynamically forced year-to-year variations of ~5%;
    - In the tropics, where halogen-driven ozone loss is small in the lower stratosphere, total column ozone has not varied significantly with ODS concentrations, except under conditions of high volcanic aerosol loading (e.g., from the eruption of Mt. Pinatubo in 1991).
- Outside the tropics, present-day (2014–2017) total ozone columns from ground-based and space-based observations remain lower than 1964–1980 column ozone by:
    - about 2.2% for the near-global average (60°S–60°N);
    - about 3.0% in the Northern Hemisphere mid-latitudes (35°N–60°N);
    - about 5.5% in the Southern Hemisphere mid-latitudes (35°S–60°S).

  These values are essentially the same as in the last Assessment, given uncertainties associated with natural variability and instrumental accuracy. The larger depletion in the Southern Hemisphere is linked to the Antarctic ozone hole.

PAST CHANGES IN OZONE PROFILES

Additional and improved datasets and focused studies evaluating trend uncertainties have strengthened our ability to assess ozone profile changes. Analysis of data from the upper stratosphere shows increases that are consistent with

those suggested in the last Assessment. There is some evidence for a dynamically driven decrease in ozone in the lower stratosphere from 2000 to 2016, but robust trends have not been identified for this region. New chemistry–climate model (CCM) simulations that include realistic time variations of GHG and ODS concentrations are analyzed using the same trend model as for the observations; this allows attribution of changes in ozone to different processes.

- **Measurements show increases of ozone in the upper stratosphere over the period 2000-2016.** Following a large decline of 5 to 7% decade^{-1} through the 1980s and middle 1990s, upper stratospheric ozone has increased by 1 to 3% decade^{-1} since 2000. The largest confidence is in northern mid-latitudes, where the positive trend is statistically significant between 35- and 45-km altitude. Confidence in trends in the tropics and southern mid-latitudes is not as high due to larger discrepancies between trends from individual measurement records.

- **Model simulations attribute about half of the observed upper stratospheric ozone increase after 2000 to the decline of ODSs since the late 1990s.** The other half of the ozone increase is attributed to the slowing of gas-phase ozone destruction cycles, which results from cooling of the upper stratosphere caused by increasing GHGs.

- **There is some evidence for a decrease in lower stratospheric ozone from 2000 to 2016.** This decrease is most consistent across datasets in the tropics, but is not statistically significant in most analyses. Much of the apparent decline was reversed by an abrupt increase in ozone in 2017, indicating that longer records are needed to robustly identify trends in this region. Model simulations attribute the variations in lower stratospheric ozone over this period primarily to dynamical variability.

- **Assessing the consistency between stratospheric profile trends and total column ozone trends requires changes in tropospheric ozone to be well quantified.** A recent assessment of tropospheric column ozone trends, however, shows large disagreements in the sign and magnitude of the observed trends over the past decade and a half.

FUTURE OZONE CHANGES

The baseline climate change scenario used in the new model simulations differs from the previous Assessment, because new emissions scenarios were used. The key drivers of future ozone levels continue to be declining ODS concentrations, upper stratospheric cooling because of increased GHGs, and the possible strengthening of the Brewer-Dobson circulation from climate change. The new emissions scenarios lead to slight differences in the relative contributions of these processes in various latitude and altitude regions and a delay in return dates for ozone compared to the previous Assessment.

- **Estimated dates of return of total column ozone to 1980 values are generally a few years later than given in the previous Assessment and vary considerably between scenarios.** For the baseline scenario (RCP-6.0), they are:
    - around mid-century for near-global mean annually averaged ozone;
    - most likely before the middle of the century (~2035) for annually averaged Northern Hemisphere mid-latitude ozone;
    - around mid-century for annually averaged Southern Hemisphere mid-latitude ozone.

- **CO_2, CH_4, and N_2O will be the main drivers of 60°S–60°N stratospheric ozone changes in the second half of the 21st century.** These gases impact both chemical cycles and the stratospheric overturning circulation, with a larger response in stratospheric ozone associated with stronger climate forcing. By 2100, the stratospheric column is expected to decrease in the tropics by about 5 DU for RCP-4.5 and about 10 DU for

RCP-8.5 relative to 1980 values, with the net total column change projected to be smaller (about 5 DU) because of offsetting increases in tropospheric ozone.

- **Given that ODS levels are expected to decline slowly in coming years, a large enhancement of stratospheric sulfate aerosol in the next decades would result in additional chemical ozone losses.** Possible sources of additional stratospheric sulfate aerosol include volcanic eruptions (like Mt. Pinatubo in 1991) and geo-engineering. Even when ODS levels have declined substantially, a large injection of volcanic halogens into the stratosphere could drive substantial ozone losses in the presence of aerosol surfaces.

- **Future ozone recovery and the projected strengthening of the Brewer-Dobson circulation (BDC) are likely to lead to increases in the stratosphere-to-troposphere (STT) flux of ozone via increases in mid-latitude lower stratospheric ozone and mass flux.** The net impact of increased STT flux on the tropospheric ozone burden is highly model and scenario dependent. Most studies suggest it will be small relative to other factors, such as concurrent changes in precursor emissions, temperature, and water vapor.

Chapter 3

Update on Global Ozone: Past, Present, and Future

3.1. INTRODUCTION

This chapter updates the corresponding chapter from the previous Assessment (Chapter 2, WMO, 2014); it describes our current understanding of past changes in global (60°S–60°N) ozone and its expected future development. The chapter focuses on detection and attribution of ozone changes and the robustness of ozone trends and their associated uncertainties. The chapter also describes how ozone is expected to change in the future. This includes the modeled response to the continuing decline in stratospheric chlorine- and bromine-containing compounds and the response of ozone to climate change. A key benchmark, as always, is the date of return of ozone to its 1980 value.

3.1.1 Summary of Findings from the Previous Ozone Assessment

The 2014 Assessment (WMO, 2014) for the first time provided evidence that stratospheric ozone concentrations have increased in response to reductions in the emissions of ozone-depleting substances (ODSs) imposed by the Montreal Protocol. In particular, measurements of ozone in the upper stratosphere showed a statistically significant positive trend, which chemistry–climate models (CCMs) suggested is attributable equally to decreased ODS concentrations and to colder temperatures resulting from increased greenhouse gases (GHGs). Total column ozone had not increased significantly (1%±1.7%). Large dynamic variability and differences between datasets were shown to make trend detection difficult given the ~1% expected increase in column ozone associated with ODS decline.

CCM results indicated that a large enhancement of sulfate aerosol from either a volcanic eruption or geoengineering would result in significant ozone loss while ODS levels remain high. CCM simulations were also used to examine how assumptions about future GHG emissions affect ozone in the late 21st century, when chemical ozone destruction by halogens will be negligible. The effects of increasing nitrous oxide (N_2O), which chemically depletes global ozone, compete against the effects of increasing carbon dioxide (CO_2) and methane (CH_4), which increase ozone in the extratropics via both changes in chemistry and strengthening of the circulation. CCMs showed differences of 7% in global average total column ozone for the year 2100 between maximum and minimum radiative forcing Representative Concentration Pathways (RCPs). Significant decreases in tropical column ozone were projected under all scenarios despite increases in the upper stratosphere associated with GHG-induced cooling. The column reductions occurred primarily because strengthening of the circulation decreases tropical ozone in the lower stratosphere.

3.1.2 Major New Developments Since 2014

With four additional years of data and the advent of both new and consolidated merged datasets, this chapter revisits evidence for the detectability of positive ozone trends that might be attributable to decreases in stratospheric chlorine- and bromine-containing compounds.

The Long-term Ozone Trends and Uncertainties in the Stratosphere (LOTUS) initiative has undertaken a systematic assessment of the significance of observed ozone profile trends. LOTUS (2018) robustly quantified the degree to which ozone variability can be attributed to the various proxies used to represent natural process that drive ozone changes. It also examined available trend models and formulated a best practice, applying a common methodology to updated satellite and ground-based datasets (including merged and homogenized data). The resulting trend profiles include a traceable error characterization for the assessment of significant (recovery) trends. The new analysis confirms the general trends derived for the 2014 Ozone Assessment, but with larger estimated uncertainties, in particular in the upper stratosphere. In addition, the LOTUS trend model used for the profile observations is applied to model integrations of ozone under various scenarios, allowing a consistent

comparison of observed and modeled trends up to the present day.

The Chemistry-Climate Model Initiative Phase 1 (CCMI-1; Morgenstern et al., 2017) provides new model integrations that simulate past, present, and future ozone. For the past, free-running and "specified dynamics" model integrations are available and capture many important features of the observed ozone variability and trends. The baseline future projections use the RCP-6.0 scenario to represent climate change. In this respect, this chapter deviates from the 2014 and 2011 Ozone Assessments (WMO, 2014; WMO, 2011), where CCMVal-2 integrations were used, which are based on the SRES A1B scenario. However, the response of ozone to different climate change scenarios is evaluated using additional RCP scenarios and idealized sensitivity studies (e.g., fixed ODSs or fixed GHGs). Return dates are derived in a comprehensive way by calculating filtered multi-model mean time series and analyzing if and when 1980 ozone values are reached (Dhomse et al., 2018).

3.1.3 Data Sources

This Assessment relies on essentially the same ground-based, in situ and satellite ozone datasets as were used for the 2014 Assessment. Since then, all records have been extended to the present, and some have been revised and reprocessed, in part or in full. In addition, a few new data records have emerged. **Appendix 3A** summarizes the data records used in this chapter. Because single-instrument records do not provide sufficient temporal and/or spatial coverage to assess global long-term trends, merging is required; quantification of uncertatinties associated with merging is discussed in **Section 3.1.4**. Each approach has its merits and weaknesses, and the availability of a number of complementary, independent global ozone datasets is essential to comprehensively quantifying uncertainties in trend assessments.

3.1.4 Data Quality

Data quality is one of the key drivers of trend uncertainty, with other important contributions coming from natural variability, methodological choices in the regression analyses, and assumptions on how trend results are combined (see **Section 3.2**). Merged datasets provide comprehensive multi-instrument records, with improved temporal and spatial coverage and reduced uncertainties compared to a single-instrument data record (Tummon et al., 2015). The challenges of merged records highlighted in the last Assessment, however, are still relevant: Inter-instrument biases and drift, differences or changes in spatiotemporal sampling patterns, different (vertical) coordinate systems, and different spatiotemporal resolutions can all impact the accuracy of trends derived from merged records.

Instrument biases lead to time-dependent artifacts ("jumps") when continuous or partially overlapping records are merged without prior adjustment to a common absolute reference (Ball et al., 2017; Weatherhead et al., 2017). The accuracy of such bias corrections increases with the amount of data available and depends on the length of the overlap periods for different records. Many single-instrument records were revised in recent years (**Appendix 3A**), and a series of intercomparisons revisited and refined the estimated biases between satellite data records (Kramarova et al., 2013; Frith et al., 2014, 2017; Tegtmeier et al., 2013; Coldewey-Egbers et al., 2015; Rahpoe et al., 2015; Froidevaux et al., 2015; Davis et al., 2016; Sofieva et al., 2017), ground-based datasets (Van Malderen et al., 2016; Deshler et al., 2017), and ground-based and satellite data records (Koukouli et al., 2015; Hubert et al., 2016; Thompson et al., 2017; Garane et al., 2018; Sterling et al., 2018). Single-sensor ozone profile datasets agree to within about 5% in the height range of 20–45 km. Once adjustments are made by the merging algorithms, the residual inter-instrument biases are reduced considerably. However, it is likely that uncertainties associated with bias corrections are, in some cases, not negligible; e.g., for the merged SBUV satellite data records (due to short overlap periods; Ball et al., 2017; Frith et al., 2017) and for the SAGE-MIPAS-OMPS satellites (due to a sparse sampler that acts as transfer standard between MIPAS and OMPS; LOTUS, 2018).

Removing inter-instrument drift is a challenge that requires considerable temporal overlap of data records and a reliable statistical analysis (Stolarski and Frith, 2006). Drift correction schemes have been developed for combined data from dense nadir-viewing samplers (Coldewey-Egbers et al., 2015), but thus far such corrections have only rarely been tested for limb merging algorithms (Eckert et al., 2014; Damadeo

et al., 2018). Intercomparisons between single records generally show inter-instrument drifts below 1% decade^{-1} for total column data (Frith et al., 2014; Koukouli et al., 2015; Garane et al., 2018) and less than 3–5% decade^{-1} for profilers (Kramarova et al., 2013; Rahpoe et al., 2015; Hubert et al., 2016; Frith et al., 2017). Large drifts (i.e., 5% decade^{-1} or more) found in previous versions of the OSIRIS and SCIAMACHY satellite data records (Hubert et al., 2016) have been corrected, improving agreement with other datasets (Sofieva et al., 2017; Bourassa et al., 2018; LOTUS, 2018). Instabilities in the NCEP temperature data in the 1980s (McLinden et al., 2009; Maycock et al., 2016) have been shown to have introduced a ~6% decade^{-1} systematic error on the trend in SAGE II v6.2 volume mixing ratio data in the tropical upper stratosphere (Froidevaux et al., 2015; Ball et al., 2017). The current SAGE II v7.00 release, used by all merged limb records considered here, utilizes MERRA temperature profiles that substantially reduce this systematic error.

Time-dependent biases can appear in datasets that are based on a collection of observations with non-homogeneous sampling (e.g., SAGE, HALOE, and ACE-FTS). This can also be true for an instrument such as SBUV that drifts in local overpass time. Ignoring SBUV data close to the terminator avoids most, but not all, of this issue. A study comparing trends regressed from monthly zonal mean (MZM) solar occultation data to those from data close to the native resolution of the measurements (**Figure 3-1**) inferred that diurnal sampling biases that change over time affect the MZM-derived trends by about 1% decade^{-1} in the mid-latitude upper stratosphere, which

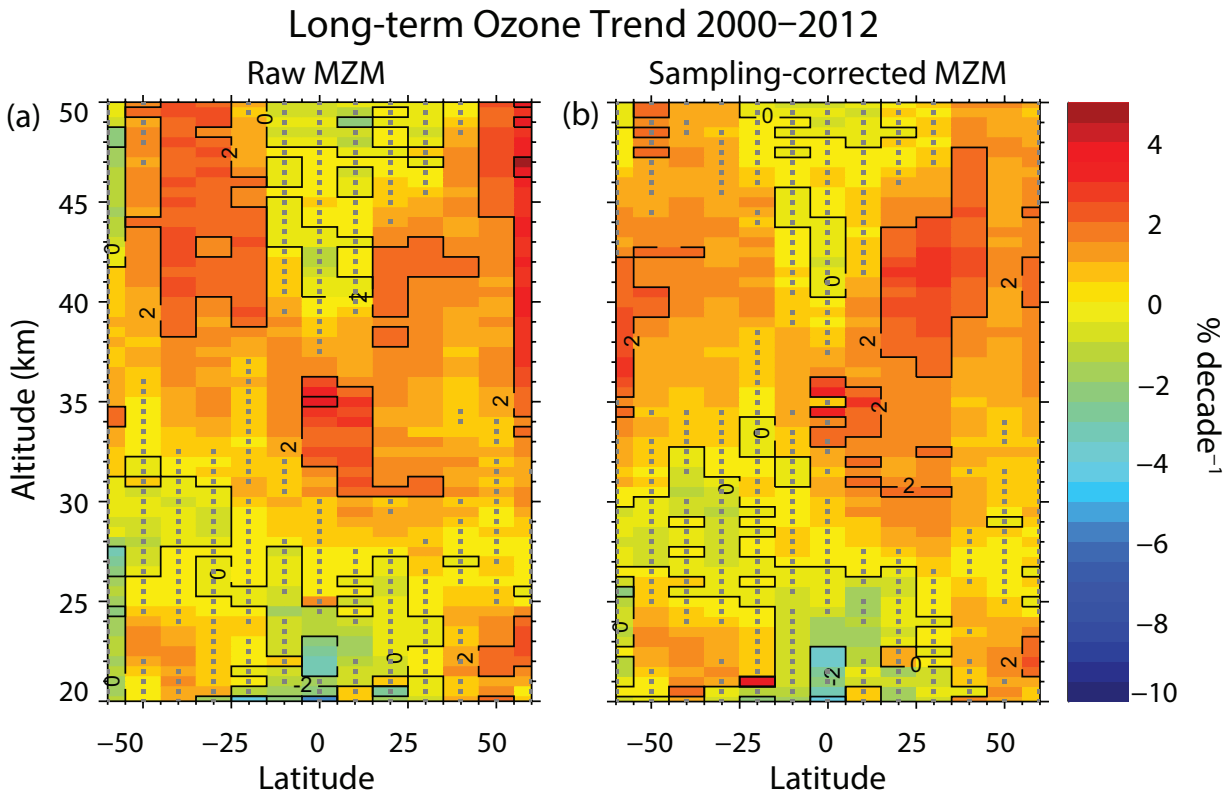

Figure 3-1. Long-term ozone trends in % decade^{-1} for the period 2000–2012 derived from both (a) a regression of monthly zonal mean data (MZM) and (b) monthly zonal mean data corrected for sampling biases due to the diurnal and seasonal cycle. The diurnal correction has the greatest influence on the upper stratosphere, while the seasonal correction has the greatest influence at higher latitudes. Stippling denotes areas where the trend results are not significant at the 2σ level. Contour lines are plotted at 2% decade^{-1} intervals. Adapted from Damadeo et al. (2018).

constitutes about half of the trend in past two decades (Damadeo et al., 2018). Seasonal sampling biases were shown to be more prevalent at higher latitudes and in the tropical middle stratosphere. The analysis led to a sampling bias correction scheme for the SAGE II dataset, which was used for the SAGE-OSIRIS-OMPS record, but not for other limb records. Sampling biases in total column or limb profile data records are generally considered random in nature but are not fully quantified (Coldewey-Egbers et al., 2015; Millán et al., 2016).

The coherent propagation of uncertainties through merging algorithms is a complex challenge. Addressing this challenge by applying a Monte Carlo technique to simulate the SBUV error time series for two different merging algorithms results in a trend uncertainty of 1–2.4% decade^{-1} (1σ), which explains the differences in profile trends for the merged SBUV MOD and SBUV COH records (Frith et al., 2014, 2017; see also **Appendix 3A** and **Figure 3-2**). So far, a comprehensive error propagation analysis has not been done for the merged limb profile records. The most advanced attempt, based on singular value decomposition of the differences between four merged limb and nadir profile data records, estimated uncertainties of up to 5% for earlier versions of MZM data from the GOZCARDS and SWOOSH data records (Ball et al., 2017). However, the impact of measurement uncertainties on trends was not investigated.

Differences in merged data records are dominated by the selection of instruments rather than the choice of the merging technique (Tummon et al., 2015). Differences are smallest in the mid-latitude lower and middle stratosphere (5%) and increase in the upper stratosphere (8%) and tropical lower stratosphere (10%), consistent with the biases between single-instrument data records. Recent modifications to profile records have addressed, at least partially, some of the identified issues, and current versions of merged ozone profile records are in better agreement than the versions used in the previous Assessment (LOTUS, 2018). Differences between merged space- and ground-based total column records (compared as monthly zoone mean total column datasets) are on average less than 1–2% and they drift apart less than 0.5–1% decade^{-1} (Chiou et al., 2014; Bai et al., 2017).

Recent reanalysis datasets (Dee et al., 2011; Dragani 2011; and Wargan et al., 2017) have been shown to produce a "realistic representation of total ozone" (Davis et al., 2017), but they are not included in this Assessment.

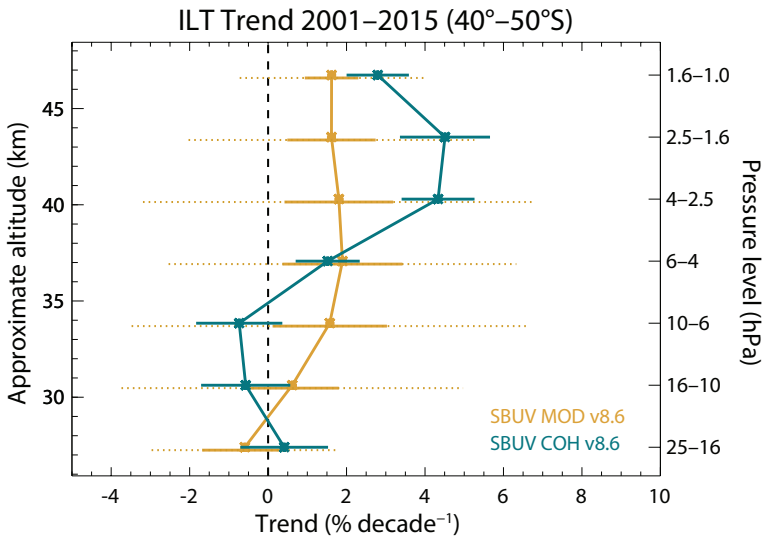

Figure 3-2. Independent linear trends (ILTs) fit from 2001 to 2015 using SBUV MOD (dark yellow) and SBUV COH (green) merged ozone records. Trends are in % decade^{-1} and plotted as a function of pressure layers for 40–50°S. Horizontal lines indicate trend uncertainty (2σ): Solid lines represent the statistical uncertainty from the unexplained variability in the multiple linear regression (MLR) analysis (**Section 3.2.1**), and dotted lines show the total uncertainty obtained by adding the statistical and merging uncertainty in quadrature. The latter is estimated from Monte Carlo simulations that model how uncertainties in individual SBUV data records propagate through the merging chain. Adapted from Frith et al. (2017).

3.2 NATURAL OZONE VARIATIONS AND TREND DETECTION

3.2.1 Natural Variability

The natural variation and long-term trends of stratospheric ozone are generally quantified using multiple linear regression (MLR) models. Such models have been discussed in previous ozone assessments (e.g., WMO, 2014). They use explanatory variables (i.e., predictors) to describe natural and anthropogenic variability in long-term ozone time series. The typical multi-linear regression can be written in the following form (e.g., Chehade et al., 2014, Steinbrecht et al., 2017, Weber et al., 2018):

$$Z(t) = Z_o + Trend \cdot (t - t_o) + \sum_{i=0}^{n} a_i P_i(t) + \varepsilon(t) \quad (1)$$

where $Z(t)$ represents a monthly or yearly averaged ozone time series and Z_0 is the value at t_0. The time series usually describes deviations from a climatology rather than the absolute amount of ozone. The *Trend* term is discussed in **Section 3.2.2**. The predictors, or proxies, $P_i(t)$ are the variables used to explain ozone interannual and long-term variability. The predictors most commonly used in ozone trend studies are listed in **Table 3-1** and are discussed in detail below. The last term, $\varepsilon(t)$, is the residual variability not explained by the MLR, which most analyses assume to be first order autoregressive noise. The terms in the model must be linearly independent and are assumed to be sufficiently orthogonal to provide independent pieces of information such that the regression can attribute, with confidence, ozone variability in the observed or modeled time record (see **Section 3.2.2**). When terms exhibit significant covariations, as is the case, for example, for the quasi-biennial oscillation (QBO) and the El Niño–Southern Oscillation (ENSO) over particular time periods, the ability of MLR to determine attribution is detrimentally impacted and confidence intervals, which take into account the covariance matrix of the regression coefficients, are correspondingly larger.

While MLR models are often applied to zonally averaged satellite data, there can be large longitudinal asymmetries in the influence of some of the processes represented by the various proxies on ozone. In particular, ENSO and the North Atlantic Oscillation (NAO) have large regional impacts that can be seen in non-zonally averaged data, as discussed in more detail in the sections below.

3.2.1.1 Solar Variability

The solar cycle influences ozone through photochemical and dynamical processes in the stratosphere (Haigh, 1994; Hood and Soukharev, 2003). Ozone in the upper-middle atmosphere is produced at wavelengths shorter than 242 nm, and it is primarily destroyed at longer wavelengths through photochemical processes. Understanding changes in UV irradiance is therefore important for the ozone and radiation budget. The solar ozone response (SOR) to changes in solar irradiance further plays a potentially important role in climate variability through modulation of stratospheric temperatures and wind. These changes in the stratosphere can influence tropospheric climate through both direct radiative effects and dynamical coupling, with impacts on extratropical modes of variability (e.g., Gray et al., 2010). Thus, understanding of the coupling between solar cycle variability, ozone changes, and circulation is of great importance for assessing the climate response to solar cycle change.

The 2014 Assessment reported a 2–4% variation of SOR in the upper stratosphere (3% in total ozone) in phase with the 11-year solar cycle. However, it was stated that the "exact shape of the solar response profile depends on the type of data and/or analysis, the length of data records, and the time periods under investigation." In the 2014 Assessment, the uncertainties regarding solar-induced variability in observed ozone fields were related to the brevity of ozone records (spanning only a few solar cycles) as well as incomplete understanding of the accuracy of modern solar spectral irradiance (SSI) observed records (i.e., data from the SORCE satellite; McClintock et al., 2005). The lack of sufficient spectral resolution in the radiation schemes of global climate models was also noted as the reason for the models not being able to reproduce the solar–ozone relationship detected in observations.

Since the last Assessment, several papers have re-evaluated SOR estimates using both updated satellite observations and models. Uncertainties in the magnitude and structure of SOR estimates remain and continue to complicate the validation of atmospheric chemistry models (Dhomse et al., 2016). The primary

Table 3-1. Table of proxies used in Equation (1), including representative data sources. The proxies and data sources used in analyses presented in **Section 3.3** are shaded in dark orange.

Proxy	Parameter	Data Sources
Solar cycle	10.7 cm solar radio flux	NOAA National Centers for Environmental Information: https://www.ngdc.noaa.gov/stp/solar/flux.html National Research Council Canada Dominion Radio Astrophysical Observatory: ftp://ftp.geolab.nrcan.gc.ca/data/solar_flux/
	30 cm solar radio flux	CNES Collecte Localisation Satellites Space Weather Services: https://spaceweather.cls.fr/services/radioflux/
	Core-to-wing ratio of Mg II doublet (280 nm)	University of Bremen: http://www.iup.uni-bremen.de/UVSAT/Datasets/mgii
QBO1 and QBO2 (orthogonal components of the quasi- biennial oscillation, QBO)	EOF1 and EOF2	Free University of Berlin: www.geo.fu-berlin.de/en/met/ag/strat/produkte/qbo/
	Tropical zonal winds at 2 pressure levels (e.g., 30 hPa and 50 hPa or 10 hPa and 30 hPa)	NOAA National Weather Service Climate Prediction Center: http://www.cpc.ncep.noaa.gov/data/indices/
ENSO	Multivariate ENSO index	NOAA Earth System Research Laboratory: https://www.esrl.noaa.gov/psd/enso/mei/
	Niño 3.4 index	NOAA National Weather Service Climate Prediction Center: http://www.cpc.noaa.gov/data/indices/ http://www.cpc.ncep.noaa.gov/products/precip/CWlink/MJO/enso.shtml
	Southern Oscillation index	
Aerosols	Mean aerosol optical depth at 550 nm	NASA Goddard Institute for Space Studies: https://data.giss.nasa.gov/modelforce/strataer/tau.line_2012.12.txt
		Khaykin et al. (2017) https://www.atmos-chem-phys.net/17/1829/2017/acp-17-1829-2017.pdf
Other Dynamical Proxies	Brewer–Dobson circulation (BDC): eddy heat flux (EHF) at 100 hPa	NOAA National Weather Service Climate Prediction Center: http://www.cpc.ncep.noaa.gov/products/stratosphere/polar/polar_body.html
	North Atlantic Oscillation (NAO) index (daily or monthly)	NOAA National Weather Service Climate Prediction Center: http://www.cpc.ncep.noaa.gov/products/precip/CWlink/pna/nao.shtml
	Arctic Oscillation (AO) index (daily or monthly)	NOAA National Weather Service Climate Prediction Center: http://www.cpc.ncep.noaa.gov/products/precip/CWlink/daily_ao_index/ao.shtml
	Antarctic Oscillation (AAO) index (daily or monthly)	NOAA National Weather Service Climate Prediction Center: http://www.cpc.ncep.noaa.gov/products/precip/CWlink/daily_ao_index/aao/aao.shtml
	Tropopause pressure (TP)	NOAA Earth System Research Laboratory https://www.esrl.noaa.gov/psd/data/gridded/data.ncep.reanalysis.tropopause.html NASA Global Modeling and Assimilation Office: https://gmao.gsfc.nasa.gov/reanalysis/MERRA/data_access/ https://gmao.gsfc.nasa.gov/reanalysis/MERRA-2/data_access/

new result, shown by two studies, is that updated SAGE II and SBUV mixing ratio datasets suggest a decrease in the magnitude of the SOR in the tropical upper stratosphere relative to earlier assessments (from ~4% in the 2014 Assessment to ~1% here) (Maycock et al., 2016; Dhomse et al., 2016). The SAGE II v7.0 number density dataset is consistent with v6.2, but the mixing ratio dataset exhibits a smaller signal, largely due to the use of a different temperature reanalysis product to convert ozone number densities to mixing ratios. SBUV MOD VN8.6 also shows a smaller and less significant SOR in the tropical upper stratosphere than the SBUV Merged Cohesive VN8.5 and closely resembles the SAGE II v7.0 mixing ratio data. However, given known issues with reanalysis temperatures, the authors concluded that the use of number density is more robust for SOR analyses than converting to mixing ratio for data records for which number density is the native coordinate, in agreement with previous findings (Remsberg et al., 2014). One of the studies also showed that the SAGE–GOMOS merged number density datasets are consistent with the SOR in SAGE II alone while SAGE-OSIRIS is not (Maycock et al., 2016). It further notes that limb sampling is too sparse to extract sub-annual variations in the SOR but that the SBUV MOD VN8.6 dataset suggests substantial month-to-month variations, particularly in the winter extratropics.

The investigations of SSI data and their reproducibility by solar models is important for the simulation of solar cycle effects on both stratospheric ozone and surface climate (e.g. Ermolli et al., 2013, and Matthes et al., 2017). Two new studies find that at pressures <5 hPa, the ozone response to solar variability simulated using output from solar models, such as SATIRE-S and NRLSSI, as forcings in climate models is consistent with observations, while simulations using SORCE data are not (**Figure 3-3;** Dhomse et al., 2016; Ball et al., 2016). These studies support earlier evidence that SORCE measurements strongly overestimate solar cycle variability in the UV range. Large differences in the amplitude and spectral features of the most recent solar cycle (C24, which began in December 2008) from earlier periods, including a reduction in total solar irradiance amplitude of 35% from the previous cycle, are an area of active investigation.

Previous studies have reported a secondary maximum in the ozone response to the solar cycle in the tropical lower stratosphere (e.g., Soukharev and Hood, 2006; Gray et al., 2010). This lower stratospheric signal is generally attributed to a dynamical response to increased heating in the upper stratosphere during solar maxima, but it could be a result of aliasing in MLR analyses due to the presence of volcanic eruptions at solar maxima (Chiodo et al., 2014). However, further evidence for the dynamical response comes from the fact that the secondary peak has also been seen in IASI satellite data (2008–2013) using daily solar flux measurements in the regression analysis (Wespes et al., 2016).

3.2.1.2 Quasi-Biennial Oscillation (QBO)

The quasi-biennial oscillation (QBO) influences stratospheric ozone through its impact on dynamical and chemical processes. The QBO signal in tropical ozone consists of a primary maximum in amplitude at a pressure of ~7 hPa, a secondary maximum near 20–30 hPa, and a minimum near 15 hPa (e.g., Naoe et al., 2017). However, other modes of variability such as ENSO can also influence tropical stratospheric ozone (e.g., Oman et al., 2013; **Section 3.2.1.3**), and anomalies do not always show a direct correlation with the QBO phase (Nedoluha et al., 2015a). The QBO proxy in MLR analyses (**Table 3-1**) is often represented by the wind speeds measured at two different pressure levels by radiosonde soundings in Singapore (Baldwin, 2001) or, alternatively, by two orthogonal QBO time series derived from principal component analyses (Wallace et al., 1993; Randel and Wu, 1996).

The period since the last Assessment was marked by an unprecedented disruption of the QBO during the NH winter of 2015–2016 (Newman et al., 2016; Osprey et al., 2016; Dunkerton et al., 2016). Usually, alternating westerly and easterly zonal wind regimes propagate downward with time with a ~28-month period. In 2016, an anomalous upward displacement of the westerly phase occurred from ~30 hPa to 15 hPa, and easterly winds appeared at 40 hPa (see **Figure 3-4**). Such a disruption of the QBO has never before been observed in tropical wind measurements, which began in 1953. The first two empirical orthogonal functions (EOFs) of the QBO, which describe the primary modes of variability in tropical zonal winds, typically account for ~95% of the variance in these winds; in 2016, they explain only 71% of the variance (Tweedy et al., 2017).

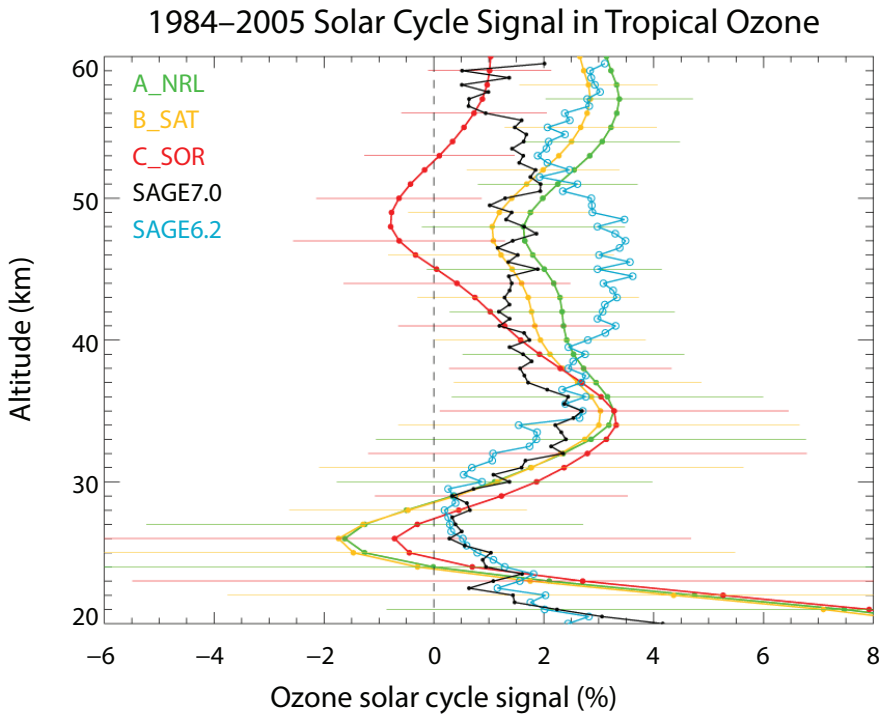

Figure 3-3. Estimated solar cycle signal in tropical ozone volume mixing ratio (VMR) from SAGE II (1984–2005) v7.0 (black) and v6.2 (light blue). The signal was dervied using a recently developed regression model (Damadeo et al., 2014). All error bars are 2-σ; none are shown for SAGE data. The modeled ozone solar cycle signals for climate model simulations using output from the NRLSSI (green) and SATIRE-S (orange) solar models and from SORCE data (red) for the 1984–2005 period are also shown. Adapted from Dhomse et al. (2016).

The anomalous zonal wind pattern drove a decrease in tropical upwelling from 50 to 30 hPa, which was associated with a positive ozone anomaly, and increased upwelling at pressures >50 hPa, which was associated with a negative ozone anomaly (**Figure 3-5**) (Tweedy et al., 2017). In the extratropics, reduced downwelling balanced the decrease in tropical ascent from 50 to 30 hPa, resulting in a negative ozone anomaly. In fact, SBUV observations show near-record low levels of total ozone in the subtropics in August 2016 of both hemispheres (Tweedy et al., 2017). At nearly the same time as the QBO disruption, there was a very strong El Niño event and a very strong stratospheric polar vortex in early to mid-winter (Nedoluha et al, 2015; Cheung et al., 2016; Hu et al., 2016; Scaife et al., 2017), which may have also contributed to ozone variability. In fact, while ENSO and QBO are assumed to be orthogonal terms in MLR analyses, they are sometimes in phase for long periods of time, complicating attribution of ozone changes (e.g., Neu et al., 2014).

The occurrence of the 2016 QBO cycle, as well as other less pronounced anomalies in the magnitude and phase of the QBO in the past decade (Nedoluha et al., 2015), are possible indications of changes in the normal behavior of the processes that impact the global stratospheric ozone distribution and inter-annual variability. The causes of this anomalous behavior and its potential implications for the future evolution of ozone are still under investigation.

3.2.1.3 El Niño–Southern Oscillation (ENSO)

El Niño–Southern Oscillation (ENSO) affects tropical upwelling, which in turn leads to fluctuations in temperature and ozone in the tropical lower stratosphere (Bodeker et al., 1998; Randel et al., 2009; and references therein). ENSO is generally represented in MLR analyses either by the Niño 3.4 index or by the multivariate ENSO index (MEI) (Wolter, 2013), which is based on the first principle component of six atmospheric parameters (**Table 3-1**). In the tropical upper troposphere and lower stratosphere (UTLS), the ENSO coefficient is negative, with low ozone during El Niño years and high ozone during La Niña years; the opposite signal is seen in mid-latitudes (e.g., Neu et al., 2014; Oman et al., 2013; Olsen et al., 2016; Wespes et al., 2016). Regression of MLS satellite measurements suggests up to a ~20 ppb K^{-1} response of ozone in the tropical lower stratosphere to changes

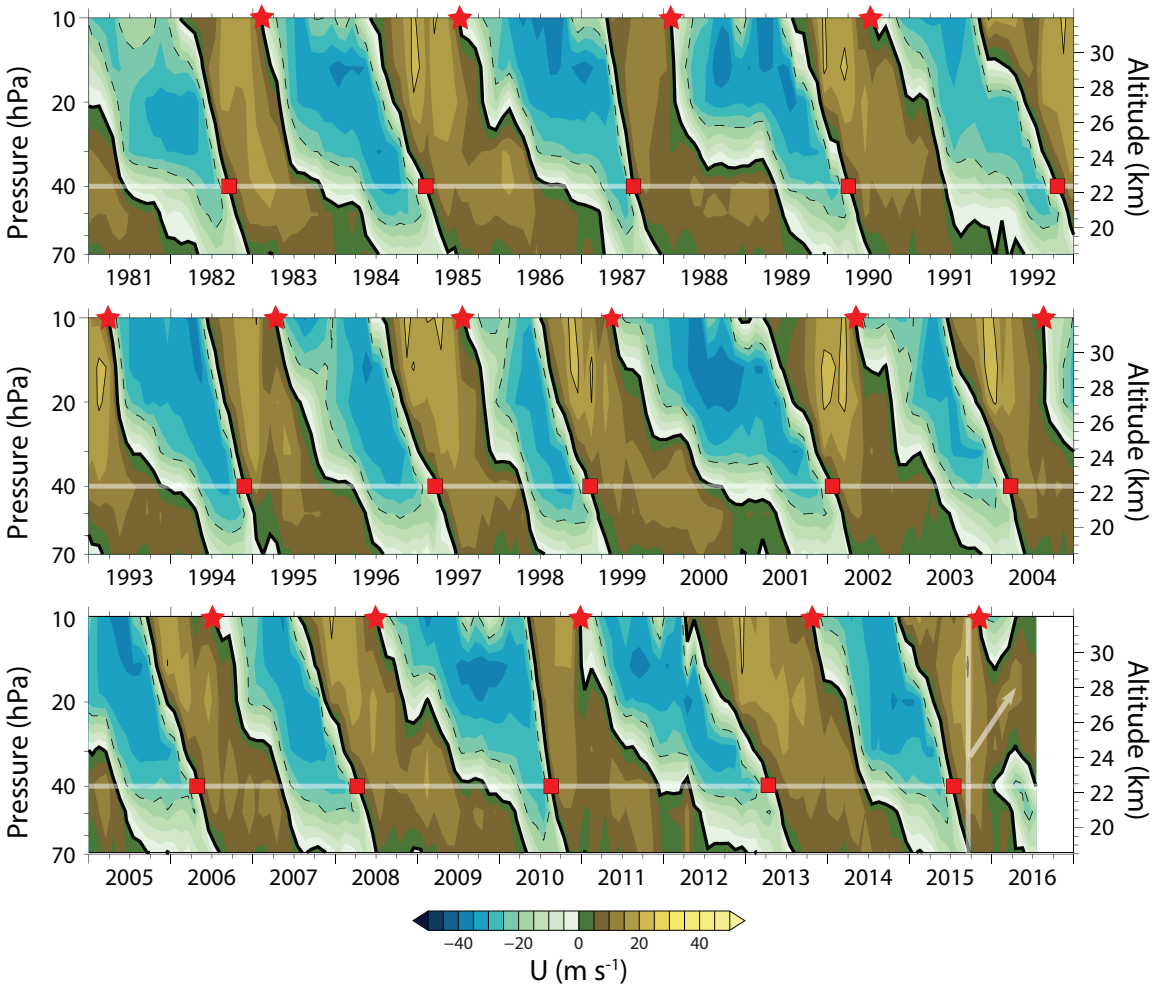

Figure 3-4. Monthly mean zonal wind U(m s^{-1}) derived from Singapore radiosondes (1°N, 104°E) between 70 and 10 hPa for 1981 through July 2016. Easterlies are shown in cyan/blue, while westerlies are shown in green/brown. Contours are every 20 m s^{-1}, with easterlies dashed and westerlies solid, and a thick black line for zero wind. The red squares show the dates of the 40 hPa easterly-to-westerly transition, while the red stars show the dates of the 10 hPa westerly-to-easterly transition. From Newman et al. (2016).

in sea surface temperatures in the Niño 3.4 region (Oman et al., 2013). This likely represents a maximum value, as ENSO and the QBO were in phase throughout much of the analyzed period, making it impossible to separate their contributions to ozone variability through linear regression (Neu et al., 2014). The period since the last Assessment has seen not only the disruption of the QBO described in **Section 3.2.1.2** but also the 2015 El Niño, which was the strongest on record since 1997 and the third strongest since 1950. The impact of this event on stratospheric ozone has not yet been assessed.

The lag between the ENSO signal in atmospheric composition and the ENSO index increases with height, and optimizing the lag has been shown to reduce trend uncertainty in the lower stratosphere (Sioris et al, 2014; Sofieva et al., 2017). One study, however, did not find that inclusion of the lag in an MLR model improved the fit to the 8-year long IASI ozone time series, perhaps due either to the brevity of the record or the broad vertical smoothing of IASI (Wespes et al. 2016). This second possibility is consistent with another analysis that found the ENSO contribution to ozone variability to be statistically insignificant in many geographical regions in low-vertical-resolution NDACC FTIR ground-based data (Vigouroux et al. 2015).

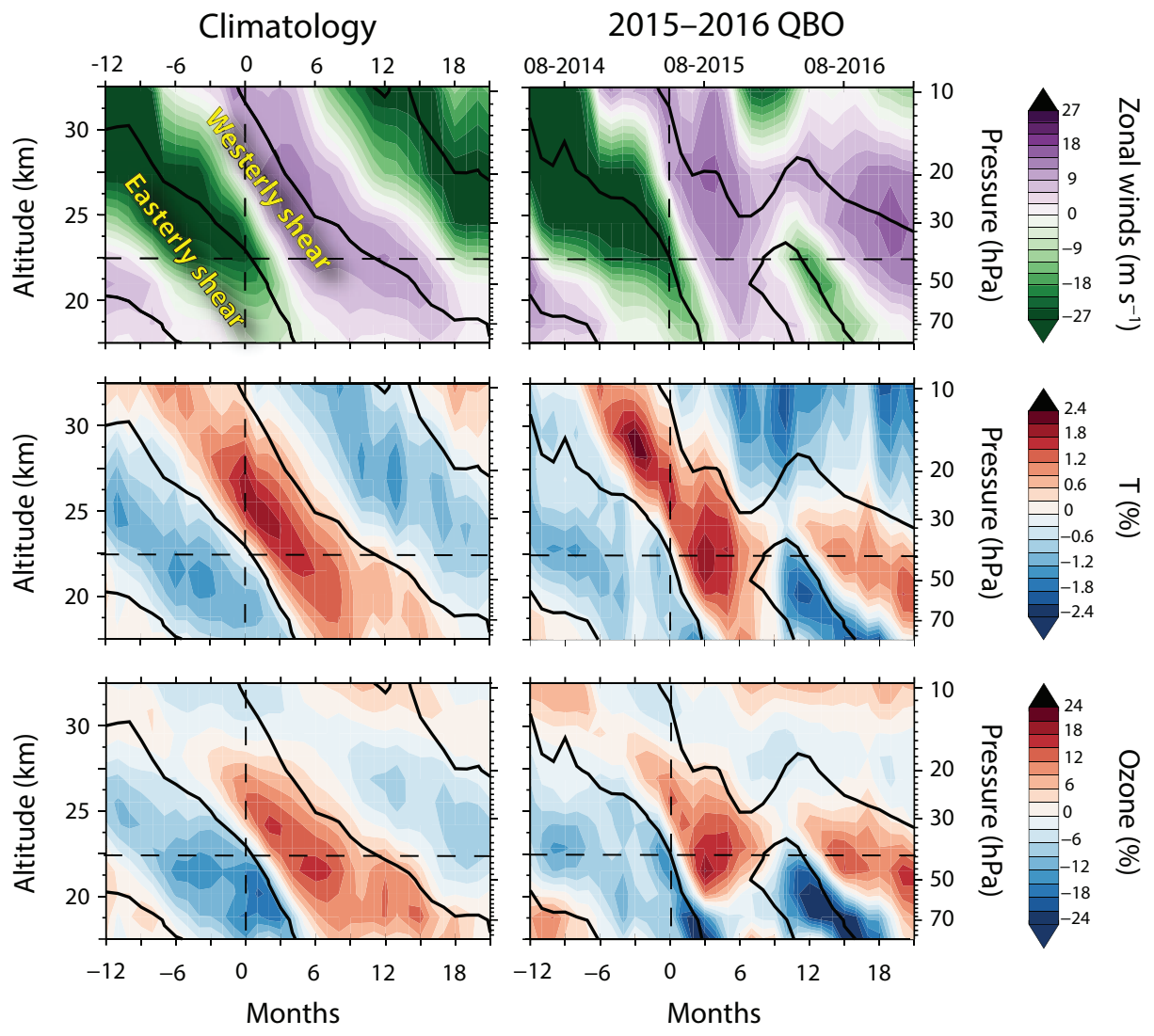

Figure 3-5. Impact of the 2015–2016 QBO disruption on stratospheric variables. The rows show (*top*) the MERRA-2 zonal-mean zonal wind component (in m s^{-1}), (*middle*) deseasonalized MLS temperature anomalies (in %), and (*bottom*) ozone anomalies (in %) as a function of time and pressure (relative to the long-term monthly averages), averaged over 5°S–5°N. The *left column* shows the composite of the easterly-to-westerly shear transitions based on 4 shear transitions at 40 hPa. The *right column* shows the 2015–2016 QBO cycle, which includes the data from April 2014 to September 2016, with month 0 (vertical dashed lines) being May 2016. The thick black contours denote the zero wind shear. The horizontal dashed lines indicate the 40 hPa level. Adapted from Tweedy et al. (2017).

Even in vertically resolved datasets, however, the ENSO impact on stratospheric ozone is regional. It changes sign between the eastern and western regions of the Pacific Ocean (Oman et al., 2013), and even in the extratropics there are large regions of both positive and negative coefficient estimates in total column ozone (Rieder et al., 2013; Frossard et al., 2013). Thus, the ENSO signal, while important for regional ozone variability, is typically small in zonal averaged ozone time series that are analyzed in this chapter (e.g, Sioris et al., 2014). LOTUS (2018) shows that inclusion of an unlagged ENSO proxy in MLR trend analyses of vertically resolved datasets changes trends by 1–2% $decade^{-1}$ and reduces trend uncertainties by 1% $decade^{-1}$.

3.2.1.4 Effects of Stratospheric Aerosol Loading

Volcanic eruptions are a major source of sulfate aerosol in the stratosphere. In the absence of volcanic eruptions, the background stratospheric aerosol layer is attributed to sulfuric gas precursors such as carbonyl sulfide (OCS) and sulfur dioxide (SO_2) that are emitted at the surface and lofted into the stratosphere by deep convection. See **Box 3-1** for a general description of the origin of stratospheric aerosols and their impacts on ozone through radiative processes and heterogeneous chemistry (e.g., Kremser et al., 2016 and references therein). Aerosol surface area has tended to undergo significant variations on decadal timescales, with major eruptions in the 1970s (Fuego), 1980s (El Chichón), and 1990s (Mount Pinatubo). There is thus potential for significant aliasing between the solar cycle and aerosol terms in MLR analysis (Solomon, 1996).

Long-term observational records of stratospheric aerosol are very important for the interpretation of global temperature changes and ozone layer variability. Ground-based lidar observations provide stable, high-quality measurements of stratospheric aerosol. Satellite data are also a very important source of information because they provide the global distribution of aerosols, although the derived aerosol surface area from satellite extinction measurements is rather uncertain (Kremser et al., 2016). In situ stratospheric aerosol measurements from optical particle counters (OPCs) have been extensively used to validate satellite measurements from SAGE II and HALOE (e.g., SPARC, 2006). The discrepancies between aerosol properties inferred from in situ and SAGE II measurements during volcanically quiescent periods have been reduced recently due to improvements in both data records (Thomason et al., 2008; Kovilakam and Deshler, 2015).

One study presented a new combined data record from continuous stratospheric aerosol lidar observations spanning 1994–2015 at the French Haute-Provence Observatory (OHP; 44°N, 6°E) compared with satellite data from SAGE II, GOMOS, OSIRIS, CALIOP, and OMPS (Khaykin et al., 2017). **Figure 3-6**, modified from this study, shows the time series of monthly averaged stratospheric aerosol optical depth between 17- and 30-km altitude derived from OHP lidars and satellite datasets. Remarkable agreement is found between all datasets despite the large variety of measurement techniques. Merged datasets such as the Global Space-based Stratospheric Aerosol Climatology (described by Thomason et al., 2018), provide input to the construction of stratospheric aerosol forcing datasets for chemistry–climate model simulations. Gap-filling of the record after the 1991 Mount Pinatubo eruption, when the stratosphere was too optically opaque for SAGE II measurements, has typically been done with ground-based lidar data. A new study finds that using CLAES measurements from the UARS satellite instead of these ground-based lidar measurements leads to less aerosol loading in the tropical lower stratosphere and less ozone loss following the eruption, in better agreement with observations (Revell et al., 2017).

As discussed in **Box 3-1**, enhanced aerosol levels following major volcanic eruptions cause ozone changes via heterogeneous chemical processes on the particle surfaces and dynamical effects related to the radiative heating of the lower stratosphere (e.g., SPARC, 2006). Ensemble sensitivity simulations using a coupled atmosphere–ocean chemistry–climate model have been used to assess how these dynamical and chemical processes affect stratospheric ozone and NH polar vortex dynamics (Muthers et al., 2015). The study found that ozone is affected globally by a volcanic eruption for several years. At current ODS levels, the dominant ozone response is depletion linked to heterogeneous chemistry involving halogen compounds, with radiative and dynamical perturbations playing a less important role. However, a major volcanic eruption could directly inject volcanic HCl into the stratosphere, triggering substantial ozone loss even when ODS levels are significantly lower than today (Klobas et al., 2017).

As seen in **Figure 3-6**, there has been no volcanic eruption with Volcanic Explosivity Index (VEI) >5 since Mount Pinatubo (VEI 6), but some small eruptions occurred in the last decade. Studies have shown that smaller volcanic eruptions can inject aerosol into the stratosphere (e.g.,Vernier et al., 2011). Therefore, it is thought that these eruptions may have impacted the ozone column at mid-latitudes over the past decade, as atmospheric chlorine levels have slowly decreased. The Calbuco volcano, which erupted in southern Chile on 22 April 2015, increased the stratospheric aerosol optical depth by a factor of 2, with an e-folding time of 90 days (Bègue et al., 2017).

Box 3-1. Origin of Stratospheric Aerosols at Mid-latitudes

C. Junge (Junge et al., 1961) discovered the presence of a layer of aqueous sulfuric acid aerosols in the stratosphere in the early 1960s. The composition of these aerosols is dominated by droplets of sulfuric acid/water (H_2SO_4–H_2O) solution, with smaller amounts of meteoritic and non-sulfate materials. The main precursors of sulfate aerosols are sulfur dioxide (SO_2) and carbonyl sulfide (OCS), which are transported to the stratosphere through dynamical transport mechanisms occurring mainly in the tropics. Volcanic eruptions can also directly inject SO_2 into the stratosphere. SO_2 and OCS are then oxidized to form H_2SO_4, which rapidly nucleates to form condensation nuclei. These nuclei grow into larger aerosol particles through condensation and coagulation mechanisms.

The key processes relating to the origin of stratospheric aerosols (adapted from Kremser et al., 2016) are given in **Box 3-1 Figure 1**:

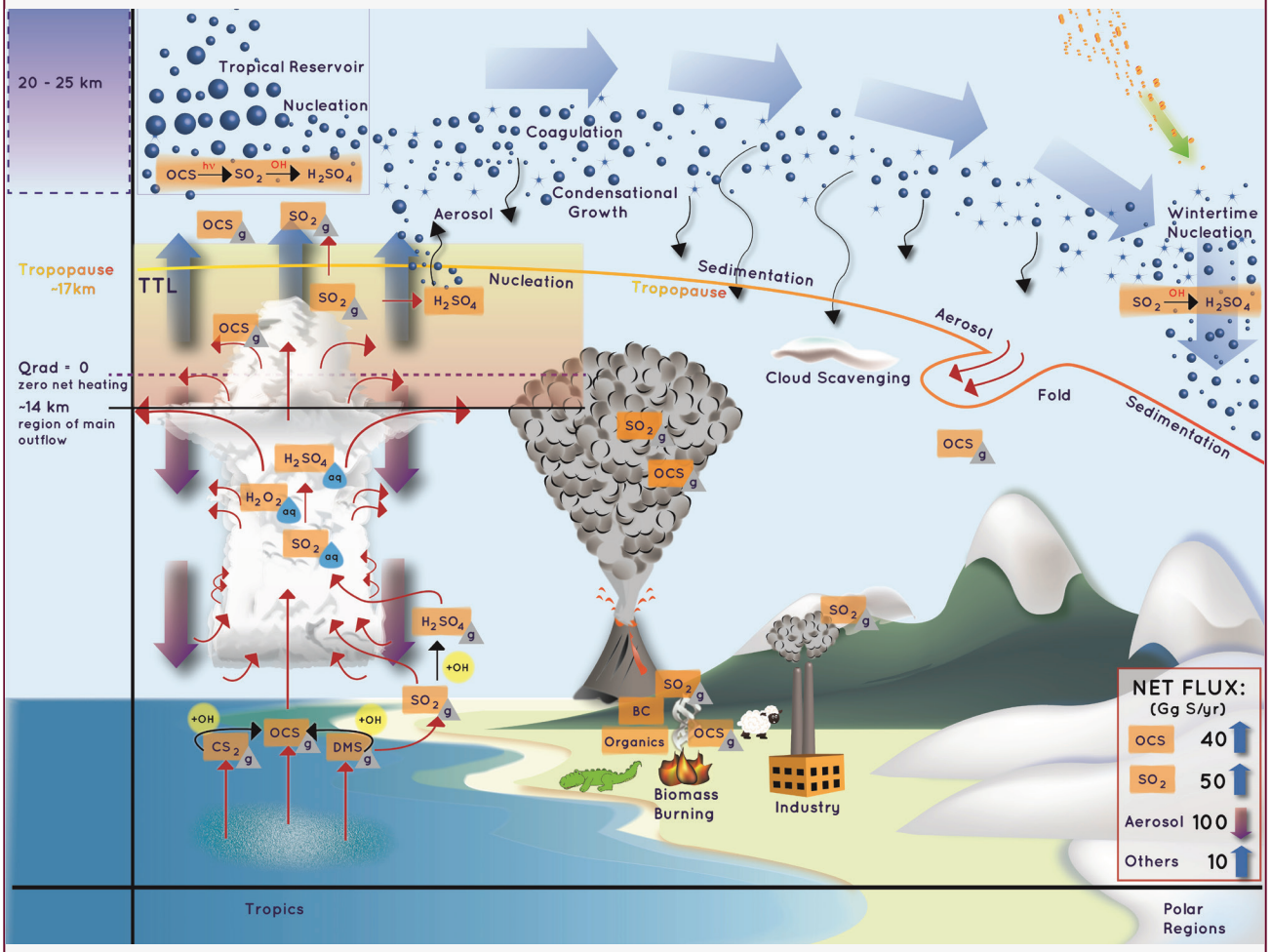

Impact of Stratospheric Aerosols on Ozone

Stratospheric aerosols play a role on the stratospheric ozone budget through chemical, radiative, and dynamical processes:

- **Chemical processes**
  - Nitrogen oxides (e.g., N_2O_5) are converted to HNO_3 through heterogeneous chemical reaction at the surface of the particles. This slows down NO_X catalytic cycles and enhances ozone in the middle stratosphere.

Box 3-1, continued.

- In the lower stratosphere, the removal of nitrogen oxides leads to increased production and decreased loss of reactive chlorine via HO_X and Cl_X cycles. This results in ozone loss in the presence of ODSs.

- **Radiative and dynamical processes**
  - Enhancement of the stratospheric aerosol layer by volcanic eruptions increases atmospheric optical depth in the solar shortwave radiation domain, inducing a cooling at Earth's surface. At the same time, volcanic aerosols increase the absorption of solar longwave radiation, inducing a heating of the lower stratosphere.
  - For volcanic eruptions occurring in the tropics, the warming of the tropical stratosphere enhances the meridional temperature gradient, which perturbs the stratospheric circulation. The enhanced upwelling linked to heating of the lower tropical stratosphere results in lower ozone levels in the tropics and higher ozone at mid-latitudes. At polar latitudes, the strengthening of the vortex due to the larger meridional gradient enhances polar ozone destruction under present-day ODS levels.

The Asian monsoon circulation has been highlighted recently as an important pathway for transport of aerosols into the stratosphere (e.g., Vernier et al., 2015, 2011). Both the Asian and North American summer monsoon circulations are accompanied by low temperatures in the lowermost stratosphere subtropics. Using a nudged chemistry–climate model, one study showed that significant heterogeneous chlorine activation on volcanic and non-volcanic particles could occur along the southeastern flank of the monsoon anticyclones (Solomon et al., 2016a). This conversion of HCl into reactive chlorine led to small modeled ozone decreases of 1.5–2.5% in the 16- to 18-km altitude range when averaged over 2009–2012 and 0°–30°N.

3.2.1.5 Other Dynamical Variations

The Brewer–Dobson circulation (BDC) is a residual meridional circulation driven largely by the deposition of momentum by planetary-scale waves. Changes in the BDC drive variations in ozone both through transport and chemistry. For example, variations in tropical upwelling have been shown to have a statistically significant impact on ozone in the mid-latitude lower stratosphere (Neu et al., 2014); Nedoluha et al. (2015) hypothesized that a significant decrease in tropical ozone from 2004 to 2013 seen near 10 hPa in measurements from MLS and other satellites (Kyrola et al., 2013; Gebhardt et al., 2014; Eckert et al., 2014), for which an increase in tropical upwelling was deemed an insufficient explanation (Eckert et al., 2014), could have instead resulted from chemical changes associated with a decrease in upwelling over the period (Aschmann et al., 2014). Using a 2-dimensional model, this study showed that such a decrease in upwelling would increase the residence time of N_2O and therefore its conversion into NO_y, which would in turn deplete ozone near the ozone maximum, where it is very sensitive to NO_y.

Because year-to-year variations in the BDC can have such an important influence on ozone variability (e.g., Fusco and Salby, 1999; Newman et al., 2001; Dhomse et al., 2006), they are often taken into account in MLR analyses. However, variability in middle-stratospheric tropical upwelling associated with the QBO and ENSO can be as large as 40% (Flury et al., 2013; Neu et al., 2014; Minschwaner et al., 2016), making it unclear to what degree BDC proxies provide information independent of these terms in MLR analyses, particularly in the tropics. As discussed in **Section 3.2.1**, the LOTUS study found that inclusion of an eddy heat flux (EHF) proxy, which is a measure of the vertical group velocity of planetary-scale waves and is proportional to the vertical component of the BDC, has a negligible impact on ozone profile trends computed from zonal average ozone fields (LOTUS, 2018). However,

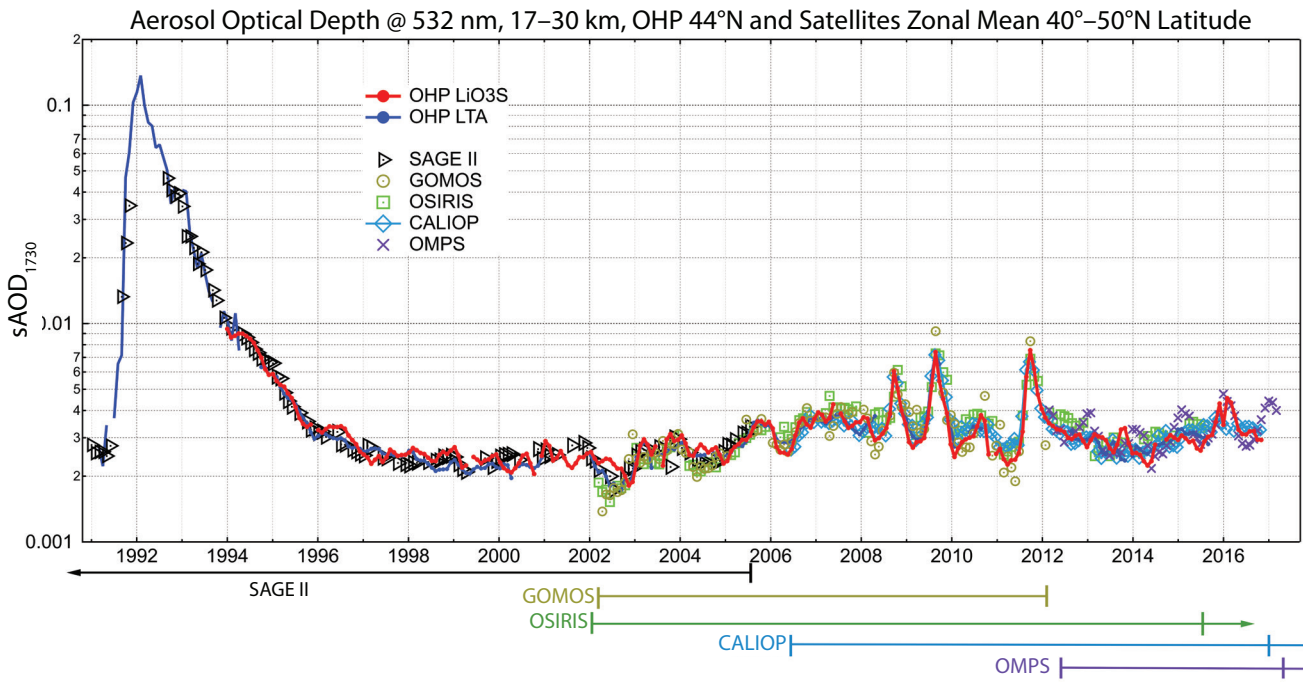

Figure 3-6. Time series of monthly mean stratospheric aerosol optical depth between 17- and 30-km altitude ($sAOD_{1730}$) from OHP lidars and monthly and zonal mean $sAOD_{1730}$ within 40–50°N from satellite sounders. From Khaykin et al. (2017).

another study found that while the QBO dominates total column ozone (TCO) variability in the tropics, using a winter-mean EHF at 100 hPa as a proxy for the BDC accounts for most of the variability in TCO from 50 to 60° in both hemispheres, with an explained variance of up to 7 DU in the SBUV MOD v8.6 and GSG datasets and a 15–35% larger signal in SBUV MOD 8.0 (Chehade et al. 2014; see **Appendix 3A** for a description of these datasets). While studies that utilize a BDC proxy tend to focus on interannual changes in ozone and on the lower-stratospheric circulation, Ball et al. (2016) developed a new upper-branch Brewer–Dobson circulation (UBDC) index based on mid-latitude temperature variations near 5 hPa that reflect rapid changes in the upper branch of the BDC that occur on timescales of a month or less. They found that this index explains more of the variability in ozone at 2 hPa (up to 60%) than the QBO index and reduces uncertainties on the estimated trend in upper-stratospheric equatorial ozone by up to 20%.

Other dynamical terms in MLR analyses include tropopause pressure, which has been shown to be a strong predictor of short-term variability in Fourier transform infrared (FTIR) ground-based ozone records (Vigouroux et al., 2015), and the Arctic Oscillation (AO), North Atlantic Oscillation (NAO), and Antarctic Oscillation (AAO) indices. The AO and NAO are essentially different ways of describing NH high-latitude pressure gradients, which influence the zonality of the jet stream. The AAO is the SH counterpart of the AO (e.g., Weiss et al., 2001; Frossard et al., 2013; Rieder et al., 2013; and references therein). The NAO/AO and AAO contributions to zonally averaged ozone variations are generally small (Chehade et al., 2014; Wespes et al., 2016; LOTUS, 2018), but these oscillations explain much of the variability in ozone at individual ground stations (Petropavlovskikh et al., 2015; Vigouroux et al., 2015). This is likely due to the fact that there are large regions of both positive and negative coefficients for the NAO north of 40°N and for the AAO south of 50°S that are associated with the shift in the jet stream between positive and negative phases (Rieder et al., 2013; Frossard et al., 2013).

3.2.1.6 Attributing Variability in Regression Analysis

In addition to there being covariances between the various proxies describing natural variability, these proxies are not fully orthogonal to the trend term and thereby influence trend estimates and their sensitivity. This long-recognized issue has been the subject of continued efforts in recent years to quantify trend sensitivity to the combination and description of natural proxies (de Laat et al., 2015; LOTUS, 2018). **Figure 3-7** shows an example of an ozone time series, the proxies for natural variability used in the LOTUS analysis (scaled by their regression coefficients), and the ozone fit residuals resulting from subtraction of those proxy terms.

As discussed in **Section 3.2.1.5**, inclusion of the AO, AAO, NAO, or EHF proxies has a negligible impact on trends for most zonally averaged satellite profile datasets (LOTUS, 2018). Trend uncertainties are slightly affected by these terms but not to the extent that insignificant trends become significant, or vice versa. The use of solar, QBO, and ENSO proxies is well established. Their omission results in 1–2% decade^{-1} changes in piecewise linear profile trends and a decrease in overall significance levels (LOTUS, 2018). The impact of the solar cycle term on upper-stratospheric trends diminishes to 0.5% decade^{-1} for regression analyses of data extending past 2014. Furthermore, the choice of solar proxy is found to be not particularly important for time series of this length (LOTUS, 2018). Using a lag for the ENSO term (see **Section 3.2.1.3**) mainly affects trend uncertainties, not the trends, but no consistent picture emerges regarding the magnitude of the impact or the parts of the atmosphere for which a lag is important. Adding a third QBO EOF into the regression has negligible impacts on the trend and uncertainty results (LOTUS, 2018).

Including an aerosol proxy primarily affects trend results in the lower stratosphere. Some aerosol dependence is seen across datasets in the middle to upper stratosphere, and coherence of this dependence across datasets adds confidence that it is likely real (LOTUS, 2018). The proxy terms for El Chichón and Mount Pinatubo scale differently, and it is often necessary to separate them and use different time lags for each term. It is quite important to accurately represent the Pinatubo event, because it tends to have a large impact on the trend term, especially when using piecewise linear trends. In recent years, there have been numerous small volcanic eruptions (Solomon et al., 2016b; **Section 3.2.1.4**), and the aerosol proxy time series have not yet been extended to cover these events. A pragmatic approach used in LOTUS is to repeat the last month of the aerosol proxy time series (September 2012) to extend the record (LOTUS, 2018). This choice has a negligible effect on trend results since the aerosol regression term is primarily constrained by the period immediately following the Pinatubo eruption rather than by aerosol loading during the last five years (**Figure 3-7**).

3.2.2 Trend Models

The proxies discussed in **Section 3.2.1** describe periodic or transient variations in ozone in Equation (1), with the longer-term evolution characterized by the *Trend* term in Equation (1). Trends are often modeled as two linear terms that are either connected (piecewise linear trend, PLT) or disconnected (independent linear trend, ILT). Alernatively, an additional proxy function (e.g., equivalent effective stratospheric chlorine, EESC) can be used to attribute long-term changes in ozone to a particular process, such as changes in ODSs.

Both PLT and ILT trend estimates are sensitive to the start- and endpoints of the time series, but this sensitivity decreases as the length of the time series increases. For stratospheric ozone trends, the advantages of ILT over PLT are that outliers in the mid 1990s affect only one trend, not both, and that no linear model is forced during the turnaround period, when the time series behaves nonlinearly. The inflection time in the PLT model is generally fixed to ~1997 (Harris et al., 2008; Kyrölä et al., 2013; Chehade et al., 2014; Damadeo et al., 2014), coinciding with the turnaround in ODS concentrations (see **Chapter 1**). Changing this inflection point impacts PLT trends in the upper stratosphere; for datasets that end in 2016, PLT trends systematically increase by up to 0.3% decade^{-1} (at mid-latitudes) for every forward shift in inflection time of one year. Changing the start year for recovery in the ILT analyses from 1997 to 2000 leads to a change in the trends of up to 1–1.5% decade^{-1} (**Figure 3-8**; LOTUS, 2018). Hence, trends calculated over different time periods are not directly comparable, and the level of disagreement depends on the trend model and the dataset (LOTUS, 2018).

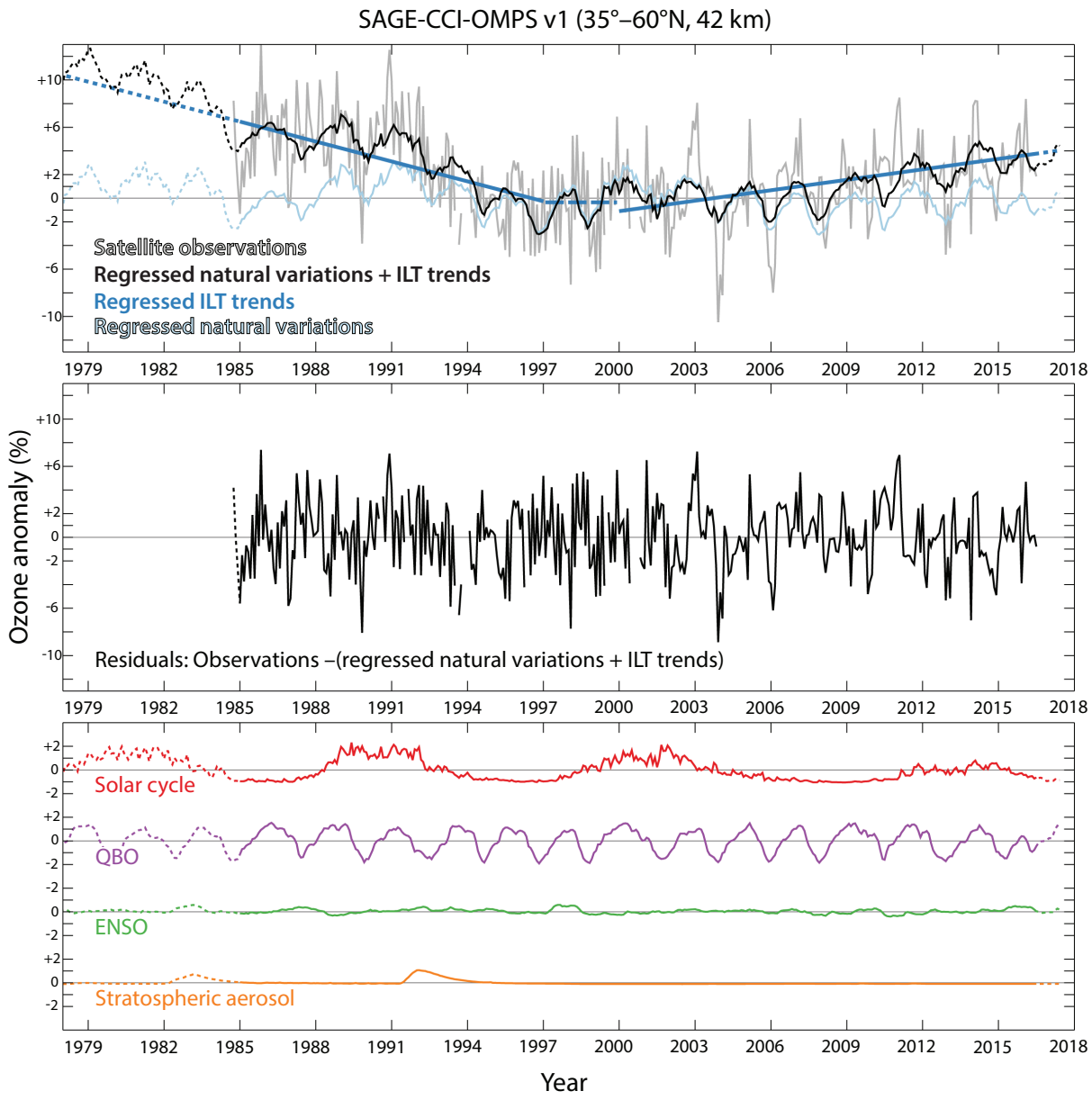

Figure 3-7. Terms in the regression of monthly deseasonalized ozone anomalies from SAGE-CCI-OMPS at 42 km in the 35°–60°N zonal band. The *top panel* shows observed monthly mean anomalies (in %; gray line) relative to the annual cycle of ozone. The black line is the result of the regression model including the independent linear trends (ILTs; thick blue lines). The light blue line shows the sum of the terms of the regression model without the ILTs included. The *middle panel* shows the residual in the observed ozone when the long-term trend and regressed natural variations are subtracted. The *bottom panel* shows the relative contributions of (from *top to bottom*) the solar flux, QBO, ENSO, and aerosols to the reconstructed time series (light blue line) in the top panel. The same vertical scale is used for all time series. Dashed lines fall outside the period used by the MLR. Observations and regression model are those used by LOTUS (2018).

This issue should not be overlooked when comparing trends and their significance from different analyses.

Long-term changes in ozone can also be represented as a nonlinear process; e.g., proportional to a measure of total stratospheric halogen loading such as an EESC proxy. EESC is calculated from emission rates of chlorofluorocarbons and related halogenated compounds, given their individual Ozone Depletion Potentials (ODPs) and certain assumptions regarding transport

times into the stratosphere. EESC-derived trends are primarily used for attribution studies. They are not well suited to detection of recent trends because the model uses a single fit coefficient, which is primarily constrained by the early period of large EESC increases and ozone depletion rates. The small ozone changes observed in recent years are poorly described by the modest post-turnaround decline in EESC (Damadeo et al., and 2014; Frith et al., 2017). In fact, the strong anti-correlation between EESC and ozone in the early period can force an erroneous, statistically significant positive trend in the latter period, even through synthetic time series in which EESC does not decrease (Kuttippurath et al., 2015). Models with two orthogonal EESC terms avoid such trend bias by effectively leaving the turnaround time and ozone depletion/recovery rate as free parameters (Damadeo et al., 2014, 2018), but this renders attribution of trends to changes in ODSs less straightforward. Adaptive techniques, such as dynamic linear regression models (DLMs; Laine et al., 2014, and Ball et al., 2017) and ensemble empirical mode decomposition (EEMD) methods

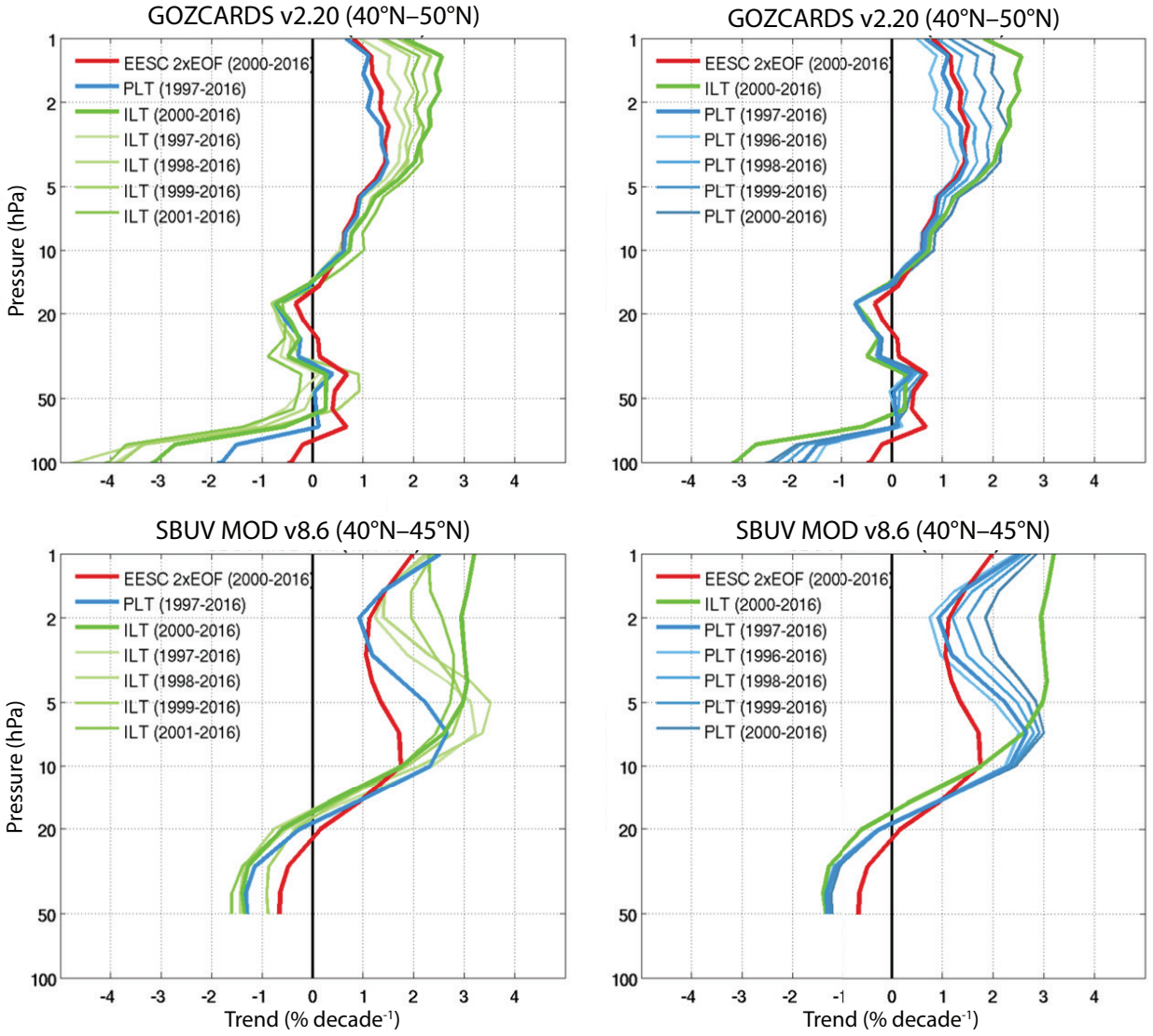

Figure 3-8. Sensitivity of ozone profile trend estimates to the modeling of the trend in the regression (independent, piecewise, or EESC) and its starting point. Results are shown for GOZCARDS v2.20 (*top row*) and SBUV MOD v8.6 (*bottom row*) at mid-northern latitudes for the past two decades. Trends in the upper stratosphere vary by 1–2 % decade^{-1} depending on the trend model and regression period. Adapted from LOTUS (2018).

(Bai et al., 2017), do not rely on a priori information for the long-term behavior of ozone. Trends are allowed to evolve over time, more accurately reflecting observed changes, especially when compared to single EESC models (Bai et al., 2017). The diagnosed difference of several percent per decade between PLT and DLM trends is not significant. However, uncertainties of DLM trends are generally larger, such that they are more likely to be insignificant than PLT trends. Tests on synthetic data hint that the DLM method provides more accurate errors (Ball et al., 2017).

Artifacts in the time series—such as sudden changes in the mean value or noise level, or more gradual changes due to drifting satellite orbits or instrument performance (e.g., Weatherhead et al., 2017)—are usually not modeled in a regression. Some artifacts are large and contribute considerably to the random component of the trend uncertainty budget, while others contribute to the systematic error. Accurate estimates of the latter remain challenging for a number of reasons, despite considerable progress in recent years, particularly in analysis of data from the middle and upper stratosphere (**Section 3.1.4**).

Random errors derived from regression residuals are typically in the range of 0.5–1% decade^{-1} (1σ). Discrepancies in trends for individual merged data records are estimated to range from 1.1 to 3.2% decade^{-1} (1σ). Uncertainties in the regression analysis contribute 0.5–1% decade^{-1}, and uncertainty in the long-term stability of satellite profile data records is currently thought to be about 1–3% decade^{-1} (LOTUS, 2018). Averaging different trend results reduces some of the biases, assuming they are uncorrelated between the data analyses, but the assumptions going into the combination of trends derived from individual data records can play a considerable role in quantifying uncertainties in long-term changes (Harris et al., 2015; Steinbrecht et al., 2017; and LOTUS, 2018). This is further discussed in **Section 3.3.2**.

3.3 PAST OZONE IN OBSERVATIONS

3.3.1 Changes in Total Column Ozone

The time series for (near) global mean, mid-latitude, and tropical total column ozone are shown in **Figure 3-9** (Weber et al., 2018).

3.3.1.1 Interannual Variations

As discussed in **Section 3.2.1**, a large fraction of the total ozone variability is related to natural processes. The impact of these processes on the ozone layer depends on season and latitude. To illustrate this, **Figure 3-10** shows a time–latitude cross section of total ozone deviations from the 1964–1980 annual cycle, clearly showing a large degree of interannual variability. However, the ozone deviations in the extratropics are mostly negative (relative to pre-1980 levels) after the mid-1980s, indicating an overall decrease in ozone.

Polar ozone depletion contributes to these negative anomalies as ozone-depleted polar air moves into lower latitudes. Strong negative anomalies at SH high latitudes in late 2015 to early 2016 reflect a large Antarctic ozone hole, whose extent was close to the all-time record. Record low temperatures likewise occurred in the Arctic stratosphere in late 2015 to early 2016 (see **Chapter 4**). In the Arctic, however, one study estimates that polar ozone depletion is responsible for only about one-third of the variability in NH mid-latitude ozone in spring, with dynamically driven differences in ozone transport between warm and cold winters responsible for the other two-thirds (Strahan et al., 2016).

The 2015–2016 boreal winter was also characterized by an unprecedented disruption in the downward propagation of the QBO westerly phase (Newman et al., 2016; see **Section 3.2.1.2**). The associated decrease in tropical upwelling led to a positive perturbation in tropical total ozone, while weaker extratropical downwelling decreased extratropical total ozone from April to September 2016 (Tweedy et al., 2017; and Weber et al., 2017).

3.3.1.2 Total Ozone Trends

The total ozone trend estimates presented below are based on the ILT approach (Weber et al., 2018). The regression model (see **Section 3.2.1**) also includes seasonal, QBO, solar, and ENSO terms using the proxy data sources described in **Table 3-1**.

The five bias-corrected merged time series (**Appendix 3A**) for the tropical (20°S–20°N) and mid-latitude (35–60°S and N) zonal bands, along with ILT trend fits to the time series, are shown in **Figure 3-11**. Prior to 1997, total ozone trends over the mid-latitudes of both

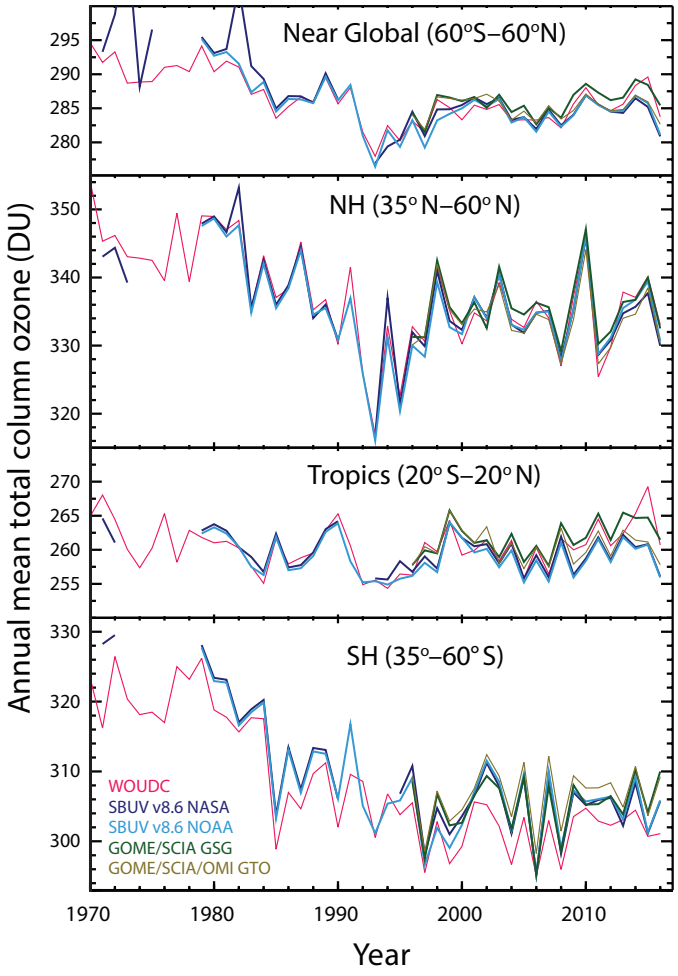

Figure 3-9. Time series of annual mean total ozone in four zonal bands. Data are from WOUDC ground-based measurements combining Brewer, Dobson, SAOZ, and filter spectrometer data (red lines; Fioletov et al. 2002); the BUV-SBUV-SBUV/2 v8.6 merged products from NASA (MOD v8.6; dark blue lines; Chiou et al., 2014, Frith et al., 2014), and NOAA (light blue lines; Wild et al., 2016); the GOME-SCIAMACHY-GOME-2 (GSG) product from the University of Bremen (dark green lines; Weber et al., 2011) and GTO product from ESA/DLR (light green lines; Coldewey-Egbers et al., 2015). WOUDC values for 2016 are preliminary because not all ground station data were available. From Weber et al. (2018).

hemispheres were about −3% ± 1.5% (2σ) decade^{-1}. The 35°–60°S and 35°–60°N trends for 1997–2016 are about +0.6% decade^{-1} and +0.2% decade^{-1}, respectively, based on the average of trend estimates for five datasets. The total column ozone trends are not statistically significant except for the GSG and GTO datasets (**Appendix 3A**) in the SH, which show a +0.7% ± 0.7% decade^{-1} increase that just reaches the 2σ uncertainty level. Given the large (~5%) year-to-year variability in mid-latitude total column ozone, the observed trends for 1997–2016 are consistent with the expected trends from EESC changes, which are about +1% decade^{-1}. Note that the two independent linear fits are almost joined together in the SH but not in the NH. The tropical belt trends are nearly zero.

Total ozone trends for the same five datasets are shown as a function of latitude for 5-degree latitude bins in **Figure 3-12.** The latitudinal dependence of the pre-1997 decrease was discussed in previous Assessments. The trend is nearly zero at the equator and becomes negative and statistically significant toward the poles. The trends over middle and high latitudes are about −3 to −6% decade^{-1}, or about −5.5 to −11% over the entire 1979–1996 period. The trends over the 1997–2016 period, on the other hand, do not show any clear latitudinal dependence. They are close to zero over the equator and NH middle and high latitudes (35°–60°N). Positive values of up to 0.8% decade^{-1} are seen over the 30°–60°S latitude band, though they are not statistically significant. The trend at 20°N is positive and statistically significant in some datasets. An increase at that latitude can also been seen in **Figure 3-10,** where ozone values in the mid-1990s are noticeably lower than in recent years.

As discussed in **Section 3.2.2**, a common approach to estimating total ozone trends is to fit the ozone time

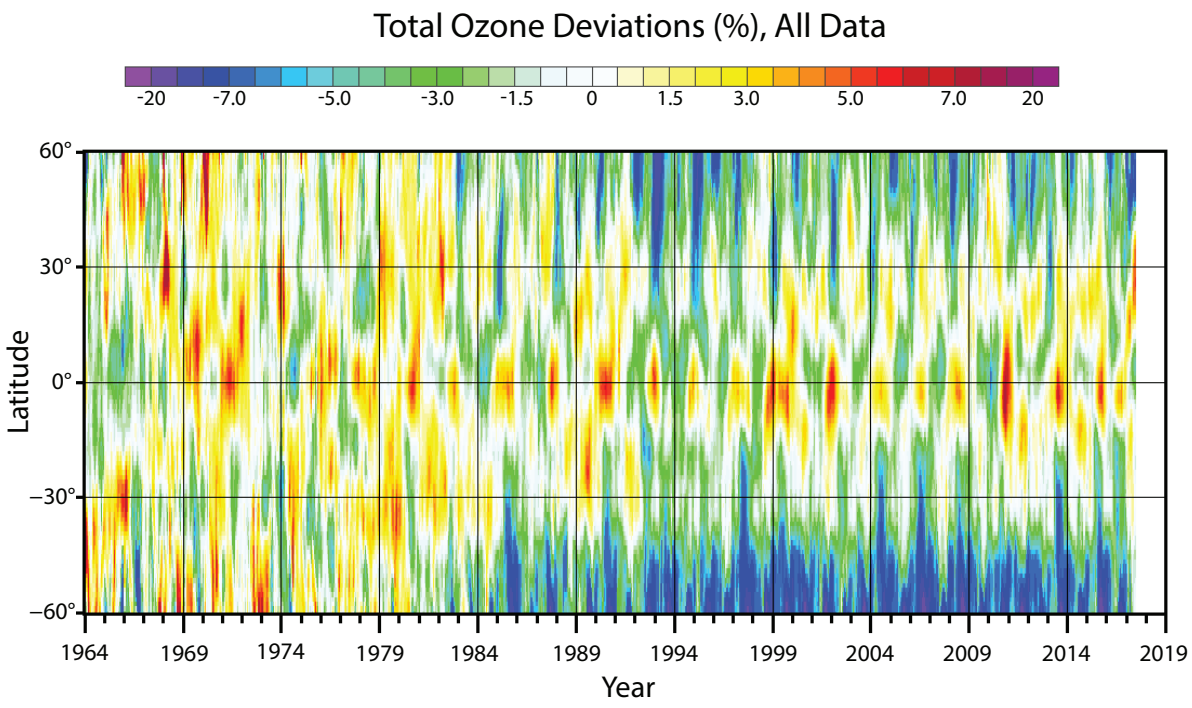

Figure 3-10. Latitude–time cross section of deviations (%) of total ozone from the long-term (1964–1980) mean, estimated from the five datasets shown in Figure 3-9. Measurements from 1964–1970 are from the WOUDC ground-based dataset. Zonal averages were calculated for each dataset for each month of the year using data averaged over the years 1997-2016, when data from all five data sets are available. These monthly zonal averages for each dataset were subtracted from the original data, yielding monthly deviations (in percent) for the entirety of each data record. The deviations then were averaged over all of the datasets for each zonal band to form a single set of monthly zonal deviations. Finally, baseline monthly mean, zonal mean deviations were calculated from the 1964-1980 average, and differences from these baseline deviations were plotted.

series using EESC. This approach works particularly well for ozone data integrated over the globe (with or without the polar regions), because dynamical fluctuations are largely reduced by the global integration. **Figure 3-13** shows global ozone with seasonal, QBO, solar, and volcanic effects removed and the best fit for the EESC curve overlaid, providing a picture of the extent of "unexplained" ozone variability (updated from WMO, 2011). While this method does not estimate the rates of ozone change prior to and after the turning point separately, it is useful as an illustration because it indicates the overall agreement of ozone and ODS changes.

One study used a different technique, called a four-step adaptive ozone trend estimation scheme, to isolate the long-term zonal ozone variability related to anthropogenic forcing (Bai et al, 2017). The technique does not require any a priori assumptions about the shape of the ozone trend. With this technique, the turning point of the ozone change was determined to occur in the year 2000; i.e., later than the maximum of stratospheric ODSs and also later than the turning point typically used in ILT analyses. Otherwise, the study's conclusions were similar to those from conventional methods. It finds that the rate of ozone change is positive after 2000 but that the record is still too short to identify a significant trend.

The datasets discussed above are based on measurements in the UV or visible parts of the spectrum. Fourier transform infrared (FTIR) measurements of the solar spectrum can also provide total ozone columns. The records of ground-based FTIR measurements are now long enough to examine the trends. Data from eight FTIR sites with records starting from

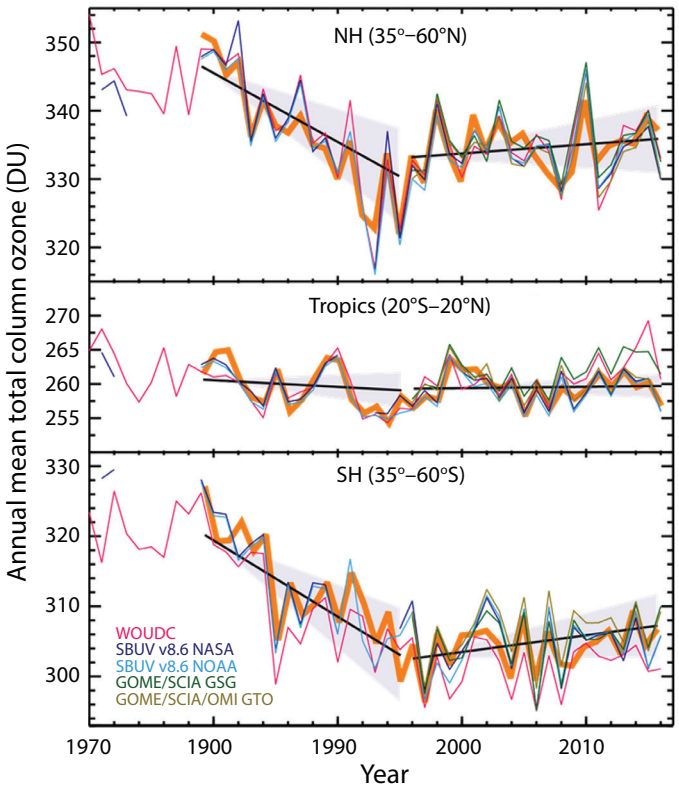

Figure 3-11. Annual mean total ozone time series of five bias-corrected, merged datasets in the 35°–60°S, 35°–60°N and 20°S–20°N latitude bands. The thick orange lines are the result from applying a multiple linear regression (MLR) model. The solid black lines indicate the linear trends before and after the ODS peak in 1997, respectively. The shaded areas show the 2σ uncertainty of the MLR trend estimates. Adapted from Weber et al. (2018).

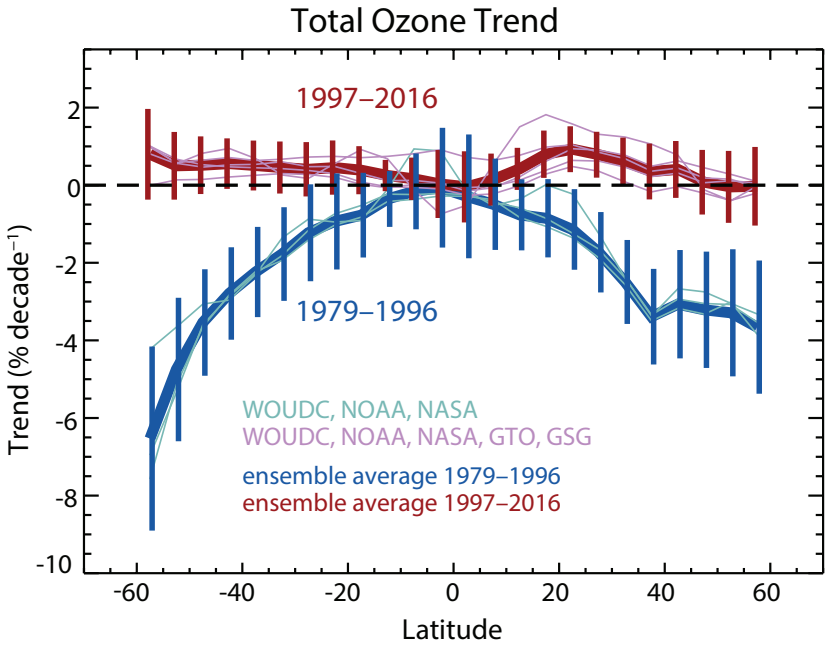

Figure 3-12. Total ozone linear trend in % decade^{-1} as a function of latitude for 1979–1996 (bluish colors) and 1997–2016 (reddish colors) estimated for NASA MOD, NOAA SBUV, GTO, GSC, and WOUDC datasets. The thick blue line with blue 2σ error bars and the thick red line with red 2σ error bars represent a weighted mean trend from the five (or three before 1996) datasets for 1979–1996 and 1997–2016, respectively. The weights are the inverses of the trend uncertainties from the individual datasets. Trends estimated using the individual datasets are shown by the thin lines as indicated. The 1979–1996 trends are not shown, as the GSG and GTO are available only after 1995. The uncertainty of the mean trend is the weighted standard deviation resulting from the averaging. However, the uncertainties are sometimes very small, as all datasets agree at some latitudes very well. Therefore, the larger value of the weighted standard deviation and the mean of the individual uncertainties is plotted (in most cases, it is the latter). Adapted from Weber et al. (2018).

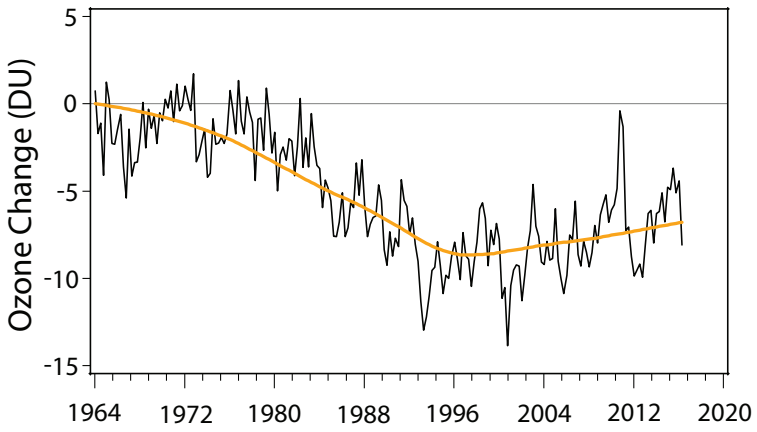

Figure 3-13. Deseasonalized, area-weighted total ozone deviations for 60°S–60°N from the WOUDC dataset, adjusted for seasonal, solar, volcanic, and QBO effects (black line). The orange line represents the component of ozone variability due to changes in the equivalent effective stratospheric chlorine (EESC) based on a fit to data from 1964–2016. The EESC curve for the mid-latitude lower stratosphere is used for this plot.

around 1995 have been found to be consistent with UV/VIS measurements (Vigouroux et al., 2015). The total ozone trends over middle and low latitudes are small and not significant for all stations except for Wollongong, located at 34°S, where the 1996–2012 trend was 1.9% ± 1.1% decade^{-1}.

Total ozone changes during the solstice seasons for 35°–60°S and 35°–60°N for the period 1970–2016 are shown in **Figure 3-14**. The ozone variability over mid-latitudes is highest during winter and is much lower during summer, though the winter and summer deviations are highly correlated. The long-term ozone decline in the Northern Hemisphere shows a seasonal dependence, with the average winter and spring 1997–2016 deviations from pre-1980 levels of 3–4% and summer and autumn deviations of ~2–2.5%. In contrast, there is no seasonal difference in the ozone decline in the Southern Hemisphere. The average 1997–2016 values are about 6% lower than the pre-1980 level for all seasons. In the Northern Hemisphere, large winter–spring ozone deviations such as those seen in 1993 and 1995 (**points a** and **b** in **Figure 3-14**) which were related to the Mount Pinatubo eruption, have not occurred recently. Summer deviations in 2011 and 2016 (**points c** and **d** in **Figure 3-14**) however, are among the largest in the record and comparable to those that occurred in 1993 and 1995. The large Arctic ozone depletion events in 2011 and 2016, as well as the QBO disruption in 2016 (**Section 3.2.1.2**) and the large 2015 ENSO event (**Section 3.2.1.3**) may have contributed to these large deviations. However, it is difficult to quantify these effects. Unlike in the Northern Hemisphere, summertime ozone values in the Southern Hemisphere are affected by the ozone hole and dilution of polar ozone to mid-latitudes (e.g., Fioletov and Shepherd, 2003).

Long-term total ozone variations and trends are generally determined from zonal or global averages, but zonal asymmetries do exist. One study investigated the ENSO impact on the detectability of regional trends in total ozone (Coldewey-Egbers et al., 2014). Both it and another study (Knibbe et al., 2014) that used a different dataset (van der A et al., 2010, 2015) found that the effect of ENSO on total ozone is primarily seen over the Pacific. The contributions from most other factors showed little longitudinal dependence.

In summary, the main results of this Assessment related to total column ozone are similar to those from the 2014 Assessment (WMO, 2014): column ozone remains below pre-1980 levels by 2–3% over NH mid-latitudes (35°–60°N) and by 5–6% over SH mid-latitudes (35°–60°S), with no major changes over the tropical region (20°S–20°N). Despite the fact that it has been nearly 20 years since the ODS turning point in 1997, we still do not see a statistically significant positive total ozone trend over the NH mid-latitudes. The trend is only +0.2% decade^{-1}, which is consistent with expectations given the slow rate of ODS decline and large interannual variability. The trend over the

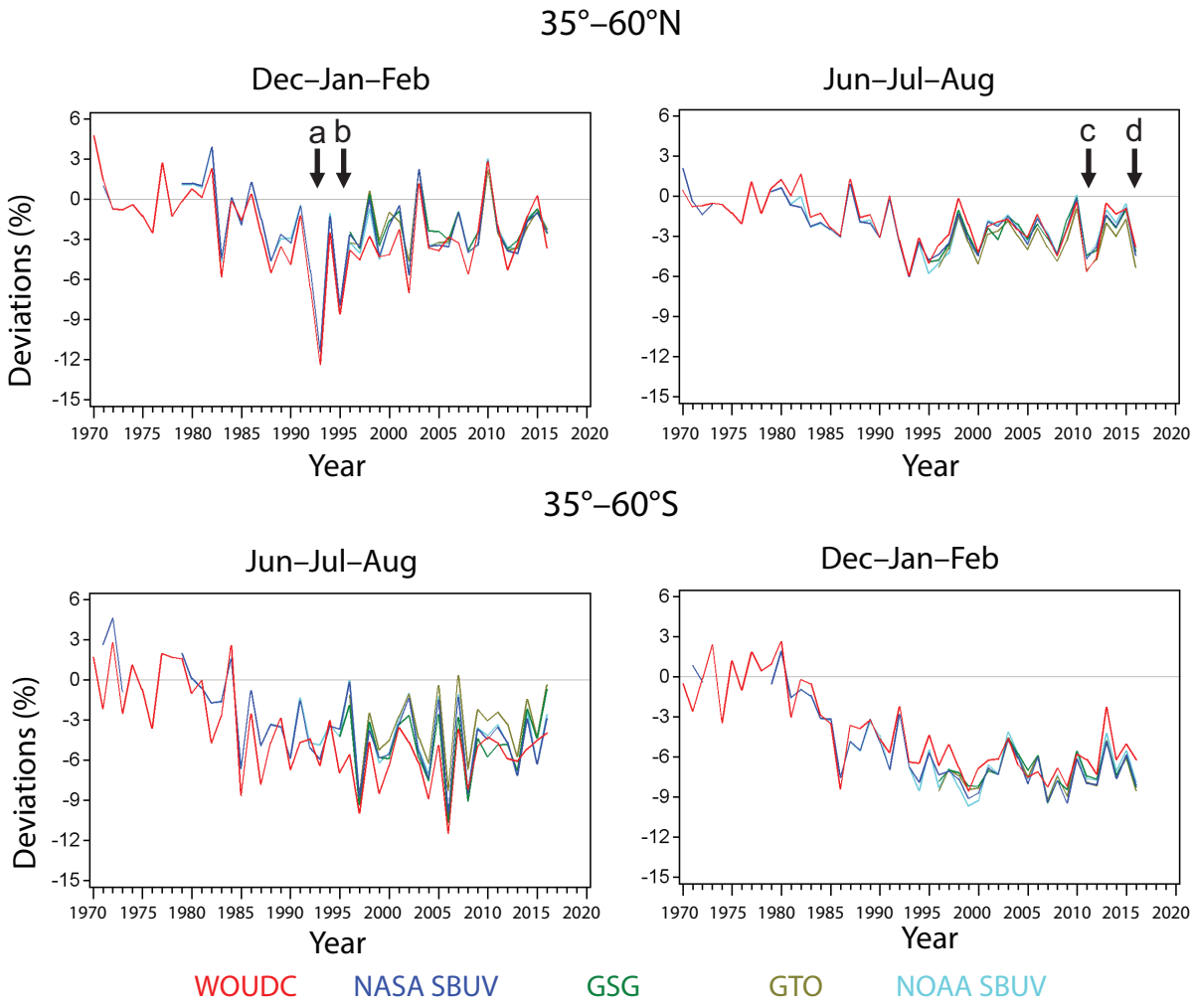

Figure 3-14. Seasonal, area-weighted total ozone deviations from the 1964–1980 means, calculated for four seasonal averages for the latitude bands 35°–60°N (*top row*) and 35°–60°S (*bottom row*). The years on the horizontal scale correspond to the first month of the season. The arrows indicate large NH ozone deviations that occurred in the winter–spring of 1993 (a) and 1995 (b), as well as in the summer of 2011 (c) and 2016 (d) that are discussed in the text. Updated from WMO (2007).

SH mid-latitudes is about +0.7% decade^{-1}, which is just above the 2σ uncertainty level.

3.3.2 Trends in Ozone Profiles

3.3.2.1 Time Series

Figures 3-15 and 3-16 show time series of annual mean ozone concentration anomalies at four pressure levels from 70 to 2 hPa from various ground-based and satellite-based measurements records (**Appendix 3A**), averaged over four latitude bands (LOTUS, 2018). Chemistry–climate model simulations from CCMI-1 are also shown. Ozone anomalies are relative to the 1998 to 2008 climatology of each individual dataset. **Figures 3-15** and **3-16** show overall consistency among observations and between observations and models at the various pressure levels and latitude bands. The relatively narrow model ranges, as compared to the interannual variability of the observations, can be explained to some extent by the lack of volcanic perturbations in some of the CCMI-1 simulations, as well as by a 3-year smoothing applied to the model output. The larger variability of ground-based

observations relative to the satellite measurements is expected, given the small number of measurement stations providing long-term ozone measurements. As in the last Assessment, all datasets show an ozone decline up to the late 1990s, with a leveling off since then. At 2 hPa, most records indicate a slight increase of ozone over the 2000–2016 period that is most pronounced in the Northern Hemisphere. In the CCMI-1 simulations, the ozone decline before 2000 is linked to increasing ODS levels. After 2000, the ozone increase due to ODS decline is enhanced by upper-stratospheric cooling associated with increases in GHGs (e.g., Randel et al., 2016) (**Section 3.3.3**). At pressures greater than 10 hPa, no increase in ozone is seen in the observational records, in broad agreement with the range of model simulations at these pressure levels.

Figure 3-15. Evolution of annual mean deseasonalized ozone anomalies at the 2-hPa/42-km (*left column*) and 10-hPa/31-km (*right column*) levels. Satellite data and measurements from ground-based stations are averaged over four different latitude bands. Gray shadings correspond to the 10th–90th percentiles of the CCMI-1 model results. The model mean and median are also plotted, together with the ±2σ range of the models (gray lines). All anomalies are calculated relative to the base period 1998–2008; CCMI-1 model data are shown as 3-year weighted running means with a double weight for the central year (i.e., 1-2-1 weighting). Adapted from LOTUS (2018).

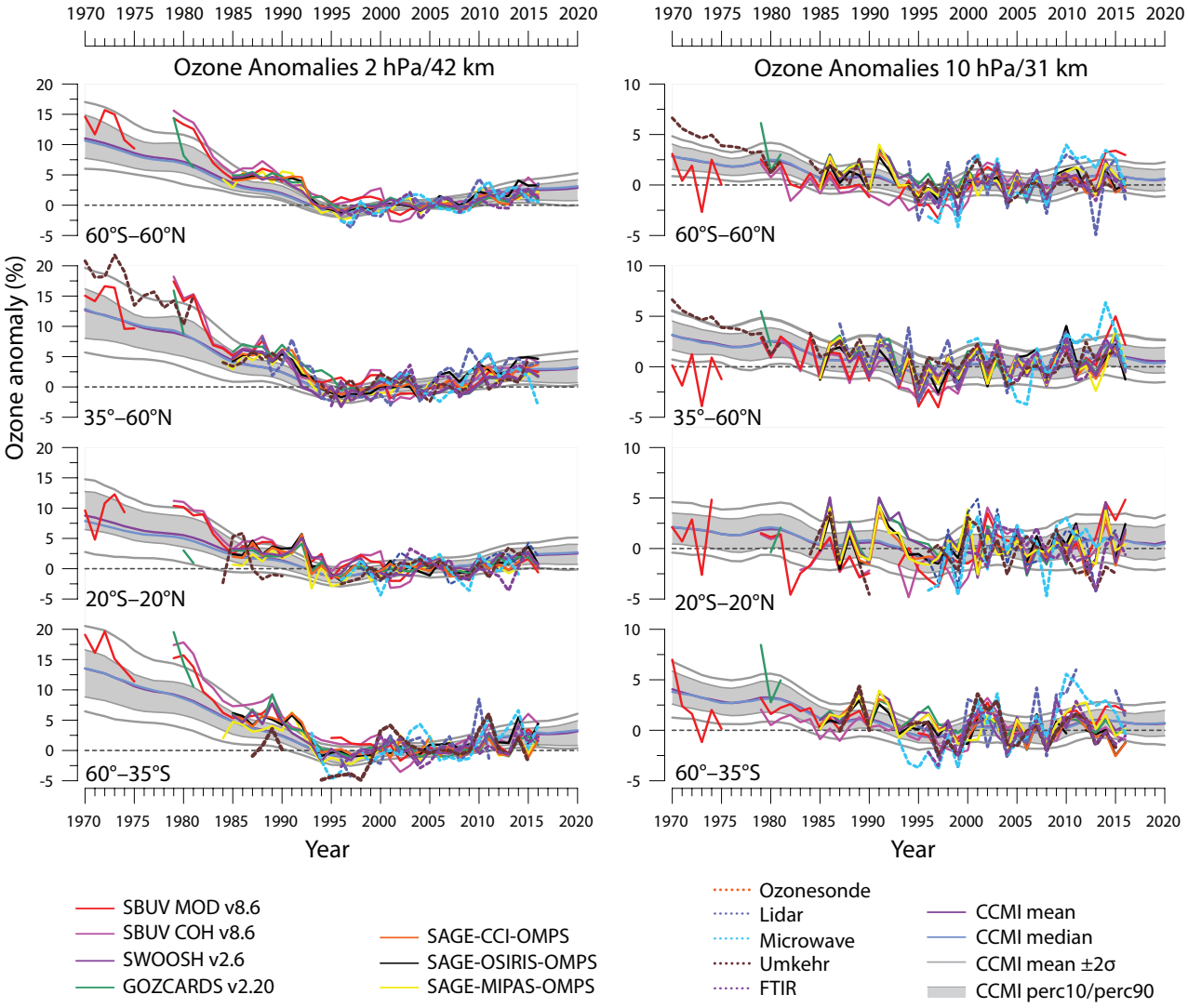

3.3.2.2 Ozone Trends 2000–2016

The last Assessment examined ozone profile trends for both the period of ODS increases, up to about 1997, and after the turnaround in ODS concentrations. For the first part of the record, it confirmed the large negative trends of about −6 to −8% decade^{-1} in the upper stratosphere (around 2 hPa or 35–45 km altitude) that had been found in previous Assessments. For the period after the ODS peak, it reported a significant increase in ozone of 2.5–5% at around the same altitudes in the mid-latitudes and in the tropics. These findings were in agreement with CCMVal-2 model simulations, which attributed about half of this upper-stratospheric ozone increase to declining ODSs. The other half was attributed to increasing GHGs, which cool the upper stratosphere and reduce catalytic ozone loss rates.

Shortly after the release of the 2014 Assessment, several papers that reassessed ozone trends were published as part of the SPARC/IO3C/IGACO-O3/NDACC (SI2N) initiative. The most prominent study re-evaluated long-term ozone profile trends from ground-based, single-satellite and merged satellite ozone records over the period 1979–2012 (Harris et al., 2015). Trends obtained before the ODS peak

Figure 3-16. Same as **Figure 3-15** but for levels 20 hPa/26 km (*left*) and 70 hPa/19 km (right). Adapted from LOTUS (2018).

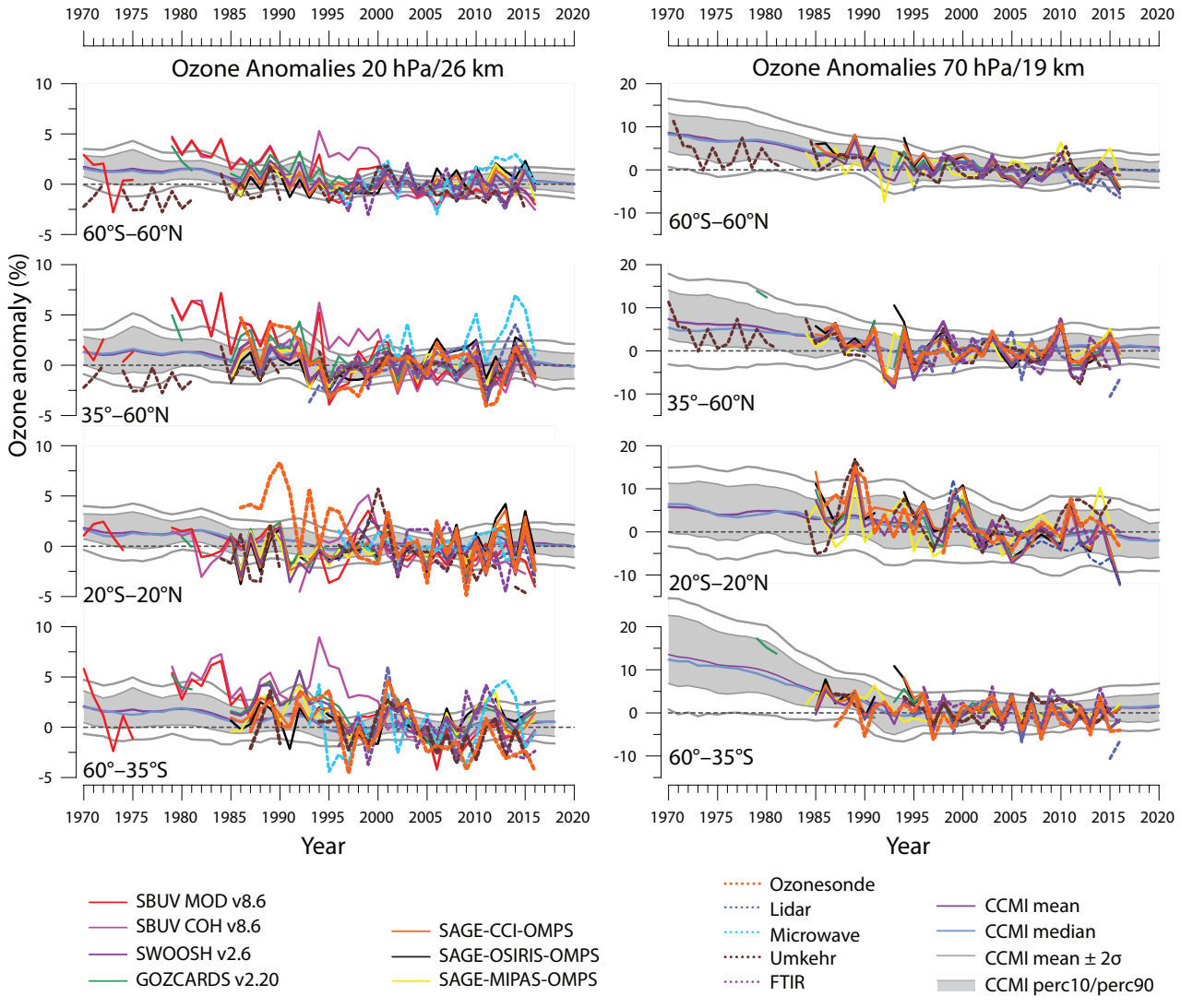

were found to be similar to those reported previously, including in the 2014 Assessment. For the period after the peak in ODS concentrations, positive trends of ~2% decade^{-1} in mid-latitudes and ~3% decade^{-1} in the tropics were found in the upper stratosphere. However, several methods were used to investigate the significance of the increasing trends and in all cases they were found to be insignificant throughout the stratosphere. One method, similar to that used in the previous Assessment, estimated the uncertainty of average trends from the weighted mean of the individual variances but added an extra term for measurement drift, which was found to be ±3–5% decade^{-1} in the 20–40 km altitude range and larger elsewhere (Hubert et al., 2016). A second method used the joint distribution of the individual variances around the arithmetic mean of the estimators e.g., (SPARC 2013). The main conclusion of the Harris et al. (2015) study was that the analyses included in the 2014 Assessment had underestimated the uncertainties in the combined ozone records and that, given these uncertainties, it was too early to detect a significant trend given the length of the "recovery" period (1997–2012).

The differences in the conclusions regarding the significance of increasing ozone trends between the 2014 Assessment and Harris et al. (2015) were revisited under the LOTUS initiative (LOTUS, 2018). In parallel, one study using both newly released merged satellite records and ground-based datasets (Steinbrecht et al., 2017) and another using just satellite records (Sofieva et al., 2017) re-evaluated ozone profile trends using multi-linear regression analyses. Both studies found significant ozone increases in the upper stratosphere of about 2–2.5% decade^{-1} in the mid-latitudes of both hemispheres. Other recent analyses using ground-based datasets have also reported significant positive trends of ozone in the upper stratosphere (e.g., Moreira et al., 2015; Nair et al., 2015; Vigouroux et al., 2015).

However, at least in the case of SBUV long-term observations, inclusion of uncertainties in the calibration and drift of individual instruments in ozone profile merged datasets can result in relatively large errors in ozone trend results. When Monte Carlo simulations are used to estimate uncertainties in ozone trends based on the SBUV MOD merged dataset over the period 2000–2015, the significant ozone trends derived over the 1.6–1.0 hPa range from standard multi-linear regression analyses become insignificant at the 2σ level (Frith et al., 2017).

Altitude–latitude cross sections of ozone trends derived from the merged satellite ozone datsets considered in the LOTUS initiative are shown in **Figures 3-17** and **3-18** for the periods 1985–1997 and 2000–2016, respectively. Trends were determined using the ILT regression model (**Section 3.2.2**). In **Figure 3-17**, the negative trends obtained in the upper stratosphere (e.g., above 35 km) are consistent in magnitude with previous studies. These trends range from −4 to −9% decade^{-1}, depending on the satellite record, with larger negative trends in the Southern Hemisphere in some cases. For the 2000–2016 period (**Figure 3-18**), most records show significant positive ozone trends in the upper stratosphere, consistent with the recent studies discussed above. These positive trends are largest in the mid-latitudes of both hemispheres and range from 2 to 4% decade^{-1}. Both SBUV merged records also show significant positive trends in the tropical upper stratosphere, although the significance is likely overestimated due to omission of the merging uncertainies of the SBUV datasets (**Section 3.1.4**; Frith et al., 2017). Some significant negative trends are found in the tropical middle to lower stratosphere; these are seen primarily in the SBUV and SWOOSH records (LOTUS, 2018). While merging uncertainties were not available for all datasets and thus not explicitly considered within LOTUS, they are to some extent taken into account in that the final trend uncertainty (**Section 3.3.2.3**) was derived from the trend ensemble using the noise in the regression residuals and the spread in the derived trends.

3.3.2.3 Trend Profiles

Figure 3-19 shows individual trend profiles derived from the various data records used in LOTUS (2018) in four broad latitude bands. The pre-1997 trends are very similar across the datasets, within the uncertainties of the measurements; the exceptions are both SBUV merged records, which show large differences from the other datasets in some regions due to larger merging uncertainty in the mid 1990s (LOTUS, 2018). In the post-2000 period, all individual merged records show significant trends, ranging from 2 to 5% decade^{-1}, in the 5–2 hPa pressure range for 35°–60°N. Smaller positive trends are found in the other latitude bands, and some trend values are not significant,

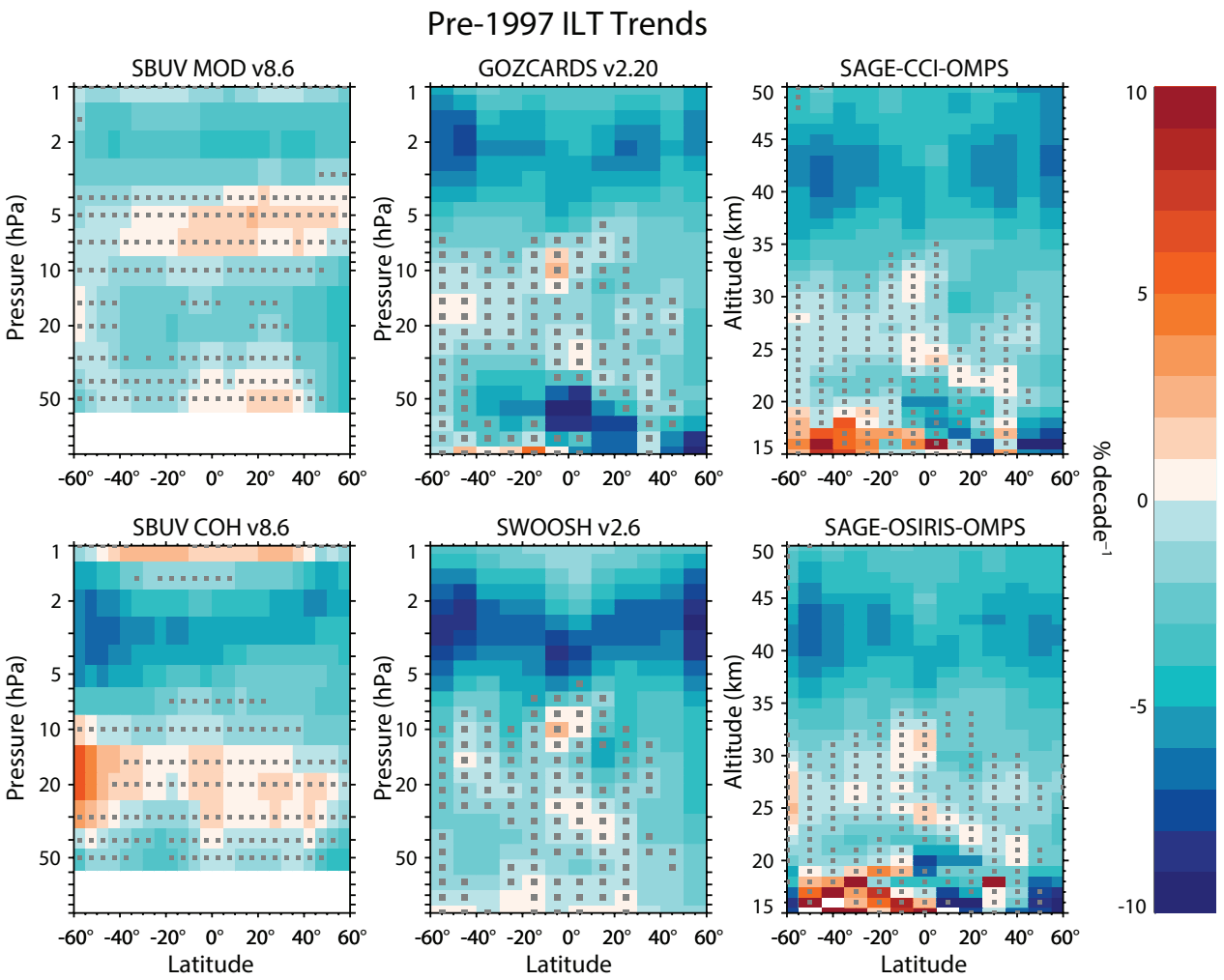

Figure 3-17. Ozone trends for the period 1985–1997 estimated from six satellite data records using the independent linear trend (ILT) model. Gray stippling denotes results that are not significant at the 2σ level. Data are presented on the latitudinal grid and vertical coordinates associated with each dataset. Adapted from LOTUS (2018).

especially in the tropics. In the middle and lower stratosphere, trends are generally not significantly different from zero. This includes the NH mid-latitudes, where most records show negative but not significant trends below 70 hPa.

To facilitate comparison with model simulations, it is useful to calculate an average ozone trend profile from the individual trends derived from each observational record. However, the use of different averaging techniques and different approaches to the calculation of average trend uncertainties can result in contradicting statements regarding the significance of ozone recovery in the stratosphere (**Figure 3-20**). Various techniques have been used to merge the uncertainties in the past (e.g., Harris et al., 2015; Steinbrecht et al., 2017); LOTUS (2018) introduced a new, more statistically robust method. This method includes both simple error propagation, which captures uncertainties introduced by the data and the analyses, and the standard error of the mean, which captures systematic uncertainties such as those introduced by drifts between datasets. Another important parameter that impacts the uncertainty of combined trends is the estimated number of independent datasets. In LOTUS (2018), this number is determined from the correlation of the fit residuals from the trend simulations; it

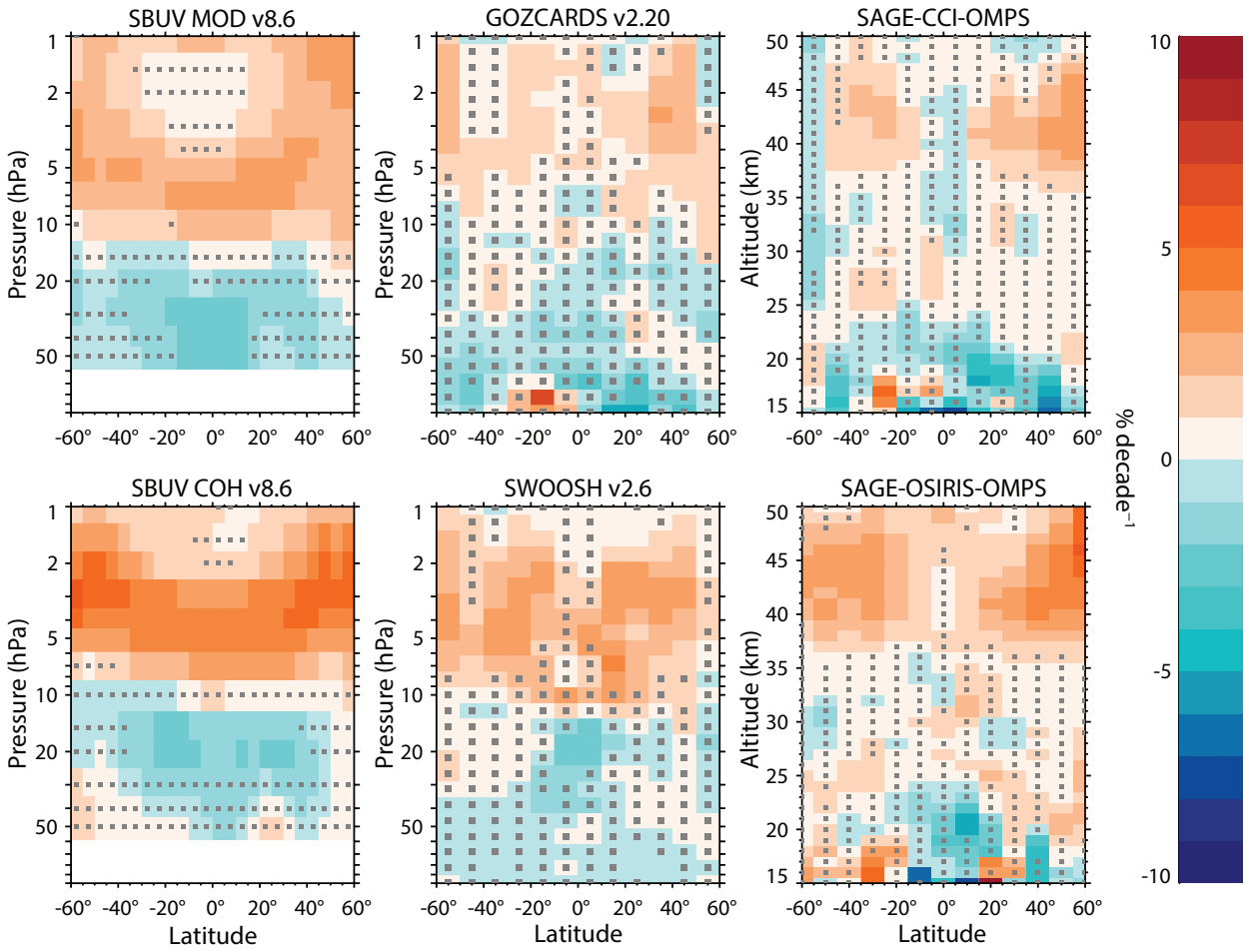

Figure 3-18. Ozone trends for the period 2000–2016 estimated from six satellite data records using the independent linear trend (ILT) model. Gray stippling denotes results that are not significant at the 2σ level. Data are presented on the latitudinal grid and vertical coordinates associated with each dataset. Adapted from LOTUS (2018).

has been more subjectively determined in previous studies (Steinbrecht et al., 2017). The combined trends from the merged satellite datasets used in the LOTUS (2018) study are shown in **Figure 3-21** and compared to the results from the last Ozone Assessment, as well as from the two major studies on ozone profile trends published since then (Harris et al., 2015; Steinbrecht et al., 2017). A significant ozone increase is found in the NH mid-latitude upper stratosphere regardless of the method used. In the tropics and SH mid-latitude upper stratosphere, however, trends are smaller, and their degree of significance depends on the method used to evaluate combined uncertainties.

3.3.2.4 Consistency of Total Column Trends and Integrated Profile Trends

As shown in **Figure 3-12**, total ozone trends for the 1997–2016 period are close to zero over all latitudes, with small positive but not statistically significant values at middle and high latitudes. Despite the small magnitude of these trends, the time series of global mean total ozone is, in fact, consistent with changes in EESC resulting from ODS changes (**Figure 3-13**).

However, ozone profile trends (**Section 3.3.2**) show a significant increase in ozone mixing ratios in the upper stratosphere; this is also thought to be due

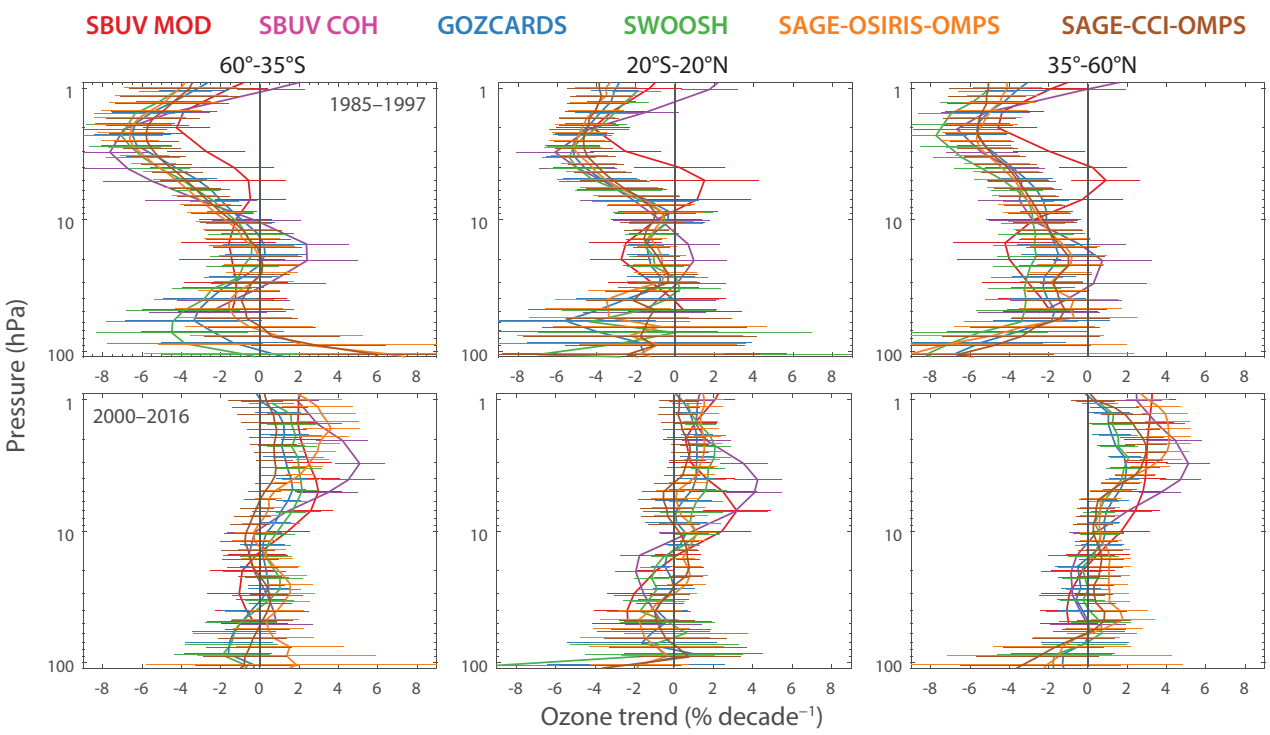

Figure 3-19. Ozone profile trends with 2σ uncertainties for the 1985–1997 (*top row*) and 2000–2016 time periods (*bottom row*) from the ILT regression for latitude bands 35°–60°S (*left column*), 20°S–20°N (*center column*), and 35°–60°N (*right column*). Colored lines are the trend estimates from six individual merged datasets on their original vertical grid. Adapted from LOTUS (2018).

to the decline in ODSs, with enhancement of upper-stratospheric cooling associated with increases in GHGs (**Section 3.3.3**). Though the contribution of the upper stratosphere to column ozone changes is small, it is necessary to understand the consistency or lack thereof among ozone trends in the upper, middle, and lower stratosphere and their relationship to total column changes.

There is recent evidence for a continuous decline in lower-stratospheric ozone, based on merged SWOOSH-GOZCARDS-SAGE II-CCI-OMPS and SAGE II-OSIRIS-OMPS data (Ball et al., 2018). Partial column ozone anomalies (60°S–60°N) were calculated for three layers: the upper stratosphere (10–1 hPa), the middle stratosphere (32–10 hPa), and the lower stratosphere (100–32 hPa). The study found that for the 1998–2016 period, there was a highly probable recovery in the upper stratosphere, a relatively flat trend in the middle stratosphere, and a continuous decrease in ozone in the lower stratosphere.

Similar observational results showing a decline in lower-stratospheric ozone have also been noted by others (e.g., Bourassa et al., 2014, 2018; Steinbrecht et al., 2017; Sofieva et al., 2017) and can be seen in **Figures 3-18** and **3-19** of this report. These figures show that the decline is largest and most consistent across datasets in the tropics. Several studies have addressed attribution of ozone trends in the tropical lower stratosphere (see **Section 3.3.3.2**).

Ball et al. (2017) also found that stratospheric column ozone, which is dominated by lower-stratospheric ozone, decreased from 1998 to 2016. Using the OMI/MLS tropospheric ozone residual column (Ziemke et al., 2006), the study suggests that the total column change is near zero because of increases in tropospheric ozone that compensate for the decline in the stratosphere.

Though there does appear to be evidence from merged satellite datasets for a decrease in lower-stratospheric

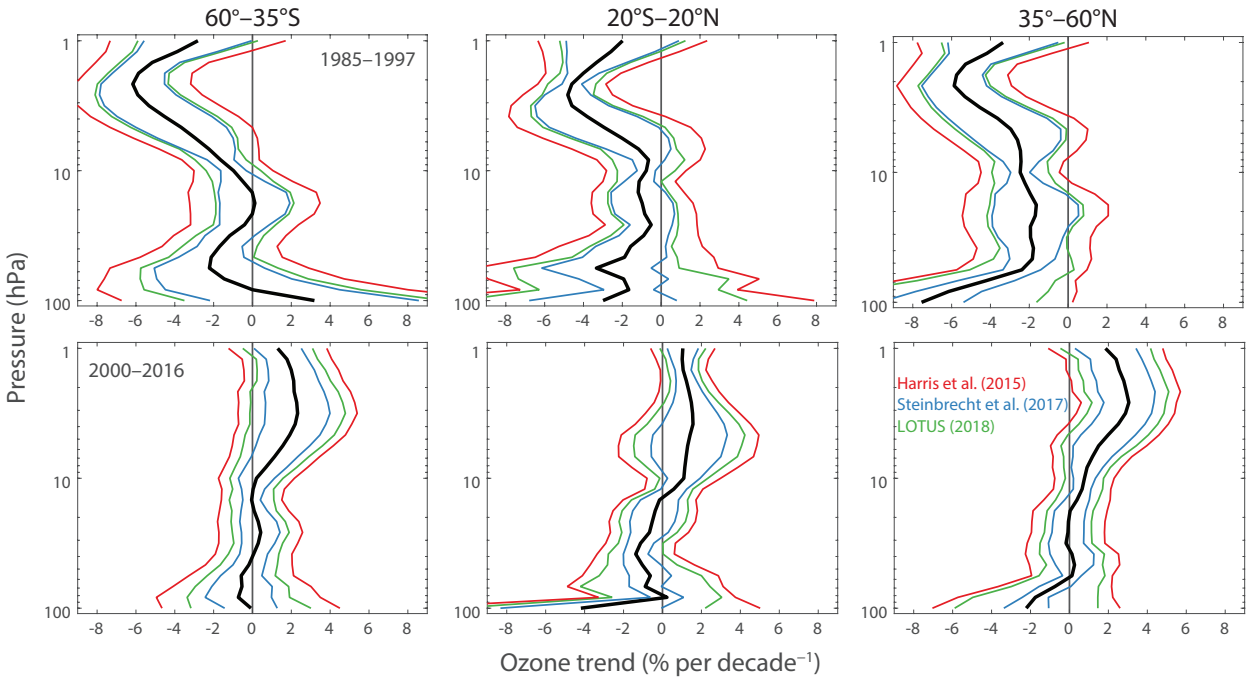

Figure 3-20. Combined trends of six satellite data records with 2σ uncertainties for the pre-1997 period (*top row*) and the post-2000 period (*bottom row*) from the LOTUS analysis for three latitude bands 35°–60°S (*left column*), 20°S–20°N (*center column*) and 35°–60°N (*right column*). Central trend estimates are identical for all methods (black lines). Green lines represent uncertainties calculated using the LOTUS method (Equation 5.1 in LOTUS, 2018); Blue lines represent the method of Steinbrecht et al. (2017) with the number of independent datasets estimated as 2 for pre-1997 and 3 for post-2000 trends; and red lines represent the J-distribution method used by Harris et al. (2015). Results shown here for the latter two methods were obtained using formulae that were modified to use an unbiased estimator of sample variance. Adapted from LOTUS (2018).

ozone over the 1998–2016 period, it is not easy to assert the statistical significance of the trends because the uncertainties are very large there, as seen in **Figure 3-19**. In particular, the lower stratosphere is one of the most difficult regions for obtaining accurate satellite observations because of steep vertical gradients in various atmospheric parameters around the tropopause. Natural variability is also large in the lower stratosphere. In fact, in a 9-member ensemble of a free-running CCM, 1998–2016 trends in the lower stratosphere varied from −6% decade^{-1} to +6% decade^{-1} among the ensemble members (Stone et al., 2018). Furthermore, a recent study showed that lower-stratospheric ozone and the total ozone column both increased sharply from 2016 to 2017, reversing much of the apparent decline in recent years (Chipperfield et al., 2018). Using a chemistry-transport model, that study concluded that the observed changes in lower-stratospheric ozone have been dominated by dynamically driven variability and that there is no need to invoke the VSLS-driven ozone loss suggested by Ball et al. (2018) to explain them. Enhanced isentropic transport between the tropical and extratropical lower stratosphere from 1998 to 2016, particularly in the NH mid-latitudes, has been proposed as a mechanism for this dynamically driven decrease in ozone in the lower stratosphere (Wargan et al., 2018).

The tropospheric ozone trend and its role in total column changes require further investigation. OMI/MLS

is the only record of tropospheric ozone to show continuous, near-global, monotonic increases in tropospheric ozone since 2004 (Gaudel et al., 2018). Other OMI records based on profile retrievals show much smaller increases, and IASI measurements actually show a decline in tropospheric ozone since 2008. There is currently no consistent picture of changes in ozone throughout the troposphere over the past decade (**Figure 3-22**).

3.3.3 Impacts of Changes in Ozone-Depleting Substances and Greenhouse Gases on Ozone Trends

A comprehensive interpretation of observational records must be supported by chemistry–climate or chemistry-transport modeling. CCMI-1 modeled ozone profile trends are in excellent agreement with the observed trends (**Section 3.3.2.3**), except in the

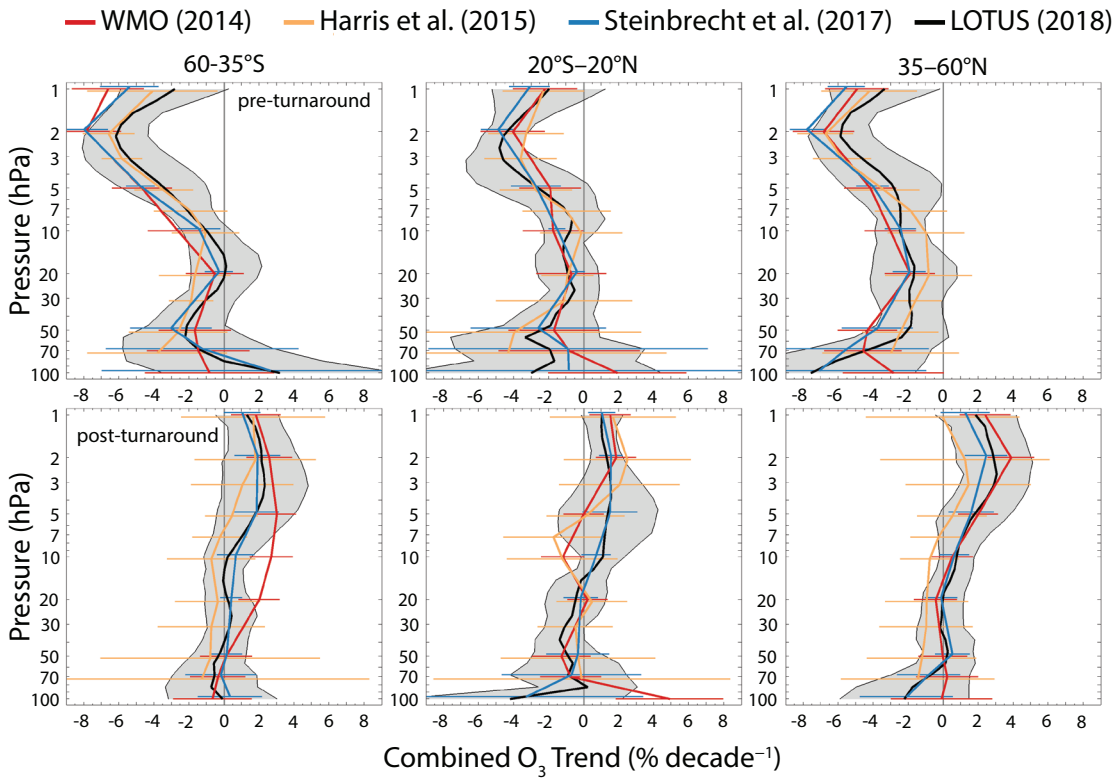

Figure 3-21. Ozone profile trends from WMO (2014), Harris et al. (2015), Steinbrecht et al. (2017), and LOTUS (2018) are shown in red, orange, blue, and black, respectively[1]. The top row shows trends before the turnaround of ODSs; the bottom row shows trends since the turnaround. Shaded areas and error bars represent the 95% confidence interval for the combined trend. Colored profiles are slightly offset on the vertical axis for display purposes. Steinbrecht et al. (2017) did not report or discuss pre-1997 trends but did calculate them and made them available for comparison here. Adapted from LOTUS (2018).

[1]Data included in the trends from each study are from the following periods:

	Pre-turnaround	**Post-turnaround**
WMO (2014)	May 1970 / Feb 1979 / Oct 1984–1997	Jan 2000–Dec 2013
Harris et al. (2015) (Sections 2.1 & 2.2)	Feb 1979 / Oct 1984–Dec 1997	Jan 1998–Dec 2012
Steinbrecht et al. (2017) (Table 3)	May 1970 / Feb 1979 / Oct 1984–Dec 1996	Jan 2000–Dec 2016
LOTUS (2018) (Table ES.1)	Jan 1985–Dec 1996	Jan 2000–Dec 2016

SH lowermost stratosphere during the period of ozone depletion (**Figure 3-23**). Idealized scenarios run by a subset of these models allow the attribution of ODS and GHG effects on ozone changes.

The evolution of stratospheric ozone in a changing climate depends on (in addition to ODS change): cooling of the stratosphere due to increases in GHGs; changes in transport (Brewer–Dobson circulation); and changes in ozone chemistry (N_2O/NO_x and CH_4/HO_x).

While past changes in stratospheric ozone were primarily due to anthropogenic emissions of ozone-depleting substances (ODSs), the evolution of stratospheric ozone in the 21st century will be controlled not only by the decline in ODSs but also, to a large extent, by the increase in greenhouse gases (GHGs) such as CO_2, CH_4, and N_2O. This section updates the attribution of past changes in ozone to changes in ODSs and GHGs, separated for the periods 1979–1996 and 2000–2016. This attribution is based on a multi-model analysis of simulations from CCMI-1 (**Figure 3-24**).

Figure 3-24 provides an update of the attribution of ozone trends due to ODS and GHG changes, based on output from the seven CCMI-1 models that performed all of the required simulations. In addition to the standard (REF-C2) model simulations including all forcings (ODSs and GHGs), a set of sensitivity simulations was run with either changes in ODSs only (i.e., with fixed GHGs) or with changes in GHGs only (i.e., with fixed ODSs). In the REF-C2 simulations, ODS and GHG concentrations follow the RCP-6.0 scenario, consistent with observed concentrations before 2005. Sea surface temperatures were either prescribed from an offline model simulation, which was performed using either the same model or a different model, or they were internally calculated via a coupled ocean model (Morgenstern et al., 2017). Trends were calculated as independent linear trends (ILTs) consistent with observed trends, using proxies derived from the variability in each model for QBO, ENSO, solar cycle, and aerosol optical depth.

In line with previous results, this analysis shows that negative ozone trends over the period 1979–1996 are primarily due to the increase in ODS concentrations. Model simulations with fixed ODSs exhibit small, statistically insignificant trends, except in the tropical lower stratosphere. In this region, the simulations indicate that the 1979–1996 ozone decrease may mostly

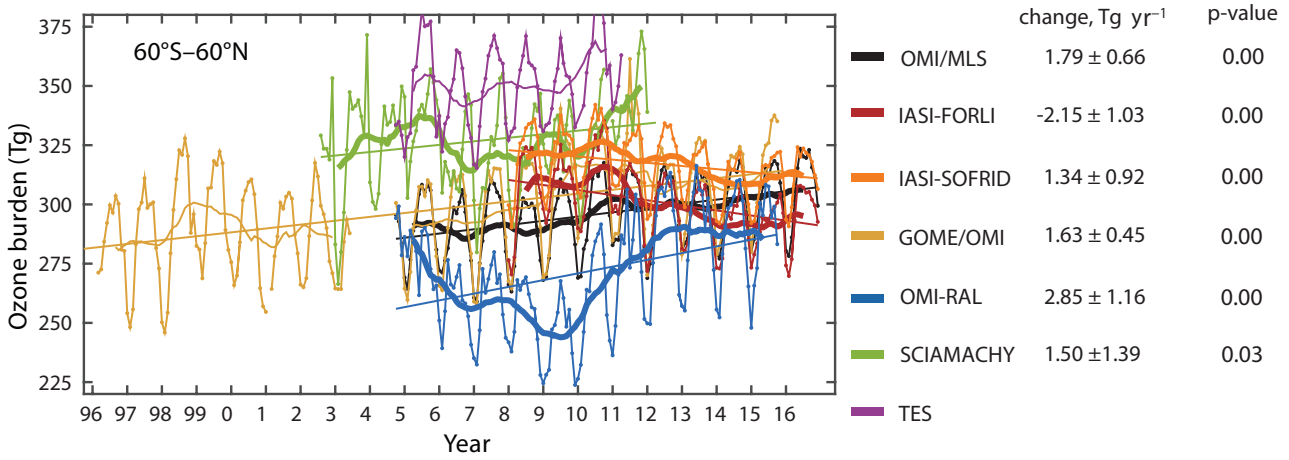

Figure 3-22. Time series of the tropospheric ozone burden, calculated from measured tropospheric ozone columns for seven satellite records. All instruments are nadir-viewing and have differing vertical sensitivities. The black line is the OMI/MLS tropospheric ozone residual product; the dark red and orange lines are IASI retrievals using the Fast Optimal Retrievals on Layers (FORLI) and SOftware for a Fast Retrieval (SOFRID) algorithms; respectively; the blue line is the OMI optimal estimation retrieval from Rutherford Appleton Laboratories (RAL); and the gold line is a combined GOME and OMI time series from Smithsonian Astrophysical Observatory. The green and purple lines are standard products from SCIAMACHY and TES, respectively. See Gaudel et al. (2018) and references therein. Adapted from Gaudel et al. (2018).

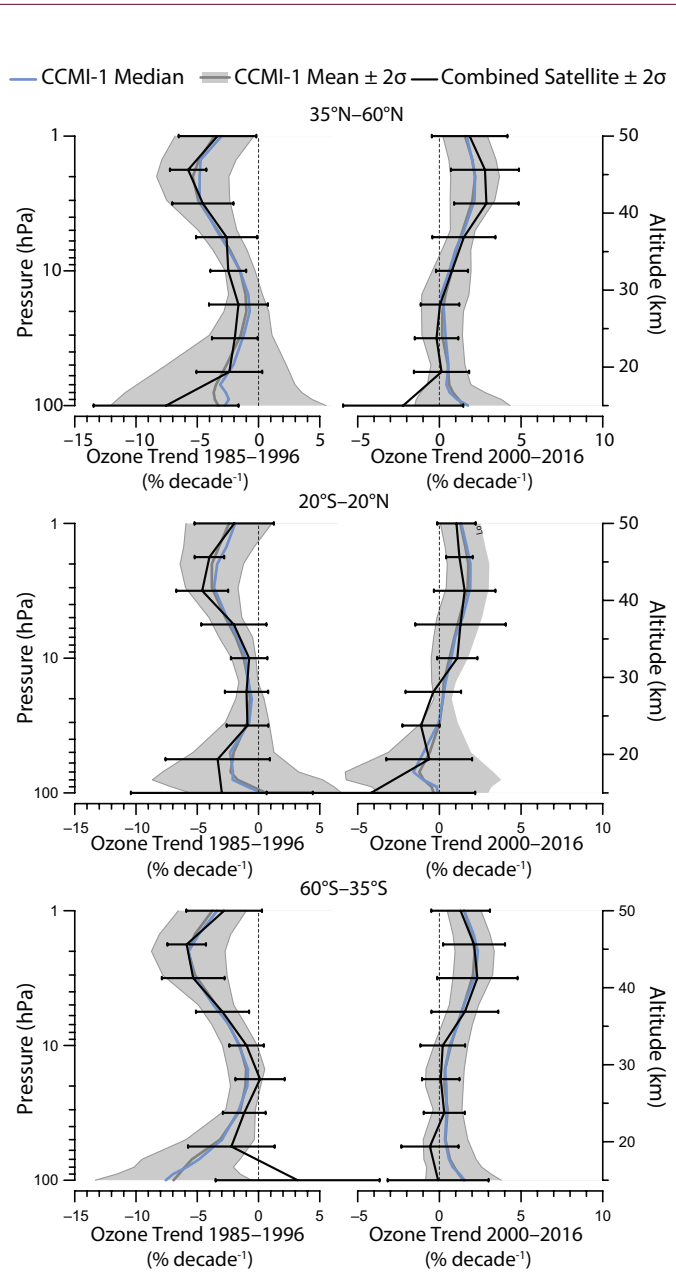

Figure 3-23. Measured and modeled ozone trends for the NH mid-latitudes (*top row*), tropics (*middle row*), and SH mid-latitudes (*bottom row*) for the pre-1997 (*left column*) and post-2000 (*right column*) periods. The black line is the combined satellite-based ozone trend from LOTUS, with 2σ uncertainties, the blue line is the median model, and the gray line is the multi-model mean. The gray envelope shows the 2σ variance of the models. CCMI-1 REF-C2 simulations are shown.

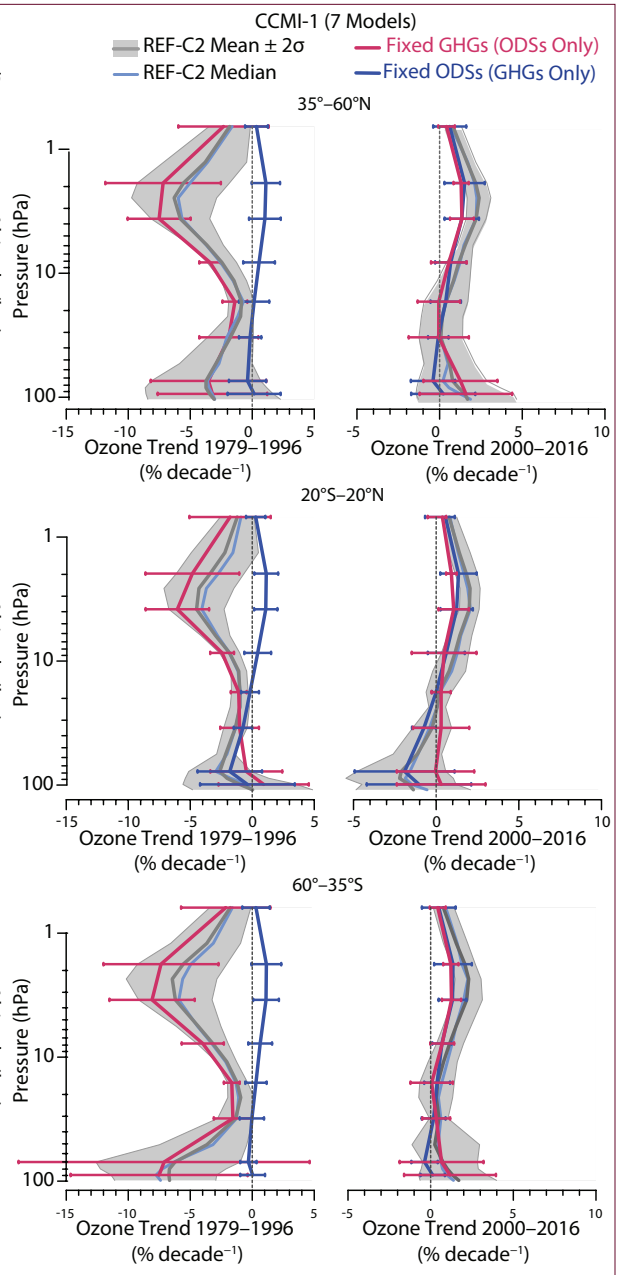

Figure 3-24. Attribution of stratospheric ozone profile trends for 1979–1996 (*left column*) and 2000–2016 (*right column*) due to ODSs and GHGs based on CCMI-1 model simulations. The top row shows the trends for NH mid-latitudes (35°–60°N); the middle row, for the tropics (20°N–20°S); and the bottom row, for SH mid-latitudes (60°–35°S). The gray lines show the multi-model mean of seven REF-C2 simulations including all forcings, with the shading indicating the 2σ range. The light blue lines show the median for all forcings. The red and blue lines represent the median trends due to ODSs only (i.e., with fixed GHGs) and due to GHGs only (i.e., with fixed ODSs), respectively. The same subset of seven models are used in all cases. Adapted from LOTUS (2018).

be due to an increase in GHGs. However, uncertainties in the lower stratosphere are large, as expressed by the relatively large spread in model results. Positive ozone trends in the lower stratosphere over the 2000–2016 period in the mid-latitudes of both hemispheres are consistent with the decline in ODSs, as the all-forcing REF-C2 simulations show positive ozone trends in this region similar to the ODS-only simulations.

In the upper stratosphere, ODS and GHG changes both contribute more or less equally to the positive ozone trends over the 2000–2016 period, again largely in agreement with previous results. The GHG-induced ozone increase in the upper stratosphere is primarily a result of cooling associated with GHGs, which reduces catalytic ozone loss rates. Furthermore, these simulations confirm previous findings that in the upper stratosphere, the effects of declining ODSs and increasing GHGs add approximately linearly.

3.3.3.1 Effects of Very Short-Lived Substances

Halogens from very short-lived substances (VSLSs; i.e., from halogenated ozone-depleting substances with lifetimes shorter than a few months) may contribute to ozone trends, in particular in the lowermost stratosphere, even when the concentrations of VSLSs themselves exhibit no trend (e.g., Dvortsov et al., 1999; Salawitch et al., 2005; Sinnhuber et al., 2009). They do so by providing additional chemical reaction partners for bromine and chlorine from anthropogenic long-lived source gases. One study described simulations with the chemistry–climate model EMAC over the timeframe 1960–2005 with and without the inclusion of brominated VSLSs (Sinnhuber and Meul, 2015). It found that a constant contribution of brominated VSLSs, producing about 6 ppt of additional bromine, led to column ozone changes in better agreement with observations and a stronger negative ozone trend in the mid-latitude lowermost stratosphere for the 1979–1995 period. The study also found a stronger positive trend for the 1996–2005 period, but the considered time period was too short for a robust estimate of the effect on ozone trends. The largest effect of brominated VSLSs on ozone was found for polar winter–spring ozone loss in the lower stratosphere and, in particular, the Antarctic ozone hole (**Chapter 4, Sections 4.3.3** and **4.5.3.4**).

Model calculations show that column ozone is reduced by about 1% at low latitudes and about 5% at high latitudes relative to a model simulation without VSLSs when best estimates for the present-day stratospheric loading of brominated and chlorinated VSLSs are used (**Figure 3-25;** Hossaini et al., 2015). The largest ozone reductions due to VSLSs occur in the lowermost stratosphere below 20-km altitude, where present-day ozone reductions due to VSLSs could be almost half as large as the ozone depletion due to long-lived ODSs, depending on the assumed VSLS scenario (**Figure 3-25**). Although the effectiveness of VSLSs to deplete ozone depends on the anthropogenic halogen loading, VSLSs have contributed to the lower-stratospheric ozone decrease since preindustrial times. Lower-stratospheric ozone changes due to the presence of brominated VSLSs have resulted in an estimated radiative forcing of about 0.02 W m^{-2} since the preindustrial period (Hossaini et al., 2015).

Brominated VSLSs are emitted primarily from biogenic oceanic sources (such as phytoplankton and seaweed) and contribute significantly to the current stratospheric bromine loading (see **Chapter 1**); in contrast, chlorinated VSLSs are emitted primarily from anthropogenic sources (although there are also significant natural sources of methyl chloride) and currently contribute little to stratospheric chlorine loading. However, some of the chlorinated VSLSs, and in particular CH_2Cl_2, have shown relatively large increases in recent years (Hossaini et al., 2015; Hossaini et al., 2017; Oram et al., 2017). The impact of anthropogenic chlorinated VSLSs on past ozone trends is still small (Hossaini et al., 2015), but may become important in the future if the observed increase in emissions of CH_2Cl_2 continues (Hossaini et al., 2017).

All CCMI-1 models now include additional bromine from VSLSs (Morgenstern et al., 2017). Two studies have investigated the impact of VSLSs on ozone recovery in chemistry–climate model simulations, with a focus on polar ozone, where the effects are largest (Oman et al., 2016; Fernandez et al., 2017; see **Chapter 4, Section 4.5.3.4**).

3.3.3.2 Tropical Ozone Changes

Past Assessments (WMO, 2011; WMO, 2014) have reported observed negative ozone trends in the tropical lower stratosphere, in overall agreement with available chemistry–climate model simulations. Modeled changes in tropical stratospheric ozone columns using the CMAM chemistry–climate model over the

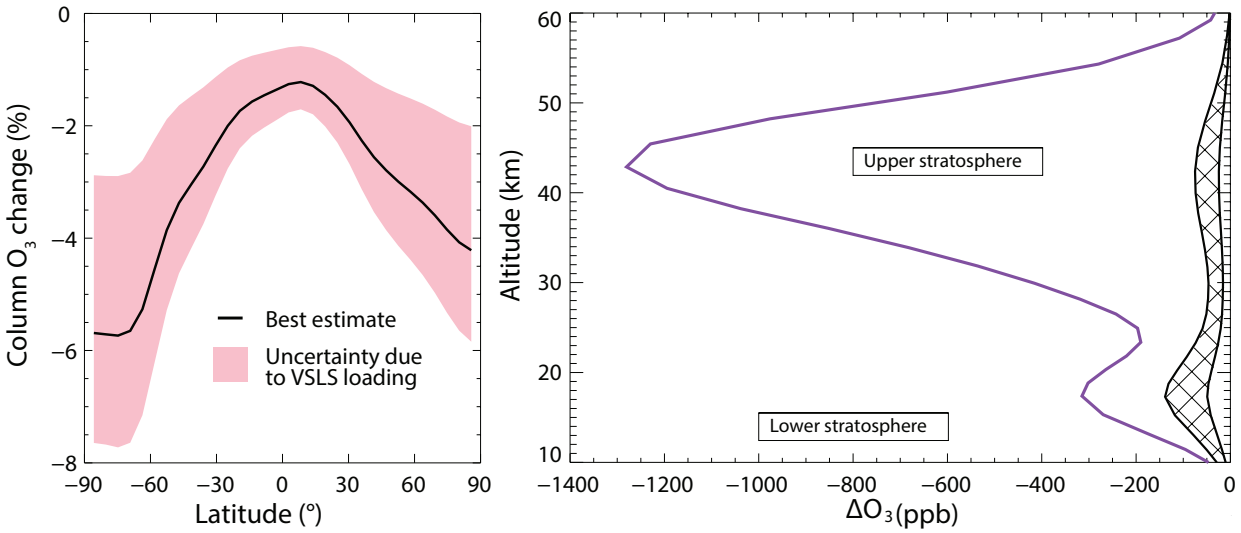

Figure 3-25. Effect of VSLSs on present-day (2011) ozone columns (calculated as the difference between simulations with and without VSLSs) as a function of latitude (*left*), and the impact of ODSs (purple) and VSLSs (black) on global mean ozone profiles (*right*). Shading indicates the range of current estimates of the contribution of VSLSs to stratospheric bromine. Adapted from Hossaini et al. (2015).

1960–2010 period are broadly consistent with satellite observations based on LIMS, SAGE I and II, and MIPAS, although the modeled decrease in tropical ozone is smaller than that deduced from SAGE II (Shepherd et al., 2014). The model shows a decrease of tropical (25°S–25°N) stratospheric ozone of 5.2 ± 1.7 DU between the 1964–1978 and 1996–2002 periods, with the largest decrease in tropical stratospheric ozone before 1990 and little change since the mid-1990s. This is consistent with results presented in this Assessment and with the analysis in the last Assessment (WMO, 2014); while both model simulations and observations show negative trends in the tropical lower stratosphere since 2000 (**Figure 3-23**), these trends are not significant except at 30–50 hPa in the SBUV MOD dataset. In CMAM, the 1990s decrease in stratospheric ozone is partly compensated by a modeled increase in tropical tropospheric ozone of 2.9 ± 0.7 DU over the same period (Shepard et al., 2014). The modeled decrease in stratospheric ozone can be largely attributed to the increase in ODSs; a model simulation with constant ODSs shows only a small and insignificant decrease in the tropical stratospheric ozone column of 0.3 ± 1.8 DU between the 1964–1978 average and the 1996–2002 average.

Another study similarly demonstrated that observed variations in tropical lower-stratospheric ozone are captured by a chemistry-transport model driven with meteorological reanalysis fields (Aschmann et al., 2014). The lack of ozone decline after the mid-1990s was explained by changes in not only the strength but also the location of the tropical upwelling region. This argument, that structural changes in upwelling are responsible for changes in tropical ozone trends, is supported by another analysis using satellite observations (Stiller et al., 2017). MIPAS measurements indicate a southward shift of up to 5 degrees in the lower- to middle-stratospheric upwelling region during the period 2002–2012. This shift also appears to explain observed hemispheric asymmetries in trends in other long-lived trace gases (Stiller et al., 2017).

Separating chemical- and transport-related effects (in particular ozone reductions due to an increase in tropical upwelling; **Chapter 5, Section 5.3.2**) is not trivial, as recent papers (Oberländer-Hayn et al., 2015; Polvani et al., 2017) have emphasized that ODS changes may have had a significant or even dominant impact on changes in tropical upwelling, thus leading to the observed decreases in tropical lower-stratospheric ozone. One study used a set of simulations from the

GEOSCCM with small ensembles of single forcings and concluded that dynamical responses to ODSs are the main driver for past changes in tropical upwelling (Polvani et al., 2017). It suggests that the mechanism of such a response may relate to changes in the thermal structure of the lower stratosphere caused by polar ozone depletion, which could alter the propagation and dissipation of planetary-scale waves. Another study, based on simulations with the EMAC chemistry–climate model, finds that ODSs contributed about equally with other GHGs to past changes in tropical lower-stratospheric upwelling (Oberländer-Hayn et al., 2015).

3.4 PROJECTED OZONE CHANGES

Models have always been tools to test process understanding and to project possible future developments. **Box 3-2** summarizes the evolution of models used in Ozone Assessments since 2002 and introduces the model runs used in this Assessment.

Box 3-2. Modelling past and future changes in ozone: Model heritage and application

Modelling in support of the Ozone Assessments has a long tradition. For example, the 2002 Assessment used a selection of early 3-dimensional (3-D) Chemistry-Climate Models (CCMs) to assess polar ozone changes. However, a large amount of information, in particular in the global ozone chapter, was derived from 2-dimensional (2-D) models. In the 2006 Assessment, 3-D Chemistry Transport Models (CTMs) were extensively used to discuss past ozone changes and were complemented with 3-D CCMs. The projected changes for the 21st century were extensively discussed in a separate chapter that used 2-D models and (very extensively) 3-D CCM results, largely emerging from the CCMVal (CCM Validation) activity. The model results were used to characterize future changes in ozone, including the return dates. The 3-D CCM modelling results for the 2010 Assessment were produced in the context of a comprehensive model evaluation in the framework CCMVal-2 (SPARC, 2010). A summary of the participating models can be found in Morgenstern et al. (2010). In the 2014 Assessment, results from this exercise were also used and complemented with results from newer publication. Prior to the 2014 report the CCMVal activity was superseded by the Chemistry-Climate Modelling Initiative (CCMI), which has a wider remit than CCMVal.

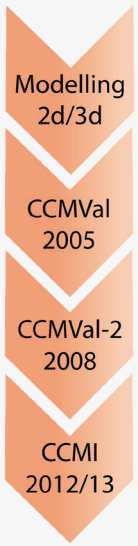

Earlier versions of most models contributing to CCMI in the context of stratospheric ozone variability and trends were evaluated in CCMVal-2. As can be expected, some models have been changed more than others; however their fidelity is always assessed by modelling the recent past. A summary of relevant models and their configurations can be found in Morgenstern et al. (2017). Generally, there is a trend to higher spatial resolution, more processes and the option to run more models with interactive ocean and sea-ice coupling. In previous CCM projections there was a clearer disjoint between model configurations used for CCMVal and model configurations used for CMIP (Coupled Model Intercomparison Project). Often, when projecting ozone changes, CCMs prescribed the future sea-surface temperatures and sea-ice coverage from their nearest CMIP relative. The CMIP model would be run without chemistry (prescribing ozone – perhaps from CCM integrations – in the radiation), but with an interactive ocean and sea-ice. This circularity can now be overcome by running atmosphere-ocean CCMs consistently. However, it is important to remember that the ozone projection will rely in both cases on the chosen climate change scenario (see table below and Meinshausen et al., 2011 for the definition of the RCPs).

Other model changes relate to the complexity of the chemistry (more emitted species, more reactions in the troposphere) and to a better understanding of the halogen budget, including the role of VSLSs. The impact of concentration and flux boundary conditions on lifetimes of halogen-containing species was evaluated in the SPARC Report No. 6 using a subset of CCMs from CCMVal-2/CCMI.

Box 3-2, continued.

Name of Simulation	Type of Simulation	Purpose	Features
REF-C1	Hindcast simulation of the period 1960–2010	To produce realistic simulations of the past atmospheric state	GHG*, ODS*, background and volcanic aerosol, solar variability, ozone and aerosol precursors, SST*, SIC*, VSLSs* are prescribed from observations
REF-C1SD	Hindcast simulation of the period 1980–2010	Same as REF-C1, but with the CCM dynamics nudged to observed meteorology	Same as in REF-C1; SSTs and SIC are consistent with meteorological reanalyses
REF-C2	Consistent simulation from the past into the future for the period 1960–2100	To produce best estimates of the future ozone and climate changes under specific assumptions of GHG and ODS evolution	Observations until 2005; then prescribed future scenarios for GHG and ozone/aerosol precursors (medium RCP6.0), ODS (WMO, 2011), background aerosol, projected solar variability, VSLSs; SST and SIC modeled
SEN-C2-RCP2.6	Same as in REF-C2 but for the period 2000–2100	To assess the future evolution of ozone and climate change under GHG scenarios other than RCP6.0	Same as in REF-C2, but GHG and ozone/aerosol precursors according to RCP2.6 scenario; SST and SIC consistent with RCP2.6 scenario
SEN-C2-RCP4.5	Same as in REF-C2 but for the period 2000–2100	To assess the future evolution of ozone and climate change under GHG scenarios other than RCP6.0	Same as in REF-C2, but GHG and ozone/aerosol precursors according to RCP4.5 scenario; SST and SIC consistent with RCP4.5 scenario
SEN-C2-RCP8.5	Same as in REF-C2 but for the period 2000–2100	To assess the future evolution of ozone and climate change under GHG scenarios other than RCP6.0	Same as in REF-C2, but GHG and ozone/aerosol precursors according to RCP8.5 scenario; SST and SIC consistent with RCP8.5 scenario
SEN-C2-fODS	Same as in REF-C2 for the period 1960-2100	To assess the effect of halogens on stratospheric ozone and climate change in the presence of climate change	Same as in REF-C2, but with halogens (ODS) fixed at 1960 levels
SEN-C2-fGHG	Same as in REF-C2 for the period 1960–2100	To assess the impact of halogens on the atmosphere in the absence of climate change	Same as in REF-C2, but with GHG fixed at 1960 levels and 1955–1964 average values from REF-C2 for SST and SIC repeating each year

*GHG: Greenhouse gases; ODS: Ozone depleting substances; SST: Sea surface temperature; SIC: Sea-ice concentration; VSLSs: Very short- lived halogenated substances

3.4.1 Expected Return to 1980 Levels and Ozone Recovery

One of the most critical roles that models play in the assessment process is to provide projections of the future evolution of ozone, with the return to 1980 values being a convenient definition of an ozone recovery milestone. Previous Assessments have discussed tropical and global annual mean total column ozone time series from individual models or multi-model means (see **Box 3-2** for a timeline of modeling and current experimental setups). In the last two Assessments, the results of the CCMVal-2 initiative have been utilized. Here, we provide an update using recent integrations from CCMI-1. The increased availability of simulations from models and ensemble integrations within CCMI-1 provides a new resource for assessing past and future ozone changes. However, the ability to discern the robustness of ozone return dates is limited by the newness of the results and the resulting lack of comprehensive validation across models.

Figure 3-26 presents the modeled total column ozone time series from 1960 to 2100 from bias-adjusted CCMI-1 multi-model means for the tropical belt and for global annual means. To provide a measure of the spread that is realistic but not overly influenced by outliers, the envelope is calculated from models that fall within 1σ of the multi-model mean (denoted MMM1S; see Dhomse et al., 2018 for details). The MMM1S return dates are generally found to be consistent with those derived from the median model (Dhomse et al., 2018).

The most appropriate (based on the chosen boundary conditions) free-running model representation of past total ozone is REF-C1 (blue lines in **Figure 3-26**). REF-C1SD (green lines) should be an even more accurate representation, as the individual models' circulation and thermal structure are relaxed toward analyzed values, thus providing extra information about "realistic" temporal changes to the models. Theoretically, REF-C1SD should provide the best representation of observed ozone anomalies (in particular the timing of low/high ozone events). However, there are large differences among models in how the specified dynamics were implemented. REF-C1 is still able to capture the long-term variability as imposed by the boundary conditions, but it does not accurately capture extremes or particular events. By construction, REF-C2 (red lines in **Figure 3-26**) should be similar to REF-C1 for the past. However, the boundary conditions are extended into the future following the RCP-6.0 scenario in REF-C2, allowing the identification of possible return thresholds in total ozone. A common point of reference is the occurrence of ozone values at 1980 levels (indicated by the horizontal dashed lines in **Figure 3-26**). For a more detailed discussion of the use of return dates, see **Box 3-3** on "Ozone return dates".

Figure 3-27 provides a comparison of the 1980 total column ozone return dates from the last Assessment (WMO, 2014) with the corresponding MMM1S results from CCMI-1 (Dhomse et al., 2018) (see also details in **Box 3-3**). Many of the 20 CCMs analyzed provided ensemble integrations of the REF-C2 scenario; if only a single model integration was available, then a 3-year boxcar smoothing algorithm was applied before ensemble mean model output and individual integrations were brought together (Dhomse et al., 2018). Due to the large number of model realizations that are combined to derive the multi-model mean, internal variability contributes only a small amount to the uncertainty in return dates (indicated by range bars in **Fig. 3-27**). However, when determining whether the 1980s total ozone threshold has been met with either measurements or output from an individual model, the year-to-year variability of ozone due to internal atmospheric variability must be considered (e.g., Keeble et al., 2018). The multi-model median return dates are in good agreement with the MMM1S results, demonstrating the robustness of the analysis, but they have larger uncertainties (Dhomse et al., 2018). The MMM1S return year is used in this Assessment because it is a more comparable metric to the analysis in the last Assessment than the median return year.

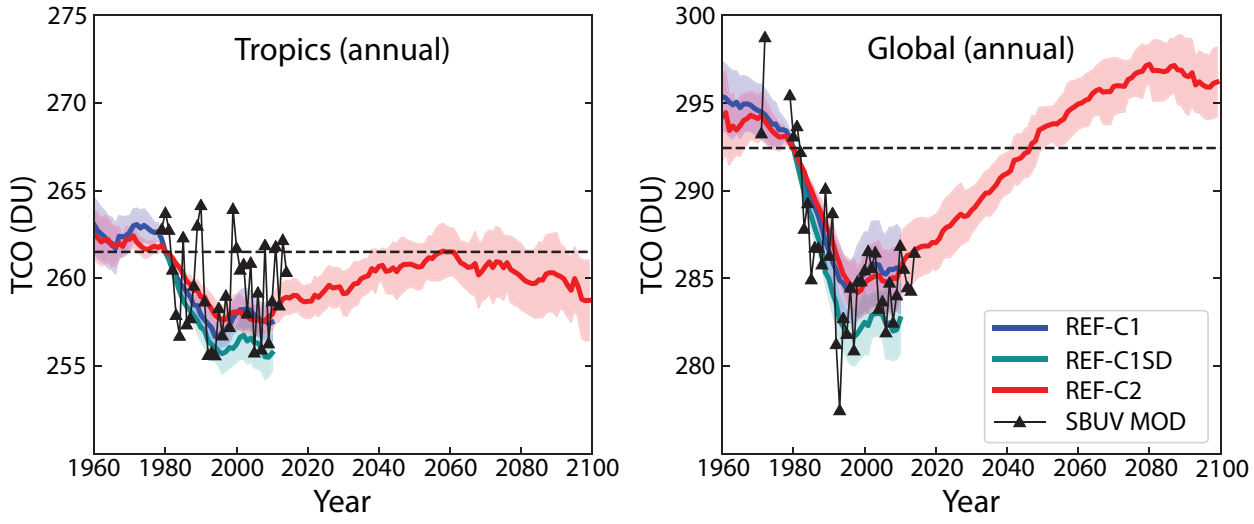

Figure 3-26. Adjusted and smoothed multi-model mean time series of annual mean tropical (*left*) and global (*right*) total column ozone (TCO) from CCMI models (colored lines) and from observations (solid black lines and symbols). Note that the multi-model mean uses a 1σ threshold (MMM1S) for filtering (for method see Dhomse et al., 2018, Figure 2, bottom). The dashed black lines represent 1980 values of TCO.

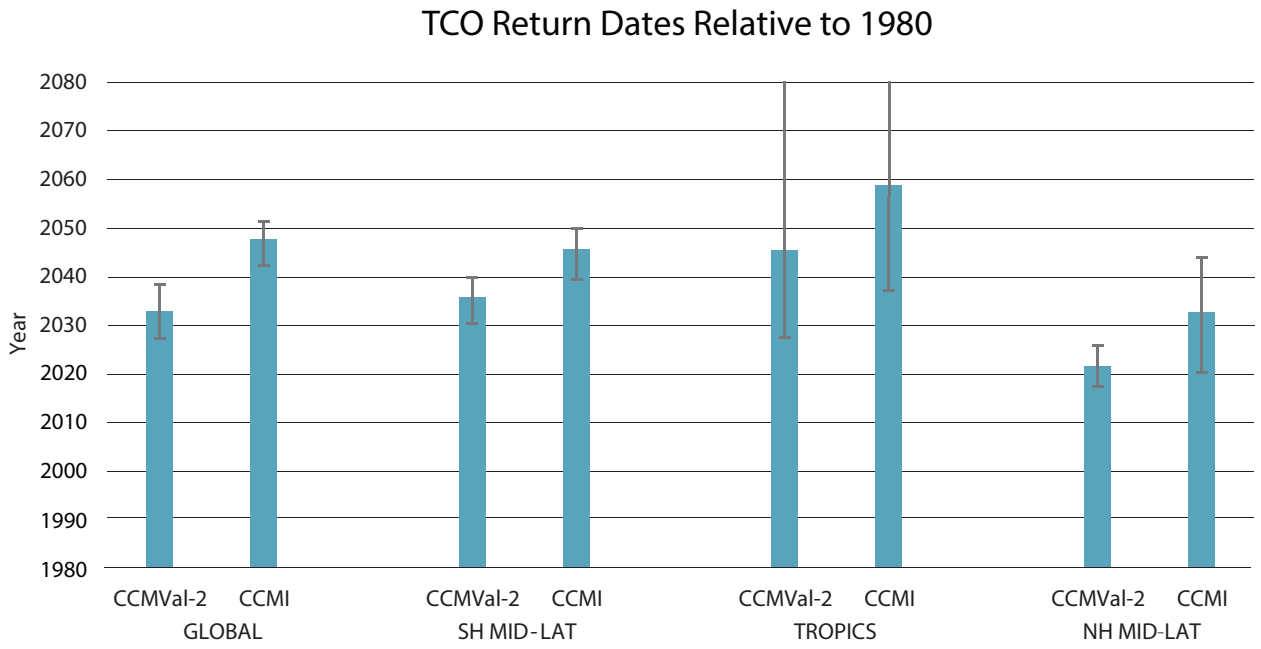

Figure 3-27. Bar chart comparing WMO (2014) projected 1980 return dates (labeled CCMVal-2) to this Assessment's CCMI-1 1980 return dates as analyzed from the multi-model mean (MMM1S) time series. The global mean refers to 90°S–90°N for WMO (2014) and to a near-global mean (60°S–60°N), consistent with the observations presented in this chapter) in the case of MMM1S. The true and near-global mean should be very similar (Dhomse et al., 2018). A comprehensive table with more details is provided by Dhomse et al. (2018).

The delay in return dates seen in this Assessment relative to the 2014 Assessment results primarily from different assumptions made in the scenarios (see **Box 3-3)**. The current best estimates for the range of years in which total ozone will return to 1980 values are 2042–2051 for the near-global mean, 2039–2050 for the SH mid-latitudes, and 2020–2044 for the NH mid-latitudes. The systematic delay of return years relative to the last Assessment (WMO, 2014) does not imply deficits in understanding, but rather reflects updates to prescribed scenarios describing the future evolution of GHGs (chosen to be in line with CMIP5) and ODSs. The extended range of return dates for the tropical belt reflects the fact that some models will not return to their 1980 ozone values in the projected time window given the competing effects of climate change (declining lower-stratospheric ozone) and declining ODSs (increasing ozone) in the tropics.

3.4.2 Effects of Future Stratospheric Temperature and Circulation Changes

As mentioned throughout this chapter, the evolution of stratospheric ozone in the 21st century will be controlled not only by the decline of ODSs but also, to a large extent, by changes in GHG concentrations, most importantly CO_2, CH_4, and N_2O. These GHGs affect stratospheric ozone through temperature and subsequent changes in dynamics and transport; CH_4 and N_2O also affect ozone chemistry (e.g., Butler et al., 2016), as discussed in more detail in **Section 3.4.3.2**. The impact of possible future GHG scenarios described by different Representative Concentration Pathways (RCPs) is discussed in **Section 3.4.3.1**.

The effects of GHG-induced temperature and circulation changes on ozone are compared to the effects of declining ODSs in **Figure 3-28,** which shows results from time-slice simulations with different forcings from the UM-UKCA chemistry–climate model

(Banerjee et al., 2016). The decrease in ODSs between the years 2000 and 2100 will lead to an ozone increase essentially everywhere in the atmosphere, with the largest percentage changes in the upper stratosphere at around 40 km and in the lower stratosphere at high latitudes, particularly in the Southern Hemisphere, where recovery of the Antarctic ozone hole is most notable. In contrast, changes in GHG concentrations will lead to a more complex pattern of ozone changes, with increases in the upper stratosphere at

Box 3-3. Ozone Return Dates

A critical role of Ozone Assessments is to provide years at which (column) ozone is expected to return to a particular, historic level – so-called return dates. This Assessment tabulates ozone return to 1980 values only. Here, we explain how return dates are computed and clarify why our current estimate for when global, total ozone will return to the 1980 level is systematically delayed relative to the 1980 return given in the prior two Assessments.

Comprehensive Chemistry-Climate Models (CCMs) project climate, and interactively calculate ozone, for prescribed future abundances of greenhouse gases (GHGs) and ozone depleting substances (ODSs). Three types of uncertainties must be considered for return date estimates: internal variability, structural uncertainty, and scenario uncertainty.

Internal Variability. CCMs exhibit internally-generated variability that impacts ozone (e.g., polar stratospheric warmings). If multiple runs from one model exist for the same climate scenario, these so-called ensembles are averaged together. If only one run is available, the model output is smoothed with respect to time, prior to being combined with results from other models. Due to the large number of runs and models that are combined to derive the multi-model mean, internal variability contributes only a small amount to the uncertainty of return dates.

Structural Uncertainty. CCMs represent processes, and their interactions, differently. This may lead to different return dates, for the same prescribed future levels of GHGs and ODSs. Several of the latest CCMs have interactive oceans and/or sea-ice modules, enlarging the degrees of freedom. In this and prior Assessments, structural uncertainty is quantified by examining output from many different models. While structural uncertainty is certainly important for quantifying the range of expected return years, the introduction of three additional CCMs for this Assessment is not responsible for the delay of the return dates relative to prior Assessments. Structural uncertainty is, however, the driving factor of lower and upper limits for the range of years given in **Table 3-4**.

Scenario Uncertainty. CCM projections use prescribed scenarios for future ODSs and GHGs. The return dates reported in WMO (2011) and WMO (2014) were based on ODSs from the baseline scenario of WMO (2007) with an adjustment for HCFCs and GHGs from the Special Report on Emissions Scenarios (SRES) A1b scenario developed in IPCC (2000). Here, we use ODSs from the baseline scenario of WMO (2011) and GHGs from the Representation Concentration Pathway (RCP) 6.0 scenario developed by Masui et al. (2011) for IPCC (2013). As illustrated below, differences in future specifications of CO_2, CH_4, and ODSs are the likely cause of the obvious delay in return of ozone to the 1980 value relative to the projections of the previous Assessments.

Most CCMs prescribe future abundances of GHGs and ODSs at the surface and compute the concentrations in the atmosphere as a function of time. Panels a) and b) on the next page show significant differences in the assumed evolution of CO_2 and CH_4 as used in model runs for the previous assessments (SRES A1b) and this assessment (RCP 6.0). Note that these differences in CO_2 and CH_4 have both direct and indirect

Box 3-3, continued.

consequences for the climate change impact on ozone. Panel c) shows effective equivalent stratospheric chlorine (EESC) that can be used as a proxy of how the halogen loading evolves within the CCMs. The approximately 5-year delay in EESC drawdown in the WMO (2011) baseline scenario used in this assessment relative to the previously-used scenario reflects new knowledge of lifetimes and emissions of various ODSs. This is another factor contributing to the overall delay in return dates.

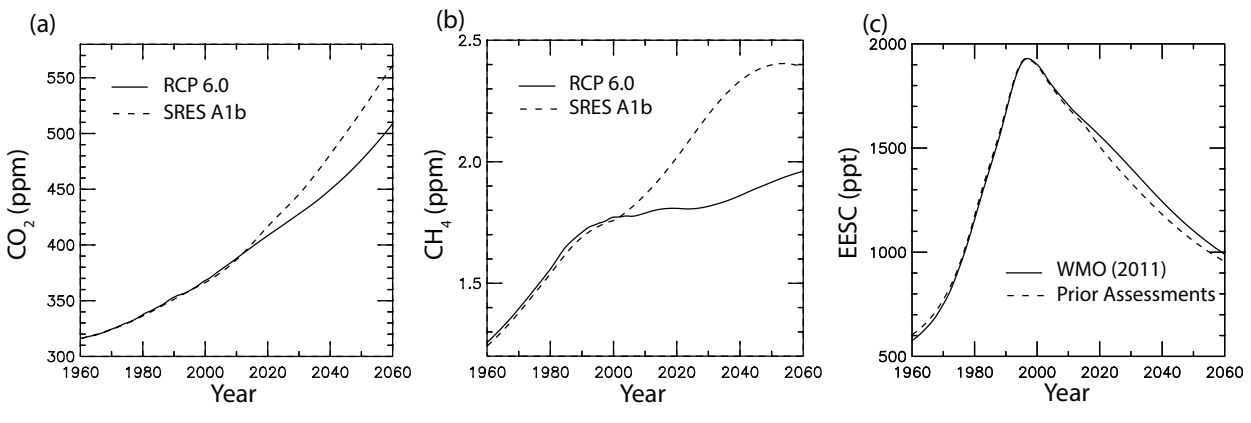

Time series of a) CO_2, b) CH_4, and c) equivalent effective stratospheric chlorine (EESC) used as boundary conditions for the CCM simulations analyzed for ozone return dates of this assessment (black solid) and of the prior two assessments (black dashed). For the baseline return dates of this assessment, future abundances of CO_2, CH_4, and all other GHGs are from the RCP 6.0 scenario developed for IPCC (2013) and ODS mixing ratios that drive EESC originate from WMO (2011). The prior two Assessments utilized time series of GHGs from the SRES A1b scenario and ODSs from WMO (2007) with an adjustment for HCFCs. The EESC curves in this figure were calculated for mid-latitude air with a lifetime of 3 years, using the Newman et al. (2007) release factors.

all latitudes, primarily due to GHG-induced cooling that slows down gas-phase ozone loss reactions. In the low-latitude lower stratosphere, however, ozone is projected to decrease due to changes in dynamics and transport, and, in particular, a strengthening of the BDC. This increase in the strength of the BDC is a robust finding in the CCMI-1 models, although there are still uncertainties in the magnitude (Morgenstern et al., 2018) and attribution of the strengthening (**Chapter 5, Section 5.3.2**). Lower-stratospheric ozone in middle to high latitudes may either increase or decrease, depending on the hemisphere and on the GHG scenario. In the more extreme RCP-8.5 scenario, the upper-stratospheric increase in ozone due to GHGs is larger than that due to ODS decline. In the tropical lower stratosphere, ozone changes due to BDC alteration that are potentially driven by GHG increases will dominate (see also **Section 3.4.3**).

A study diagnosing ozone sensitivity to varying GHGs and ODSs in CCMI-1 simulations finds varying degrees of consistency in the models' responses in ozone to individual forcings, including some considerable disagreement. It is suggested that some of these differences could be linked to circulation differences between the models (Morgenstern et al., 2018). The results in **Figure 3-28** (Banerjee et al., 2016) are therefore an illustration of principle and not a universally valid result.

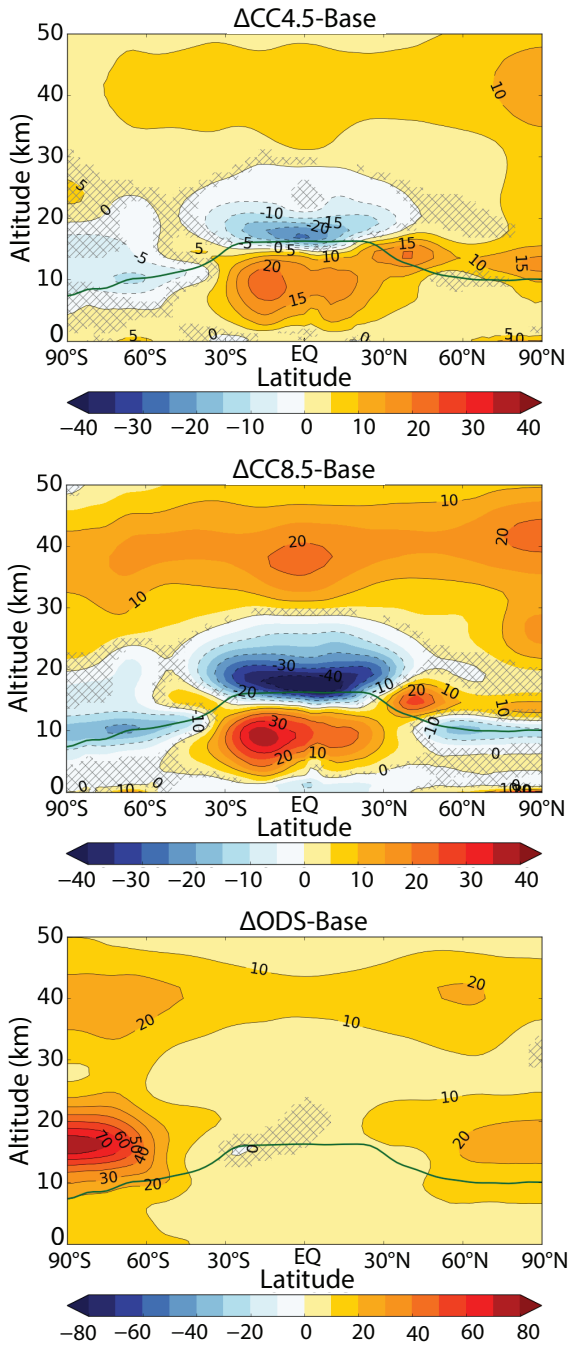

Figure 3-28. Modeled percent changes in annual mean ozone between 2000 and 2100 due to GHG changes according to RCP-4.5 (*top*) and RCP-8.5 (*middle*) and due to ODS changes (*bottom*). Shown are differences between a year-2000 baseline simulation with single forcing changes for year-2100 conditions: RCP-4.5 and RCP-8.5 assume year-2100 SST, sea-ice, and GHG concentrations with year-2000 ODS and ozone precursor emissions. From Banerjee et al. (2016).

3.4.3 Sensitivity to the Specification of Different Future Scenarios

3.4.3.1 Effects of Different Representative Concentration Pathways

A number of CCMI-1 models provide estimates of the sensitivity of ozone to changes in other traces gases using simulations with different scenarios. The different RCPs are GHG concentration trajectories first chosen for the Coupled Model Intercomparison Project Phase 5 (CMIP5) to span a range of corresponding radiative forcings by the year 2100 (see **Box 3-2**). While the standard reference simulations of CCMI-1 use the RCP-6.0 scenario, sensitivity simulations for RCP-2.6, RCP-4.0, and RCP-8.5 have also been carried out. **Figure 3-29** summarizes the evolution of total ozone columns for the different RCPs (Dhomse et al., 2018). For global mean total ozone columns, the return to 1980 values is faster and the possibility of super-recovery (i.e., the increase of ozone above historical levels) is higher for the RCPs with larger GHG increases. This effect is largest in mid-latitudes, where RCP-8.5 results in ozone increases of more than 20 DU above average 1980 levels at the end of the 21st century. RCP-4.5, in contrast, results in a return to 1980 global mean ozone columns in NH mid-latitudes by the middle of the 21st century and shows little change afterwards. Tropical ozone columns for the multi-model mean do not fully return to pre-1980 levels in any of the scenarios.

One study shows changes in tropical total column ozone for three altitude ranges (upper stratosphere, lower stratosphere, and troposphere) for three RCPs (4.5, 6.0, 8.5) from calculations with the chemistry–climate model EMAC (Meul et al., 2016; **Figure 3-30**). Upper-stratospheric ozone columns ($p<10$ hPa) recover to 1980 levels as early as ~2025 in all scenarios and show a super-recovery afterwards, with the largest super-recovery for RCP-8.5. In contrast, ozone columns in the lower stratosphere ($10\ \text{hPa} < p < 100\ \text{hPa}$) do not return to pre-1980 levels at all but continue to decrease, with the largest decrease for RCP-8.5. (These simulations show a small increase in tropical lower-stratospheric ozone columns between the late 1990s and around 2025, but it is not clear if this is significant.) Tropical total ozone columns also depend critically on the evolution of tropospheric partial column ozone, which is either decreasing or increasing in the future, depending on the RCP scenario (Igelsias-Suarez et al.,

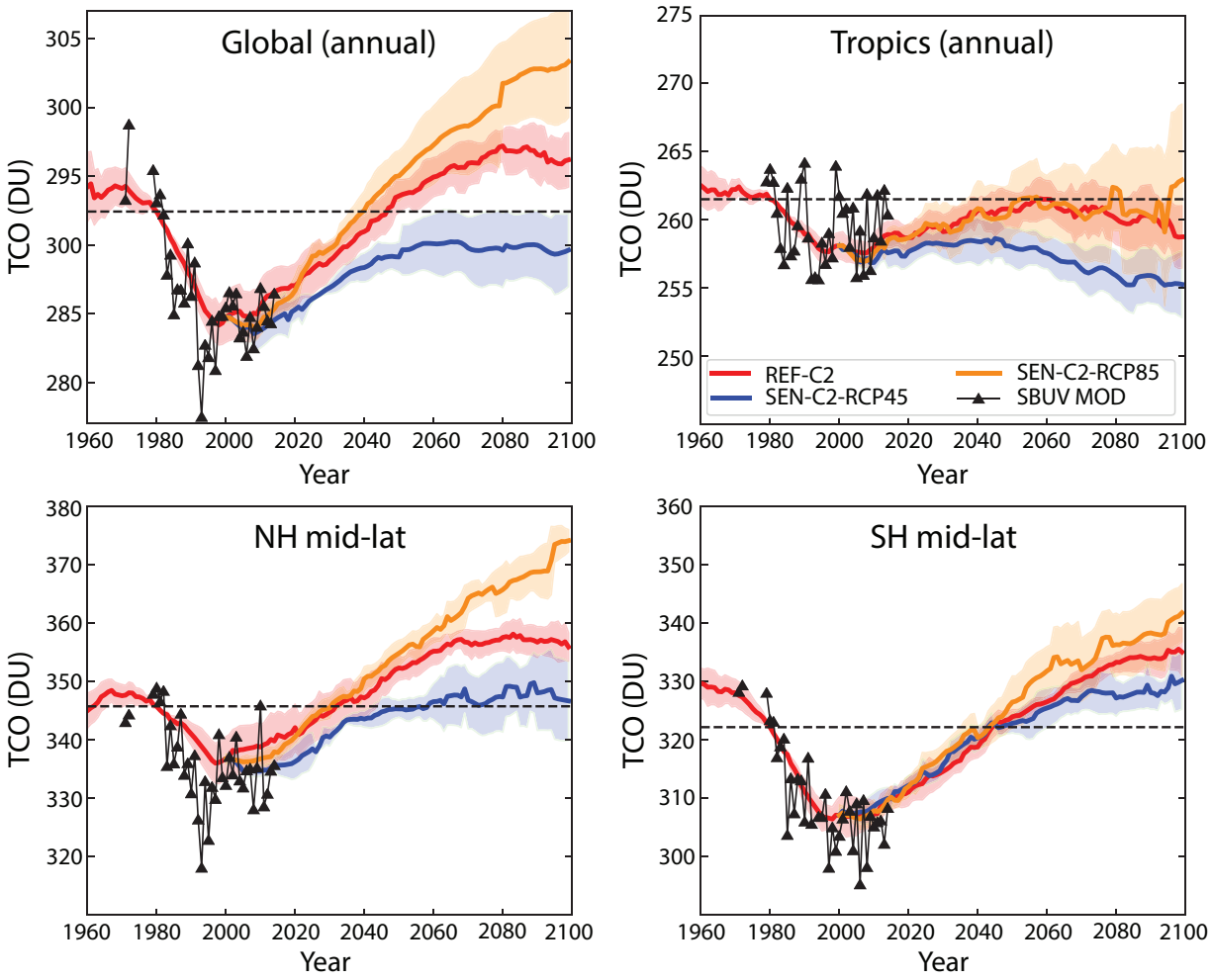

Figure 3-29. Adjusted and smoothed multi-model mean time series of annual mean TCO from observations (solid black lines and symbols) and for RCP scenarios from CCMI models: REF-C2=RCP-6.0 (red lines), SEN-C2-RCP45=RCP-4.5 (blue lines), and SEN-C2-RCP85=RCP-8.5 (orange lines). The black dashed lines represent 1980 values of TCO. From Dhomse et al. (2018).

2016; Meul et al., 2016). In most scenarios, tropical tropospheric ozone columns decrease during the second half of the 21st century, though there are large differences among models (**Section 3.4.4**). The exception is RCP-8.5, which shows a strong increase in tropical tropospheric ozone in most models due to a strong increase in methane. There is some cancelation between the projected upper-stratospheric increase in tropical ozone (e.g., due to GHG-induced cooling) and the projected decrease in lower-stratospheric ozone, but the overall effect on stratospheric ozone columns depends on the RCP scenario (Banerjee et al., 2016).

3.4.3.2 Influence of Nitrous Oxide and Methane

Methane (CH_4) and nitrous oxide (N_2O) affect stratospheric ozone not only through the temperature changes associated with their radiative forcing, but also through chemistry: N_2O is the main source of odd nitrogen (NO_y) in the stratosphere, while CH_4 is an important source for hydroxyl radicals (HO_x) but is also involved in chlorine deactivation into HCl. Currently, N_2O is the most important ODS emitted in terms of its Ozone Depletion Potential (ODP). However, the ODP metric was traditionally developed for long-lived halogen-containing ODSs. It uses CFC-11 as a reference gas, and it is not an optimal metric

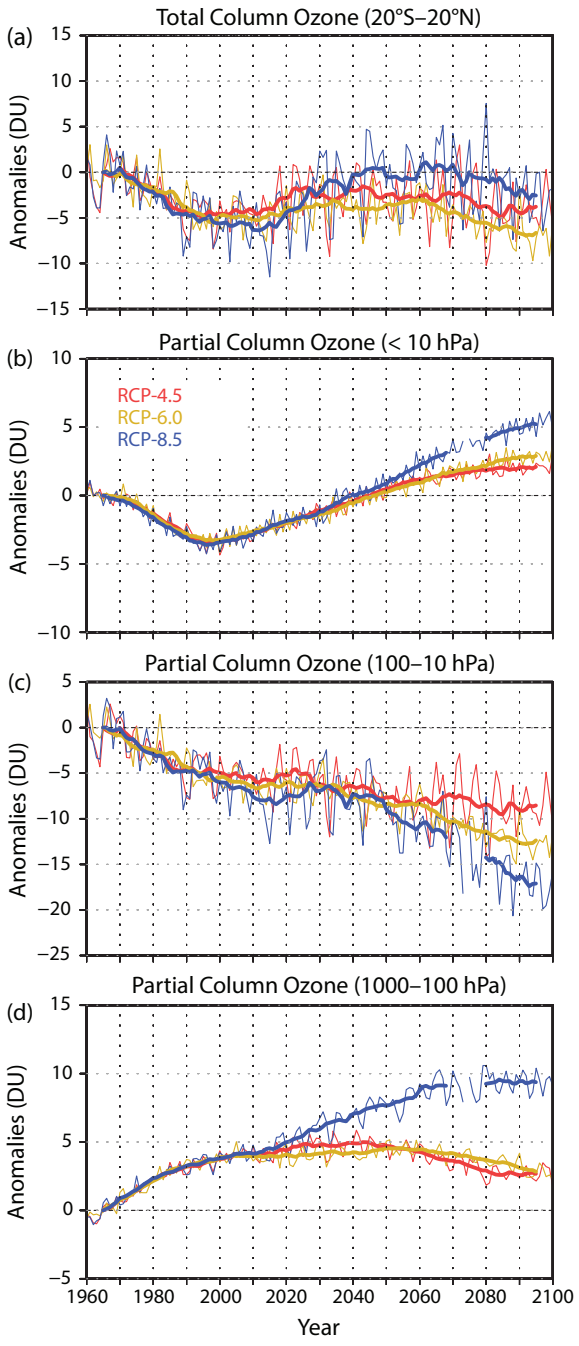

Figure 3-30. Past and projected tropical ozone for different RCPs: (a) total-column ozone, (b) upper-stratospheric partial column ozone, (c) lower-stratospheric partial column ozone, and (d) tropospheric partial column ozone. From Meul et al. (2016).

for assessing the impact of future N_2O emissions. Specifically, the ODP value for N_2O depends critically on the level of other GHGs and the degree of halogen loading. This sensitivity is due to the chemical interactions of NO_x with HO_x and ClO_x, as well as the temperature dependence of those interactions (Revell et al., 2015). The ODP of N_2O was calculated using the chemistry–climate model SOCOL (Revell et al., 2015) for year-2100 conditions under a range of different CH_4 and CO_2 concentrations (**Figure 3-31**). **Figure 3-31a** shows the calculated global mean total ozone column as a function of CO_2 and CH_4 global mean surface mixing ratios, with all other parameters held constant according to RCP-6.0. Global mean total ozone increases for increasing CO_2 and increasing CH_4 concentrations. Reductions in global mean total ozone relative to the modeled value for the year 2000 of 314 DU (white contour) are primarily due to reductions in tropospheric ozone columns resulting from reductions in ozone precursor emissions in the model scenarios (Revell et al., 2015). **Figure 3-31b** shows the calculated ODP of N_2O in the year 2100 as a function of CO_2 and CH_4. The ODP of N_2O for 2100 will, under essentially all conditions, be larger than the calculated value of 0.015 for the year 2000 because of interactions of NO_x chemistry with chlorine chemistry. Under high chlorine loading, increasing NO_x reduces ozone depletion by deactivating reactive chlorine. Higher CO_2 levels induce cooling of the stratosphere, which increases the chemical destruction of NO_x and reduces the efficiency of ozone destruction by N_2O (Stolarski et al., 2015). Higher levels of CH_4 also slow NO_x-driven ozone loss, but they lead to an increased ODP of N_2O. This is because increased CH_4 reduces the efficiency of CFC-11 at destroying ozone, and CFC-11 is used as a reference gas in the ODP concept (Revell et al., 2017).

One study analyzing the effect of N_2O and CH_4 changes on ozone from a range of CCMI-1 models shows that the global-average impact of N_2O increases on total column ozone is highly model-dependent (Morgenstern et al., 2017). Another analysis of simulations from the WACCM model with different N_2O and CH_4 scenarios concludes that extratropical total ozone could either remain weakly depleted or even

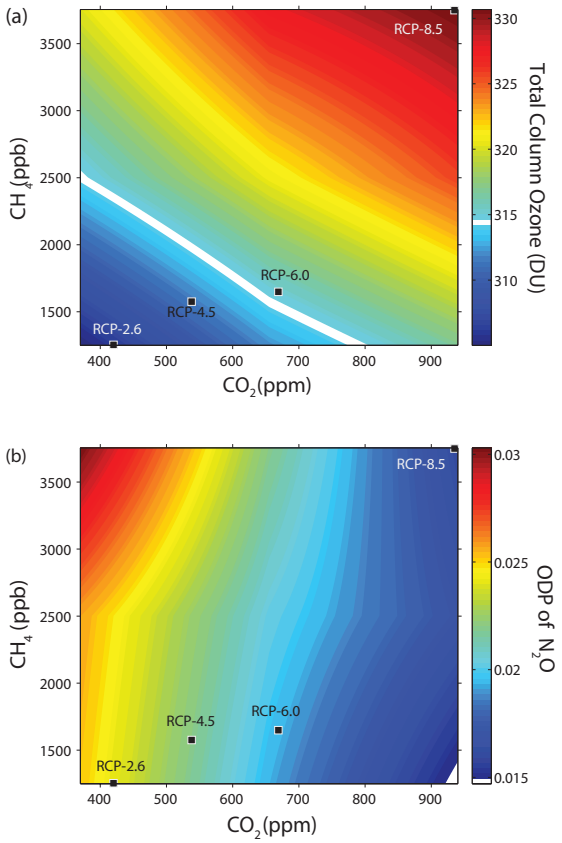

Figure 3-31. Effect of different abundances of CO_2 and CH_4 on (a) global mean total column ozone and on the (b) ODP of N_2O in 2100. Black squares indicate the CO_2 and CH_4 surface concentrations in 2100 for the various RCP scenarios. White contour lines show values of ozone (314 DU) and the ODP of N_2O (0.015) for year-2000 conditions. From Revell et al. (2015)

increase well above historical levels, depending on the CH_4 and N_2O scenario (Butler et al., 2016).

3.4.3.3 Sensitivity to Geoengineering/Solar Radiation Management

Deliberate increases in stratospheric aerosol loading to counter the effects of GHG-induced global warming have been discussed in recent years. This is often termed geoengineering or, more specifically, solar radiation management (SRM; see also **Chapter 6**). These schemes would impact stratospheric ozone in a number of ways: 1) through chemical effects of the increased aerosol loading, 2) through resulting changes in stratospheric temperature as well as changes in solar radiation and corresponding photolysis rates, both of which impact ozone chemistry, and 3) through resulting changes in stratospheric dynamics and transport. The most discussed and studied SRM schemes involve enhancement of stratospheric sulfate aerosols. **Chapter 6, Section 6.2.5** provides a detailed overview of the impact of deliberate climate interventions. A number of recent chemistry–climate modeling studies, including coordinated multi-model studies (GeoMIP, Kravitz et al., 2013), have been performed to study the impact of deliberate stratospheric sulfate aerosol enhancements on the ozone layer (e.g., Pitari et al., 2014). The effect on stratospheric ozone depends critically on the assumed stratospheric halogen loading; i.e., it will be different under a scenario where halogen loading is enhanced (e.g., for the middle of the 21st century) than under a scenario with little halogen loading (e.g., corresponding to the end of the 21st century). While much can be learned from the effects of enhanced sulfate aerosol loading following volcanic eruptions (see also **Chapter 5, Section 5.2.3**), the long-term effects of deliberate sulfate aerosol increases will be different from volcanic effects due to the different timescales involved (Pitari et al., 2014). In addition to their use in studying stratospheric chemistry perturbations taking place through the enhanced surface area density of the sulfuric acid aerosols, chemistry–climate models have been used to examine the impact on long-lived species transport due to the aerosol-driven surface cooling coupled to the stratospheric warming (Visioni et al., 2017). Perturbed concentrations of CH_4, N_2O, and other long-lived tracers would feed back on short-lived species that regulate stratospheric ozone depletion. Any significant reduction in stratospheric ozone associated with sulfate aerosol enhancement would further lead to decreases in tropospheric ozone through decreased stratosphere-to-troposphere transport (STT) of ozone and increased UV radiation (Xia et al., 2017).

More recent studies have explored strategic injections of sulfate aerosols into the stratosphere at locations other than the equator. One examination of a scenario in which injection at 15°N, 15°S and 30°N was steadily increased over the 21st century found that mean surface temperature and the equator-to-pole temperature gradients were kept near 2020 levels despite the strong climate forcing of the RCP-8.5 scenario (Richter et al., 2018). Polar column ozone

recovered to pre-ozone hole conditions by the end of the century but, in contrast to RCP-8.5, did not exceed pre-1980 levels. In the middle and high latitudes, ozone recovered and even exceeded RCP-8.5 values in some latitude bands and some months. Another study looked at differences between high- and low-altitude injections, assuming injection latitudes of 15°N and 15°S (Tilmes et al., 2018). Ozone destruction was less severe when sulfate aerosols were injected at 70 hPa rather than 30 hPa, and for middle and high latitudes, the low-altitude injections resulted in more column ozone than without geoengineering in winter.

A number of studies have also investigated the effect of solid particles for SRM schemes (e.g., Tang et al., 2014; Tang et al., 2016; Keith et al., 2016; Weisenstein et al., 2015). These highly refractive particles will lead to much less warming of the tropical lower stratosphere compared to sulfate aerosols (Keith et al., 2016). In particular salts of alkaline metals such as calcite ($CaCO_3$) have been proposed for SRM; these would have the side effect of chemically removing acids such as HCl or HNO_3 that are involved in ozone depletion. Model simulations have been used to investigate and compare the impact of proposed geoengineering schemes using sulfate, titania, and black carbon particles on the stratosphere (Jones et al., 2016). However, so far not enough information is available to assess how these proposed SRM schemes with solid aerosol particles will affect the evolution of stratospheric ozone under different GHG and ODS scenarios.

A recent chemistry–climate modeling study investigated the effect of solar radiation management schemes on stratospheric and surface ozone. It focused on the generic impact of SRM schemes; i.e., ozone changes due to the reduction in solar radiation, stratospheric temperature changes, and resulting changes in dynamics and transport (Nowack et al., 2016). In this study, the radiative forcing due to increased GHGs was balanced by a reduction in solar radiation at the top of the atmosphere without explicit treatment of stratospheric aerosol enhancements (an implementation colloquially termed space mirrors). This generic scheme thus shows some general aspects of SRM schemes without the particular chemical and radiative aspects that are specific to sulfate or other aerosol enhancements. The study shows that this generic SRM scheme would lead to strong enhancements in stratospheric ozone, with a calculated global total column increase of about 8% (Nowack et al., 2016). Because SRM schemes will not substantially reduce the upper-stratospheric cooling due to GHG increases, stratospheric ozone will strongly increase. In addition, reduced solar radiation under SRM would lead to further chemical ozone enhancement, according to this study. Increases in tropical upwelling (BDC) would be reduced with SRM, mediating the climate change-induced reduction in tropical lower-stratospheric ozone.

3.4.4 Impacts on Tropospheric Ozone

Both ozone recovery and the projected strengthening of the stratospheric circulation associated with GHG increases act to increase the downward transport of ozone from the stratosphere to the troposphere in the extratropics (e.g., Zeng and Pyle, 2003; Hegglin and Shepherd, 2009; Banerjee et al., 2016; see also **Chapter 5, Section 5.3.3**). The impact on tropospheric ozone is greatest in the upper troposphere (UT), where ozone's radiative effect is largest. Climate change has the largest impact in the subtropics, and ozone recovery primarily affects UT ozone in the extratropics (Banerjee et al., 2016). The net impacts of these processes, however, given concurrent changes in precursor emissions, temperature, and water vapor, are highly model- and scenario-dependent, as described below. **Figure 3-32** shows the sensitivity of ozone to ODSs and long-lived GHGs for seven CCMI-1 models (Morgenstern et al., 2018). There are sizable discrepancies among the models throughout the atmosphere, but these discrepancies are particularly large in the troposphere. A separate set of simulations showed a somewhat surprising sensitivity of tropospheric ozone to changes in N_2O; this sensitivity was dominated by chemical depletion of stratospheric ozone by N_2O (Morgenstern et al., 2018).

Using the UM-UKCA model under both RCP-4.5 and RCP-8.5 emissions scenarios in which the methane boundary condition was held constant, a recent study found that the projected increase in STT associated with climate change and ozone recovery offsets decreases in net chemical production associated with reductions in ozone precursor emissions (Banerjee et al., 2016), in agreement with earlier work (Sekiya and Sudo, 2014). Enhanced STT increases the global tropospheric lifetime of ozone (τ_{O3}) because it

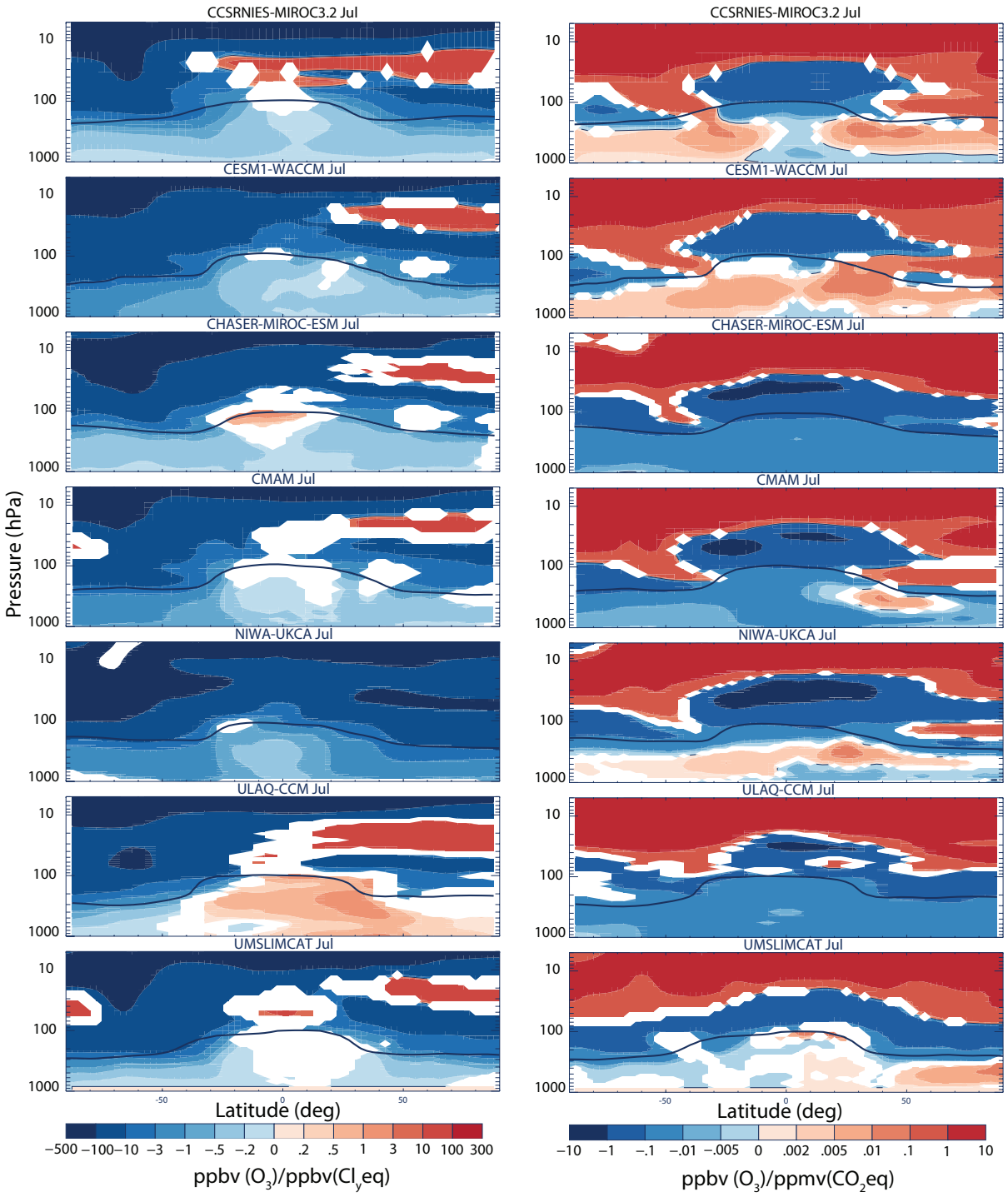

Figure 3-32. Ratio of zonal mean ozone volume mixing ratio (VMR) changes to VMR in (*left column*) equivalent Cl (Newman et al., 2007) and (*right column*) equivalent CO_2 (sum of CO_2, HFCs, PFCs, and SF_6) for seven CCMI-1 models for July. The solid black lines indicate 150 ppbv of ozone. Adapted from Morgenstern et al. (2018).

increases the ozone burden in the UT, where ozone is long lived. For climate change, this enhancement is offset by greater water vapor-induced loss of tropospheric ozone (reduction in lifetime of 0.4–6.7%, depending on scenario); for ozone recovery, the increase in τ_{O3} is enhanced by decreases in OH associated with decreased photolysis rates (increase of ~0.5%) (Bannerjee et al., 2016; Zhang et al., 2014). This decrease in OH may enhance the intercontinental transport of ozone and other pollutants, increasing ozone attributable to Asian emissions by up to 15%, or 0.3 ppbv, in the Northern Hemisphere (Zhang et al., 2014). It should be noted, however, that global models differ by nearly a factor of 2 in their predictions of OH changes associated with stratospheric ozone recovery (Madronich et al., 2015).

While ozone recovery and projected increases in the ozone flux associated with STT have a clear influence on τ_{O3}, the net change in lifetime depends strongly on changes in precursor emissions, temperature, and humidity and is highly scenario-dependent. Uncertainties in the future evolution of CH_4 dominate differences in tropospheric ozone among RCP scenarios (e.g., Revell et al., 2012, 2015; Young et al., 2013; Naik et al., 2013). Within any given scenario, changes in tropospheric ozone depend primarily on changes in ozone precursors. The SOCOL CCM, using RCP-6.0, simulates a 23% decrease in global mean tropospheric ozone between 1990 and 2060. This decrease is dominated by reductions in NO_x emissions. The increased STT associated with climate change contributes <1 ppb of additional ozone at 500 hPa between 1960 and 2090. This additional ozone, as well as that attributable to increased production of NO_x by lightning, was largely offset by increases in ozone chemical loss driven by higher temperatures in the model. Under a "solar mirror" geoengineering scenario in the HadGEM3 CCM, higher stratospheric ozone levels combined with lower atmospheric-specific humidity resulted in an overall increase in surface ozone of ~5% (Nowack et al., 2016), assuming no change in precursor emissions.

Observations cannot yet be used to evaluate projections of the tropospheric ozone response to strengthening of the stratospheric circulation and ozone recovery. However, satellite observations have been used to quantify the link between year-to-year variations in circulation strength and lower-stratospheric ozone abundances, with a 40% increase in circulation associated with a ~25% increase in NH mid-latitude lower-stratospheric ozone (Neu et al., 2014). These changes are similar to the long-term increases in circulation and ozone predicted by CCMs from 1960 to 2100 (Hegglin and Shepherd, 2009) and are associated with a ~2% increase in tropospheric ozone (Neu et al., 2014). Taken together with the modeling studies described above, this study suggests that future changes in tropospheric ozone are likely to be dominated by changes in precursor emissions, with the stratosphere playing a relatively minor role in increasing tropospheric ozone abundances and lifetime.

REFERENCES

Arosio, C., A. Rozanov, E. Malinina, K.-U. Eichmann, T. von Clarmann, and J.P. Burrows, Retrieval of ozone profiles from OMPS limb scattering observations, *Atmos. Meas. Tech.*, *11*, 2135–2149, doi:10.5194/amt-11-2135-2018, 2018.

Aschmann, J., J.P. Burrows, C. Gebhardt, A. Rozanov, R. Hommel, M. Weber, and A.M. Thompson, On the hiatus in the acceleration of tropical upwelling since the beginning of the 21st century, *Atmos. Chem. Phys.*, *14*, 12,803–12,814, doi:10.5194/acp-14-12803-2014, 2014.

Bai, K., N.-B. Chang, R. Shi, H. Yu, and W. Gao, An intercomparison of multidecadal observational and reanalysis datasets for global total ozone trends and variability analysis, *J. Geophys. Res. Atmos.*, *122*, 7119–7139, doi:10.1002/2016JD025835, 2017.

Baldwin, M.P., L.J. Gray, T.J. Dunkerton, K. Hamilton, P.H. Haynes, W.J. Randel, J.R. Holton, M.J. Alexander, I. Hirota, T. Hoinouchi, D.B.A. Jones, J.S. Kinnersely, C. Marquardt, K. Sato, and M. Takahasi, The Quasi-Biennial Oscillation, *Rev. Geophys.*, 39 (2), 179–229, doi:10.1029/1999RG000073, 2001.

Ball, W.T., J.D. Haigh, E.V. Rozanov, A. Kuchar, T. Sukhodolov, F. Tummon, A.V. Shapiro, and W. Schmutz, High solar cycle spectral variations inconsistent with stratospheric ozone observations, *Nat. Geosci., 9*, 206–209, doi:10.1038/ngeo2640, 2016.

Ball, W.T., J. Alsing, D.J. Mortlock, E.V. Rozanov, F. Tummon, and J.D. Haigh, Reconciling differences in stratospheric ozone composites, *Atmos. Chem. Phys.*, *17*, 12,269–12,302, doi:10.5194/acp-17-12269-2017, 2017.

Ball, W.T., J. Alsing, D.J Mortlock, J. Staehelin, J.D.Haigh, T. Peter, F. Tummon, R. Stübi, A. Stenke, J. Anderson, A. Bourassa, S.M. Davis, D. Degenstein, S. Frith, L. Froidevaux, C. Roth, V. Sofieva, R. Wang, J. Wild, P. Yu, J.R. Ziemke, and E.V. Rozanov, Evidence for a continuous decline in lower stratospheric ozone offsetting ozone layer recovery, *Atmos. Chem. Phys.*, *18*, 1379–1394, doi:10.5194/acp-18-1379-2018, 2018.

Banerjee, A., A.C. Maycock, A.T. Archibald, N.L. Abraham, P. Telford, P. Braesicke, and J.A. Pyle, Drivers of changes in stratospheric and tropospheric ozone between year 2000 and 2100, *Atmos. Chem. Phys.*, *16*, 2727–2746, 2016, doi:10.5194/acp-16-2727-2016

Bègue, N., D. Vignelles, G. Berthet, T. Portafaix, G. Payen, F. Jégou, H. Benchérif, J. Jumelet, J.P. Vernier, T. Lurton, J.-B. Renard, L. Clarisse, V. Duverger, F. Posny, J.-M. Metzger, and S. Godin-Beekmann, Long-range transport of stratospheric aerosols in the Southern Hemisphere following the 2015 Calbuco eruption, *Atmos. Chem. Phys.*, *17*, 15019–15036, doi:10.5194/acp-17-15019-2017, 2017.

Bhartia, P.K., R.D. McPeters, L.E. Flynn, S. Taylor, N.A. Kramarova, S. Frith, B. Fisher, and M. DeLand, Solar Backscatter UV (SBUV) total ozone and profile algorithm, *Atmos. Meas. Tech.*, *6*, 2533–2548, doi:10.5194/amt-6-2533-2013, 2013.

Bodeker, G.E., I.S. Boyd, and W.A. Matthews, Trends and variability in vertical ozone and temperature profiles measured by ozonesondes at Lauder, New Zealand: 1986 to 1996, *J. Geophys. Res.*, *103*, 28,661–28,681, doi:10.1029/98JD02581, 1998.

Bodeker, G.E., J.C. Scott, K. Kreher, and R.L. McKenzie, Global ozone trends in potential vorticity coordinates using TOMS and GOME intercompared against the Dobson network: 1978–1998, *J. Geophys. Res.*, *106*, 23,029–23,042, doi:10.1029/2001JD900220, 2001.

Bojkov, R.D., V.E. Fioletov, and A.M. Shalamjansky, Total ozone changes over Eurasia since 1973 based on re-evaluated filter ozonometer data, *J. Geophys. Res.*, *99* (D11), 22,985–22,999, doi:10.1029/94JD02006, 1994.

Boone, C.D., K. Walker, P.F. Bernath, Version 3 Retrievals for the Atmospheric Chemistry Experiment Fourier Transform Spectrometer (ACE-FTS), in The Atmospheric Chemistry Experiment ACE at 10: A Solar Occultation Anthology, edited by P.F. Bernath, 103–127, A. Deepak Publishing, Hampton, Virginia, 2013.

Bourassa, A.E., D.A. Degenstein, W.J. Randel, J.M. Zawodny, E. Kyrölä, C.A. McLinden, C.E. Sioris, and C.Z. Roth, Trends in stratospheric ozone derived from merged SAGE II and Odin-OSIRIS satellite observations, *Atmos. Chem. Phys.*, *14*, 6983–6994, doi:10.5194/acp-14-6983-2014, 2014.

Bourassa, A.E., C.Z. Roth, D.J. Zawada, L.A. Rieger, C.A. McLinden, and D.A. Degenstein, Drift-corrected Odin-OSIRIS ozone product: Algorithm

and updated stratospheric ozone trends, *Atmos. Meas. Tech.*, *11*, 489–498, doi:10.5194/amt-11-489-2018, 2018.

Boynard, A., D. Hurtmans, M.E. Koukouli, F. Goutail, J. Bureau, S. Safieddine, C. Lerot, J. Hadji-Lazaro, C. Wespes, J.-P. Pommereau, A. Pazmino, I. Zyrichidou, D. Balis, A. Barbe, S.N. Mikhailenko, D. Loyola, P. Valks, M. van Roozendael, P.-F. Coheur, and C. Clerbaux, Seven years of IASI ozone retrievals from FORLI: validation with independent total column and vertical profile measurements, *Atmos. Meas. Tech.*, *9*, 4327–4353, doi:10.5194/amt-9-4327-2016, 2016.

Butler, A.H., J.S. Daniel, R.W. Portmann, A.R. Ravishankara, P.J. Young, D.W. Fahey, and K.H. Rosenlof, Diverse policy implications for future ozone and surface UV in a changing climate, *Environ. Res. Lett.*, *11*, doi:10.1088/1748-9326/11/6/064017, 2016.

Calisesi, Y., D. Ruffieux, N. Kämpfer, and P. Viatte, The Stratospheric Ozone Monitoring Radiometer SOMORA: First validation results, in Proceedings of the Sixth European Symposium on Stratospheric Ozone, Göteborg, Sweden, 2002, *Air Pollution Research Report 79*, edited by N.R.P. Harris, G.T. Amanatidis and J.G. Levine, 92–95 pp., European Commission, 2003.

Chehade, W., M. Weber, and J.P. Burrows, Total ozone trends and variability during 1979–2012 from merged datasets of various satellites, *Atmos. Chem. Phys.*, *14*, 7059–7074, doi:10.5194/acp-14-7059-2014, 2014.

Cheung, H.H.N., W. Zhou, M.Y.T. Leung, C.M. Shun, S.M. Lee, and H.W. Tong, A strong phase reversal of the Arctic Oscillation in midwinter 2015/2016: Role of the stratospheric polar vortex and tropospheric blocking, *J. Geophys. Res. Atmos.*, *121*, 13,443–13,457, doi:10.1002/2016JD025288, 2016.

Chiodo, G., D.R. Marsh, R. Garcia-Herrera, N. Calvo, and J.A. García, On the detection of the solar signal in the tropical stratosphere, *Atmos. Chem. Phys.*, *14*, 5251–5269, doi:10.5194/acp-14-5251-2014, 2014.

Chipperfield, M.P., S. Dhomse, R. Hossaini, W. Feng, M.L. Santee, M. Weber, J.P. Burrows, J.D. Wild, D. Loyola, M. Coldewey-Egbers, On the cause of recent variations in lower stratospheric ozone, *Geophys. Res. Lett.*, *45*, doi:10.1029/2018GL078071, 2018.

Chiou, E.W., P.K. Bhartia, R.D. McPeters, D.G Loyola, M. Coldewey-Egbers, V.E. Fioletov, M. Van Roozendael, R. Spurr, C. Lerot, S.M. and Frith, Comparison of profile total ozone from SBUV (v8.6) with GOME-type and ground-based total ozone for a 16-year period (1996 to 2011), *Atmos. Meas. Tech.*, *7*, 1681–1692, doi:10.5194/amt-7-1681-2014, 2014.

Claude, H., U. Köhler, and W. Steinbrecht, New trend analyses of the homogenized ozone records at Hohenpeissenberg, in Proceedings of the XVIII Quadrennial Ozone Symposium 1996 in L'Aquila, Italy, edited by R.D. Bojkov and G. Visconti, 21–24 pp., International Ozone Commission, 1988.

Clerbaux, C., A. Boynard, L. Clarisse, M. George, J. Hadji-Lazaro, H. Herbin, D. Hurtmans, M. Pommier, A. Razavi, S. Turquety, C. Wespes, and P.-F. Coheur, Monitoring of atmospheric composition using the thermal infrared IASI/MetOp sounder, *Atmos. Chem. Phys.*, *9*, 6041 –6054, doi:10.5194/acp-9-6041-2009, 2009.

Coldewey-Egbers, M., M. Weber, L.N. Lamsal, R. de Beek, M. Buchwitz, and J.P. Burrows, Total ozone retrieval from GOME UV spectral data using the weighting function DOAS approach, *Atmos. Chem. Phys.*, *5*, 1015–1025, doi:10.5194/acp-5-1015-2005, 2005.

Coldewey-Egbers, M., Diego G., Loyola R., P. Braesicke, M. Dameris, M. van Roozendael, C. Lerot, and W. Zimmer, A new health check of the ozone layer at global and regional scales, *Geophys. Res. Lett.*, *41*, 4363–4372, doi:10.1002/2014GL060212, 2014.

Coldewey-Egbers, M., D. Loyola, M. Koukouli, D. Balis, J.-C. Lambert, T. Verhoelst, J. Granville, M. van Roozendael, C. Lerot, R. Spurr, S.M. Frith, and C. Zehner, The GOME-type Total Ozone Essential Climate Variable (GTO-ECV) data record from the ESA Climate Change Initiative, *Atmos. Meas. Tech.*, *8*, 3923–3940, doi:10.5194/amt-8-3923-2015, 2015.

Damadeo, R.P., J.M. Zawodny, L.W. Thomason, and N. Iyer, SAGE version 7.0 algorithm: Application to SAGE II, *Atmos. Meas. Tech.*, *6*, 3539–3561, doi:10.5194/amt-6-3539-2013, 2013.

Damadeo, R.P., J.M. Zawodny, and L.W. Thomason, Re-evaluation of stratospheric ozone trends from SAGE II data using a simultaneous temporal and spatial analysis, *Atmos. Chem. Phys.*, *14*, 13,455–13,470, doi:10.5194/acp-14-13455-2014, 2014.

Damadeo, R.P., J.M. Zawodny, E.E. Remsberg, and K.A. Walker, The impact of nonuniform sampling on stratospheric ozone trends derived from occultation instruments, *Atmos. Chem. Phys.*, *18*, 535–554, doi:10.5194/acp-18-535-2018, 2018.

Davis, S.M., K.H. Rosenlof, B. Hassler, D.F. Hurst, W.G. Read, H. Vömel, H. Selkirk, M. Fujiwara, and R. Damadeo, The Stratospheric Water and Ozone Satellite Homogenized (SWOOSH) database: A long-term database for climate studies, *Earth Syst. Sci. Data*, *8*, 461–490, doi:10.5194/essd-8-461-2016, 2016.

Davis, S.M., M.I. Hegglin, M. Fujiwara, R. Dragani, Y. Harada, C. Kobayashi, C. Long, G.L. Manney, E.R. Nash, G.L. Potter, S. Tegtmeier, T. Wang, K. Wargan, and J.S. Wright, Assessment of upper tropospheric and stratospheric water vapor and ozone in reanalyses as part of S-RIP, *Atmos. Chem. Phys.*, *17*, 12,743–12,778, doi:10.5194/acp-17-12743-2017, 2017.

Dee, D.P., S.M. Uppala, A.J. Simmons, P. Berrisford, P. Poli, S. Kobayashi, U. Andrae, M.A. Balmaseda, G. Balsamo, P. Bauer, P. Bechtold, A.C. Beljaars, L. van de Berg, J. Bidlot, N. Bormann, C. Delsol, R. Dragani, M. Fuentes, A.J. Geer, L. Haimberger, S.B. Healy, H. Hersbach, E.V. Hólm, L. Isaksen, P. Kållberg, M. Köhler, M. Matricardi, A.P. McNally, B.M. Monge-Sanz, J. Morcrette, B. Park, C. Peubey, P. de Rosnay, C. Tavolato, J. Thépaut, and F. Vitart, The ERA-Interim reanalysis: Configuration and performance of the data assimilation system. *Q. J .R. Meteorol. Soc.*, *137*, 553–597, doi:10.1002/qj.828, 2011.

de Laat, A.T.J., R.J. van der A, and M. van Weele, Tracing the second stage of ozone recovery in the Antarctic ozone-hole with a "big data" approach to multivariate regressions, *Atmos. Chem. Phys.*, *15*, 79–97, doi:10.5194/acp-15-79-2015, 2015.

Deshler, T., J. Mercer, H.G.J. Smit, R. Stuebi, G. Levrat, B.J. Johnson, S.J. Oltmans, R. Kivi, J. Davies, A.M. Thompson, J. Witte, F.J. Schmidlin, G. Brothers, and T. Sasaki, Atmospheric comparison of electrochemical cell ozonesondes from different manufacturers, and with different cathode solution strengths: The Balloon Experiment on Standards for Ozonesondes, *J. Geophys. Res.*, *113* (D4), D04307, doi:10.1029/2007JD008975, 2008.

Deshler, T., Observations for Chemistry (In Situ), in *Particles, Encyclopedia of Atmospheric Science, 2nd Edition*, *Vol. 1*, edited by G.R. North, J. Pyle, and F. Zhang, 379–386, Academic Press, Cambridge, Masseachusetts, 2015.

Deshler, T., R. Stübi, F.J. Schmidlin, J.L. Mercer, H.G.J. Smit, B.J. Johnson, R. Kivi, and B. Nardi, Methods to homogenize electrochemical concentration cell (ECC) ozonesonde measurements across changes in sensing solution concentration or ozonesonde manufacturer, *Atmos. Meas. Tech.*, *10*, 2021–2043, doi:10.5194/amt-10-2021-2017, 2017.

Dhomse, S., M. Weber, I. Wohltmann, M. Rex, and J.P. Burrows, On the possible causes of recent increases in northern hemispheric total ozone from a statistical analysis of satellite data from 1979 to 2003, *Atmos. Chem. Phys.*, *6*, 1165–1180, doi:10.5194/acp-6-1165-2006, 2006.

Dhomse, S.S., M.P. Chipperfield, R.P. Damadeo, J.M. Zawodny, W.T. Ball, W. Feng, R. Hossaini, G.W. Mann, and J.D. Haigh, On the ambiguous nature of the 11-year solar cycle signal in upper stratospheric ozone, *Geophys. Res. Lett.*, *43*, 7241–7249, doi:10.1002/2016GL069958, 2016.

Dhomse, S.S., D. Kinnison, M.P. Chipperfield, R.J. Salawitch, I. Cionni, M.L. Hegglin, N.L. Abraham, H. Akiyoshi, A.T. Archibald, E.M. Bednarz, S. Bekki, P. Braesicke, N. Butchart, M. Dameris, M. Deushi, S. Frith, S.C. Hardiman, B. Hassler, L.W. Horowitz, R.-M. Hu, P. Jöckel, B. Josse, O. Kirner, S. Kremser, U. Langematz, J. Lewis, M. Marchand, M. Lin, E. Mancini, V. Marécal, M. Michou, O. Morgenstern, F.M. O'Connor, L. Oman, G. Pitari, D.A. Plummer, J.A. Pyle, L.E. Revell, E. Rozanov, R. Schofield, A. Stenke, K. Stone, K. Sudo, S. Tilmes, D. Visioni, Y. Yamashita, and G. Zeng, Estimates of ozone return dates from Chemistry-Climate Model Initiative simulations, *Atmos. Chem. Phys.*, *18*, 8409–8438, doi:10.5194/acp-18-8409-2018, 2018.

Dragani, R., On the quality of the ERA-Interim ozone reanalyses: Comparisons with satellite data. *Q. J .R. Meteorol. Soc.*, *137*, 1312–1326, doi:10.1002/qj.821, 2011.

Dufour, G., M. Eremenko, A. Griesfeller, B. Barret, E. LeFlochmoën, C. Clerbaux, J. Hadji-Lazaro, P.-F. Coheur, and D. Hurtmans, Validation of three different scientific ozone products retrieved from IASI spectra using ozonesondes, *Atmos. Meas. Tech.*, *5*, 611–630, doi:10.5194/amt-5-611-2012, 2012.

Dunkerton, T.J., The quasi-biennial oscillation of 2015–2016: Hiccup or death spiral?, *Geophys. Res. Lett.*, *43*, 10,547–10,552, doi:10.1002/2016GL070921, 2016.

Dvortsov, V.L., M.A. Geller, S. Solomon, S.M. Schauffler, E.L. Atlas, and D.R. Blake, Rethinking reactive halogen budgets in the mid-latitude lower stratosphere, *Geophys. Res. Lett.*, *26*, 1699–1702, doi:10.1029/1999GL900309, 1999.

Eckert, E., T. von Clarmann, M. Kiefer, G.P. Stiller, S. Lossow, N. Glatthor, D.A. Degenstein, L. Froidevaux, S. Godin-Beekmann, T. Leblanc, S. McDermid, M. Pastel, W. Steinbrecht, D.P.J. Swart, K.A. Walker, and P.F. Bernath, Drift-corrected trends and periodic variations in MIPAS IMK/IAA ozone measurements, *Atmos. Chem. Phys.*, *14*, 2571–2589, doi:10.5194/acp-14-2571-2014, 2014.

Ermolli, I., K. Matthes, T. Dudok de Wit, N.A. Krivova, K. Tourpali, M. Weber, Y.C. Unruh, L. Gray, U. Langematz, P. Pilewskie, E. Rozanov, W. Schmutz, A. Shapiro, S.K. Solanki, and T.N. Woods, Recent variability of the solar spectral irradiance and its impact on climate modelling, *Atmos. Chem. Phys.*, *13*, 3945–3977, doi:10.5194/acp-13-3945-2013, 2013.

Fernandez, R., D.E. Kinnison, J.-F. Lamarque, S. Tilmes, and A. Saiz-Lopez, Impact of biogenic very short-lived bromine on the Antarctic ozone hole during the 21st century, *Atmos. Chem Phys.*, *17*, 1673–1688, doi:10.5194/acp-17-1673-2017, 2017.

Fioletov, V.E., G.E. Bodeker, A.J. Miller, R.D. McPeters, and R. Stolarski, Global and zonal total ozone variations estimated from ground-based and satellite measurements: 1964–2000, *J. Geophys. Res.*, *107*, doi:10.1029/2001JD001350, 2002.

Fioletov, V.E., and T.G. Shepherd, Seasonal persistence of midlatitude total ozone anomalies, *Geophys. Res. Lett.*, *30* (7), doi:10.1029/2002GL016739, 2003.

Fioletov, V.E., G. Labow, R. Evans, E.W. Hare, U. Köhler, C.T. McElroy, K. Miyagawa, A. Redondas, V. Savastiouk, A.M. Shalamyansky, J. Staehelin, K.Vanicek, M. Weber, Performance of the ground-based total ozone network assessed using satellite data, *J. Geophys. Res.*, *113*, D14313, doi:10.1029/2008JD009809, 2008.

Flury, T., D.L. Wu, and W.G. Read, Variability in the speed of the Brewer–Dobson circulation as observed by Aura/MLS, *Atmos. Chem. Phys.*, *13*, 4563–4575, doi:10.5194/acp-13-4563-2013, 2013.

Frith, S.M., N.A. Kramarova, R.S. Stolarski, R.D. McPeters, P.K. Bhartia, and G.J. Labow, Recent changes in column ozone-based on the SBUV version 8.6 merged ozone dataset, *J. Geophys. Res. Atmos.*, *119*, 9735–9751, doi:10.1002/2014JD021889, 2014.

Frith, S.M., R.S. Stolarski, N.A. Kramarova, and R.D. McPeters, Estimating uncertainties in the SBUV Version 8.6 merged profile ozone dataset, *Atmos. Chem. Phys.*, *17*, 14,695–14,707, doi:10.5194/acp-17-14695-2017, 2017.

Froidevaux, L., J. Anderson, H.-J. Wang, R.A. Fuller, M.J. Schwartz, M.L. Santee, N.J. Livesey, H.C. Pumphrey, P.F. Bernath, J.M. Russell III, and M.P. McCormick, Global OZone Chemistr And Related trace gas Data records for the Stratosphere (GOZCARDS): Methodology and sample results with a focus on HCl, H_2O, and O_3, *Atmos. Chem. Phys.*, *15*, 10,471–10,507, doi:10.5194/acp-15-10471-2015, 2015.

Frossard, L., H.E. Rieder, M. Ribatet, J. Staehelin, J.A. Maeder, S. Di Rocco, A.C. Davison, and T. Peter, On the relationship between total ozone and atmospheric dynamics and chemistry at mid-latitudes – Part 1: Statistical models and spatial fingerprints of atmospheric dynamics and chemistry, *Atmos. Chem. Phys.*, *13*, 147–164, doi:10.5194/acp-13-147-2013, 2013.

Fusco, A.C., and M.L. Salby, 1999: Interannual variations of total ozone and their relationship to variations of planetary wave activity, *J. Clim.*, *12*, 1619–1629. doi:10.1175/1520-0442(1999)012<1619:IVOTOA>2.0.CO;2, 1999.

Garane, K., C. Lerot, M. Coldewey-Egbers, T. Verhoelst, M.E. Koukouli, I. Zyrichidou, D.S. Balis, T. Danckaert, F. Goutail, J. Granville, D. Hubert, A. Keppens, J.-C. Lambert, D. Loyola, J.-P. Pommereau, M. Van Roozendael, and C. Zehner, Quality assessment of the Ozone_cci Climate Research Data Package (release 2017) – Part 1: Ground-based validation of total ozone column data products, *Atmos. Meas. Tech.*, *11*, 1385–1402, doi:10.5194/amt-11-1385-2018, 2018.

Gaudel A., O.R. Cooper, G. Ancellet, B. Barret, A. Boynard, J.P. Burrows, C. Clerbaux, P.-F. Coheur,

J. Cuesta, E. Cuevas, S. Doniki, G. Dufour, F. Ebojie, G. Foret, O. Garcia, M.J. Granados Muños, J.W. Hannigan, F. Hase, G. Huang, B. Hassler, D. Hurtmans, D. Jaffe, N. Jones, P. Kalabokas, B. Kerridge, S.S. Kulawik, B. Latter, T. Leblanc, E. Le Flochmoën, W. Lin, J. Liu, X. Liu, E. Mahieu, A. McClure-Begley, J.L. Neu, M. Osman, M. Palm, H. Petetin, I. Petropavlovskikh, R. Querel, N. Rahpoe, A. Rozanov, M.G. Schultz, J. Schwab, R. Siddans, D. Smale, M. Steinbacher, H. Tanimoto, D.W. Tarasick, V. Thouret, A.M. Thompson, T. Trickl, E. Weatherhead, C. Wespes, H.M. Worden, C. Vigouroux, X. Xu, G. Zeng, and J. Ziemke, Tropospheric Ozone Assessment Report: Present-day distribution and trends of tropospheric ozone relevant to climate and global atmospheric chemistry model evaluation, *Elem-Sci. Anthrop.*, *6* (1), doi:10.1525/elementa.291, 2018.

Gebhardt, C., A. Rozanov, R. Hommel, M. Weber, H. Bovensmann, J.P. Burrows, D. Degenstein, L. Froidevaux, and A.M. Thompson, Stratospheric ozone trends and variability as seen by SCIAMACHY from 2002 to 2012, *Atmos. Chem. Phys.*, *14*, 831–846, doi:10.5194/acp-14-831-2014, 2014.

Godin, S., G. Mégie, and J. Pelon, Systematic lidar measurements of the stratospheric ozone vertical distribution, *Geophys. Res. Lett.*, *16* (6), 547–550, doi:10.1029/GL016i006p00547, 1989.

Gray, L.J., J. Beer, M. Geller, J.D. Haigh, M. Lockwood, K. Matthes, U. Cubasch, D. Fleitmann, G. Harrison, L. Hood, J. Luterbacher, G.A. Meehl, D. Shindell, B. van Geel, W. White, Solar influences on climate, *Rev. Geophys.*, *48* (4), RG4001, doi:10.1029/2009RG000282, 2010.

Haigh, J.D., The role of stratospheric ozone in modulating the solar radiative forcing of climate, *Nature*, *370*, 544–546, doi:10.1038/370544a0, 1994.

Harris, N.R.P., E. Kyrö, J. Staehelin, D. Brunner, S.-B. Andersen, S. Godin-Beekmann, S. Dhomse, P. Hadjinicolaou, G. Hansen, I. Isaksen, A. Jrrar, A. Karpetchko, R. Kivi, B. Knudsen, P. Krizan, J. Lastovicka, J. Maeder, Y. Orsolini, J.A. Pyle, M. Rex, K. Vanicek, M. Weber, I. Wohltmann, P. Zanis, and C. Zerefos, Ozone trends at northern mid- and high latitudes – a European perspective, *Ann. Geophys.*, *26*, 1207–1220, doi:10.5194/angeo-26-1207-2008, 2008.

Harris, N.R.P., B. Hassler, F. Tummon, G.E. Bodeker, D. Hubert, I. Petropavlovskikh, W. Steinbrecht, J. Anderson, P.K. Bhartia, C.D. Boone, A. Bourassa, S.M. Davis, D. Degenstein, A. Delcloo, S.M. Frith, L. Froidevaux, S. Godin-Beekmann, N. Jones, M.J. Kurylo, E. Kyrölä, M. Laine, S.T. Leblanc, J.-C. Lambert, B. Liley, E. Mahieu, A. Maycock, M. de Mazière, A. Parrish, R. Querel, K.H. Rosenlof, C. Roth, C. Sioris, J. Staehelin, R.S. Stolarski, R. Stübi, J. Tamminen, C. Vigouroux, K.A. Walker, H.J. Wang, J. Wild, and J.M. Zawodny, Past changes in the vertical distribution of ozone – Part 3: Analysis and interpretation of trends, *Atmos. Chem. Phys.*, *15*, 9965–9982, doi:10.5194/acp-15-9965-2015, 2015.

Hase, F., T. Blumenstock, and C. Paton-Walsh, Analysis of the instrumental line shape of high-resolution Fourier transform IR spectrometers with gas cell measurements and new retrieval software, *Appl. Opt.*, *38*, 3417–3422, doi:10.1364/AO.38.003417, 1999.

Hassler, B., I. Petropavlovskikh, J. Staehelin, T. August, P.K. Bhartia, C. Clerbaux, D. Degenstein, M.D. Mazière, B.M. Dinelli, A. Dudhia, G. Dufour, S.M. Frith, L. Froidevaux, S. Godin-Beekmann, J. Granville, N.R.P. Harris, K. Hoppel, D. Hubert, Y. Kasai, M.J. Kurylo, E. Kyrölä, J.-C. Lambert, P.F. Levelt, C.T. McElroy, R.D. McPeters, R. Munro, H. Nakajima, A. Parrish, P. Raspollini, E.E. Remsberg, K.H. Rosenlof, A. Rozanov, T. Sano, Y. Sasano, M. Shiotani, H.G.J. Smit, G. Stiller, J. Tamminen, D.W. Tarasick, J. Urban, R.J. van der A, J.P. Veefkind, C. Vigouroux, T. von Clarmann, C. von Savigny, K.A.Walker, M.Weber, J. Wild, J.M., and Zawodny, Past changes in the vertical distribution of ozone – Part 1: Measurement techniques, uncertainties and availability, *Atmos. Meas. Tech.*, 7, 1395–1427, doi:10.5194/amt-7-1395-2014, 2014.

Hegglin, M. I., and T.G. Shepherd, Large climate-induced changes in ultraviolet index and stratosphere-to-troposphere ozone flux. *Nat. Geosci.*, *2* (10), 687–691, doi:10.1038/NGEO604, 2009.

Hendrick, F., J.-P. Pommereau, F. Goutail, R.D. Evans, D. Ionov, A. Pazmino, E. Kyrö, G. Held, P. Eriksen, V. Dorokhov, M. Gil, and M. Van Roozendael, NDACC/SAOZ UV-visible total ozone measurements: Improved retrieval and comparison with correlative ground-based and satellite observations, *Atmos. Chem. Phys.*, *11*, 5975–5995, doi:10.5194/acp-11-5975-2011, 2011.

Hood, L.L., and B.E. Soukharev, Quasi-decadal variability of the tropical lower stratosphere: The role of extratropical wave forcing, *J. Atmos. Sci.*, *60*, 2389–2403, doi:10.1175/1520-0469(2003)060<2389:QVOTTL>2.0.CO;2, 2003.

Hossaini, R., M.P. Chipperfield, S.A. Montzka, A. Rap, S. Dhomse, and W. Feng, Efficiency of short-lived halogens at influencing ozone through depletion of stratospheric ozone, *Nat. Geosci.*, *8*, 186–190, doi:10.1038/NGEO2363, 2015.

Hossaini, R., M.P. Chipperfield, S.M. Montzka, A.A. Leeson, S.S. Dhomse, J.A. Pyle, The increasing threat to stratospheric ozone from dichloromethane, *Nat. Commun.*, *8*, doi:10.1038/ncomms15962, 2017.

Hu, D., W. Tian, Z. Guan, Y. Guo, and S. Dhomse, Longitudinal asymmetric trends of tropical cold-point tropopause temperature and their link to strengthened walker circulation, *J. Clim., 29*, 7755–7771, doi:10.1175/JCLI-D-15-0851.1, 2016.

Hubert, D., J.-C. Lambert, T. Verhoelst, J. Granville, A. Keppens, J.-L. Baray, A.E. Bourassa, U. Cortesi, D.A. Degenstein, L. Froidevaux, S. Godin-Beekmann, K.W. Hoppel, B.J. Johnson, E. Kyrölä, T. Leblanc, G. Lichtenberg, M. Marchand, C.T. McElroy, D. Murtagh, H. Nakane, T. Portafaix, R. Querel, J.M. Russell III, J. Salvador, H.G.J. Smit, K. Stebel, W. Steinbrecht, K.B. Strawbridge, R. Stübi, D.P.J. Swart, G. Taha, D.W. Tarasick, A.M. Thompson, J. Urban, J.A.E. van Gijsel, R. Van Malderen, P. von der Gathen, K.A. Walker, E. Wolfram, J.M. and Zawodny, Ground-based assessment of the bias and long-term stability of 14 limb and occultation ozone profile data records, *Atmos. Meas. Tech.*, *9*, 2497–2534, doi:10.5194/amt-9-2497-2016, 2016.

IPCC (Intergovernmental Panel on Climate Change), *Emissions Scenerios. A Special Report of Working Group III of the International Panel on Climate Change,* edited by N. Nakicenovic, and R. Swart, 570 pp., Cambridge University Press, Cambridge, United Kingdom, 2000.

IPCC (Intergovenmental Panel on Climate Change), *Climate Change 2013: The Physical Science Basis. Contribution of Working Group I to the Fifth Assessment Report of the Intergovernmental Panel on Climate Change*, edited by T.F. Stocker, D. Qin, G.-K. Plattner, M. Tignor, S.K. Allen, J. Boschung, A. Nauels, Y. Xia, V. Bex, and P.M. Midgley, 1535 pp., Cambridge University Press, Cambridge, United Kingdom, 2013.

Jaross, G., P.K. Bhartia, G. Chen, M. Kowitt, M. Haken, Z. Chen, P. Xu, J. Warner, and T. Kelly, OMPS Limb profiler instrument performance assessment, *J. Geophys. Res. Atmos.*, *119*, 4399–4412, doi:10.1002/2013JD020482, 2014.

Jia, J., A. Rozanov, A. Ladstätter-Weißenmayer, and J.P. Burrows, Global validation of SCIAMACHY limb ozone data (versions 2.9 and 3.0, IUP Bremen) using ozonesonde measurements, *Atmos. Meas. Tech.*, *8*, 3369–3383, doi:10.5194/amt-8-3369-2015, 2015.

Jones, A.C., J.M. Haywood, and A. Jones, Climatic impacts of stratospheric geoengineering with sulfate, black carbon and titania injection, *Atmos. Chem. Phys.*, *16*, 2843–2862, doi:10.5194/acp-16-2843-2016, 2016.

Keeble, J., Brown, H., Abraham, N. L., Harris, N. R. P., and Pyle, J. A.: On ozone trend detection: using coupled chemistry–climate simulations to investigate early signs of total column ozone recovery, Atmos. Chem. Phys., 18, 7625-7637, doi: 10.5194/acp-18-7625-2018, 2018

Keith, D.W., D.K. Weisenstein, J.A. Dykema, and F.N. Keutsch, Stratospheric solar geoengineering without ozone loss, *Proc. Natl. Acad. Sci.*, *113*, 14,910–14,914, doi:10.1073/pnas.1615572113, 2016.

Khaykin S., S. Godin-Beekmann, P. Keckhut, A. Hauchecorne, J. Jumelet, J.-P. Vernier, A. Bourassa, D.A. Degenstein, L.A. Rieger, C. Bingen, F. Vanhellemont, C. Robert, M. DeLand, and P.K. Bhartia, Variability and evolution of the midlatitude stratospheric aerosol budget from 22 years of ground-based lidar and satellite observations, *Atmos. Chem. Phys.*, *17*, 1829–1845, doi:10.5194/acp-17-1829-2017, 2017.

Kiesewetter, G., B.-M. Sinnhuber, M. Weber, J.P. and Burrows, Attribution of stratospheric ozone trends to chemistry and transport: A modelling study, *Atmos. Chem. Phys.*, 10, 12,073–12,089, doi:10.5194/acp-10-12073-2010, 2010.

Klobas, J.E., D.M. Wilmouth, D.K. Weisenstein, J.G. Anderson, and R.J. Salawitch, Ozone depletion following future volcanic eruptions, *Geophys. Res. Lett.*, *44*, 7490–7499, doi:10.1002/2017GL073972, 2017.

Knibbe, J.S., R.J. van der A, and A.T.J. de Laat, Spatial regression analysis on 32 years total column

ozone data, *Atmos. Chem. Phys., 14*, 5323–5373, doi:10.5194/acpd- 14-5323-2014, 2014.

Komhyr, W.D., Electrochemical concentration cells for gas analysis, *Am Geoph. 25*, 203-210, 1969.

Koukouli, M.E., C. Lerot, J. Granville, F. Goutail, J.-C. Lambert, J.-P. Pommereau, D. Balis, I. Zyrichidou, M. Van Roozendael, M. Coldewey-Egbers, D. Loyola, G. Labow, S. Frith, R. Spurr, and C. Zehner, Evaluating a new homogeneous total ozone climate data record from GOME/ERS-2, SCIAMACHY/Envisat, and GOME-2/MetOp-A, *J. Geophys. Res. Atmos.*, *120*, 12,296–12,312, doi:10.1002/2015JD023699, 2015.

Kovilakam, M., and T. Deshler, On the accuracy of stratospheric aerosol extinction derived from in situ size distribution measurements and surface area density derived from remote SAGE II and HALOE extinction measurements, *J. Geophys. Res. Atmos.*, *120*, 8426–8447, doi:10.1002/2015JD023303, 2015.

Kramarova, N.A., S.M. Frith, P.K. Bhartia, R.D. McPeters, S.L. Taylor, B.L. Fisher, G.J. Labow, and M.T. DeLand, Validation of ozone monthly zonal mean profiles obtained from the version 8.6 Solar Backscatter Ultraviolet algorithm, *Atmos. Chem. Phys.*, *13*, 6887–6905, doi:10.5194/acp-13-6887-2013, 2013.

Kramarova, N.A., E.R. Nash, P.A. Newman, P.K. Bhartia, R.D. McPeters, D.F. Rault, C.J. Seftor, P.Q. Xu, and G.J. Labow, Measuring the Antarctic ozone hole with the new Ozone Mapping and Profiler Suite (OMPS), *Atmos. Chem. Phys.*, *14*, 2353–2361, doi:10.5194/acp-14-2353-2014, 2014.

Kramarova, N.A., P.K. Bhartia, G. Jaross, L. Moy, P. Xu, Z. Chen, M. DeLand, L. Froidevaux, N. Livesey, D. Degenstein, A. Bourassa, K.A. Walker, and P. Sheese, Validation of ozone profile retrievals derived from the OMPS LP version 2.5 algorithm against correlative satellite measurements, *Atmos. Meas. Tech.*, *11*, 2837–2861, doi:10.5194/amt-11-2837-2018, 2018.

Kravitz, B., A. Robock, P.M. Forster, J.M. Haywood, M.G. Lawrence, and H. Schmidt, An overview of the Geoengineering Model Intercomparison Project (GeoMIP), *J. Geophys. Res.*, *118*, 13,103–13,107, doi:10.1020/2013JD020569, 2013.

Kremser, S., L.W. Thomason, M. von Hobe, M. Hermann, T. Deshler, C. Timmreck, M. Toohey, A. Stenke, J.P. Schwarz, R. Weigel, S. Fueglistaler, F.J. Prata, J.-P. Vernier, H. Schlager, J.E. Barnes, J.-C. Antuña-Marrero, D. Fairlie, M. Palm, E. Mahieu, J. Notholt, M. Rex, C. Bingen, F. Vanhellemont, A. Bourassa, J.M.C. Plane, D. Klocke, S.A. Carn, L. Clarisse, T. Trickl, R. Neely, A.D. James, L. Rieger, J.C. Wilson, B. Meland, Stratospheric aerosol-observations, processes, and impact on climate, *Rev. Geophys.*, *54*, 278–335, doi:10.1002/2015RG000511, 2016.

Kuttippurath, J., G.E. Bodeker, H.K. Roscoe, and P.J. Nair, A cautionary note on the use of EESC-based regression analysis for ozone trend studies, *Geophys. Res. Lett.*, *42*, 162–168, doi:10.1002/2014GL062142, 2015.

Kyrölä, E., M. Laine, V. Sofieva, J. Tamminen, S.-M. Päivärinta, S. Tukiainen, J. Zawodny, and L. Thomason, Combined SAGE II–GOMOS ozone profile dataset for 1984–2011 and trend analysis of the vertical distribution of ozone, *Atmos. Chem. Phys.*, *13*, 10,645–10,658, doi:10.5194/acp-13-10645-2013, 2013.

Laine, M., N. Latva-Pukkila, and E. Kyrölä, Analysing time-varying trends in stratospheric ozone time series using the state space approach, *Atmos. Chem. Phys.*, *14*, 9707–9725, doi:10.5194/acp-14-9707-2014, 2014.

Lerot, C., M. Van Roozendael, R. Spurr, D. Loyola, M. Coldewey-Egbers. S. Kochenova, J. van Gent, M. Koukouli, D. Balis, J.-C. Lambert, J. Granville, C. Zehner, Homogenized total ozone data records from the European sensors GOME/ERS-2, SCIAMACHY/Envisat, and GOME-2/MetOp-A, *J. Geophys. Res. Atmos.*, *119* (3), 1639–1662, doi:10.1002/2013JD020831, 2014.

Livesey, N.J., W.G. Read, P.A. Wagner, L. Froidevaux, A. Lambert, G.L. Manney, L.F. Millán Valle, H.C. Pumphrey, M.L. Santee, M.J. Schwartz, S.Wang, R.A. Fuller, R.F. Jarnot, B.W. Knosp, E. Martinez, R.R. Lay, Earth Observing System (EOS) Aura Microwave Limb Sounder (MLS) Version 4.2x level 2 data quality and description document, JPL D-33509 Rev. D, available at https://mls.jpl.nasa.gov/data/v4-2_data_quality_document.pdf, 2018.

LOTUS (2018): *SPARC/IO3C/GAW report on Long-term Ozone Trends and Uncertainties in the Stratosphere,* edited by I. Petropavlovskikh, S. Godin-Beekmann, D. Hubert, R. Damadeo, B. Hassler, V. Sofieva, *SPARC Report No. 9, WCRP-*

17/2018, GAW Report No. 241, doi:10.17874/f899e57a20b, (accepted in May 2019), available at: http://www.sparc-climate.org/publications/sparc-reports.

Madronich, S., M. Shao, S.R. Wilson, K.R. Solomon, J.D. Longstreth, and X.Y. Tang, Changes in air quality and tropospheric composition due to depletion of stratospheric ozone and interactions with changing climate: implications for human and environmental health, *Photochem. Photobiol. Sci.*, *14*, 149–169, doi:10.1039/C4PP90037E, 2015.

Masui T., K. Matsumoto, Y. Hijioka, T. Kinoshita, T. Nozawa, S. Ishiwatari, E. Kato, P.R. Shukla, Y. Yamagata, M. Kainuma, An emission pathway for stabilization at 6 Wm−2 radiative forcing, *Clim. Change*, *109* (12), 59–76, doi:10.1007/s10584-011-0150-5, 2011.

Maycock, A.C., K. Matthes, S. Tegtmeier, R. Thiéblemont, and L. Hood, The representation of solar cycle signals in stratospheric ozone – Part 1: A comparison of recently updated satellite observations, *Atmos. Chem. Phys.*, *16*, 10,021–10,043, doi:10.5194/acp-16-10021-2016, 2016.

Matthes, K., B. Funke, M.E. Andersson, L. Barnard, J. Beer, P. Charbonneau, M.A. Clilverd, T. Dudok de Wit, M. Haberreiter, A. Hendry, C.H. Jackman, M. Kretzschmar, T. Kruschke, M. Kunze, U. Langematz, D.R. Marsh, A.C. Maycock, S. Misios, C.J. Rodger, A.A. Scaife, A. Seppälä, M. Shangguan, M. Sinnhuber, K. Tourpali, I. Usoskin, M. van de Kamp, P.T. Verronen, and S. Versick, Solar forcing for CMIP6 (v3.2), *Geosci. Model Dev.*, *10*, 2247–2302, doi:10.5194/gmd-10-2247-2017, 2017.

McClintock, W.E., G.J. Rottman, and T.N. Woods, Solar-Stellar Irradiance Comparison Experiment II (SOLSTICE II): Instrument concept and design, *Sol. Phys.*, *230*, 225–258, doi:10.1007/0-387-37625-9_12, 2005.

McDermid, I.S., S.M. Godin, and T.D. Walsh, Lidar measurements of stratospheric ozone and intercomparisons and validation, *Appl. Opt.*, *29* (33), 4914–4923, doi:10.1364/AO.29.004914, 1990.

McDermid, I.S., J.B. Bergwerff, G. Bodeker, I.S. Boyd, E.J. Brinksma, B.J. Connor, R. Farmer, M.R. Gross, P. Kimvilakani, W.A. Matthews, T.J. McGee, F.T. Ornel, A. Parrish, U. Singh, D.P.J. Swart, J.J. Tsou, P.H. Wang, and J. Zawodny, OPAL: Network for the detection of stratospheric change ozone profiler assessment at Lauder, New Zealand. Intercomparison of revised results, *J. Geophys. Res.*, *103*, 28,693–28,699, doi:10.1029/98JD02707, 1998.

McLinden, C.A., S. Tegtmeier, and V. Fioletov, Technical Note: A SAGE-corrected SBUV zonal-mean ozone dataset, *Atmos. Chem. Phys.*, *9*, 7963–7972, doi:10.5194/acp-9-7963-2009, 2009.

McPeters, R.D., D.J. Hofmann, M. Clark, L. Froidevaux, M. Gross, B. Johnson, G. Koenig, S. McDermid, F. Murcray, S. Oltmans, A. Parrish, U. Singh, J.J. Tsou, and J. Zawodny, Results from the 1995 stratospheric ozone profile intercomparison at Mauna Loa, *J. Geophys. Res.*, *104*, 30,505–30,514, doi:10.1029/1999JD900760, 1999.

Meinshausen, M., S.J. Smith, K. Calvin, J.S. Daniel, M.L.T. Kainuma, J.-F. Lamarque, K. Matsumoto, S.A. Montzka, S.C.B. Raper, K. Riahi, A. Thomson, G.J.M. Velders, D.P.P. van Vuuren, *Clim. Change*, *109*, doi:10.1007/s10584-011-0156-z, 2011.

Meul, S., M. Dameris, U. Langematz, J. Abalichin, A. Kerschbaumer, A. Kubin, and S. Oberländer-Hayn, Impact of rising greenhouse gas concentrations on future tropical ozone and UV exposure, *Geophys. Res. Lett.*, *43*, 2919–2927, doi:10.1002/2016GL067997, 2016.

Millán, L.F., N.J. Livesey, M.L. Santee, J.L. Neu, G.L. Manney, and R.A. Fuller, Case studies of the impact of orbital sampling on stratospheric trend detection and derivation of tropical vertical velocities: Solar occultation vs. limb emission sounding, *Atmos. Chem. Phys.*, *16*, 11,521–11,534, doi:10.5194/acp-16-11521-2016, 2016.

Minschwaner, K., H. Su, and J.H. Jiang, The upward branch of the Brewer-Dobson circulation quantified by tropical stratospheric water vapor and carbon monoxide measurements from the Aura Microwave Limb Sounder, *J. Geophys. Res. Atmos.*, *121*, 2790–2804, doi:10.1002/2015JD023961, 2016.

Moreira, L., K. Hocke, E. Eckert, T. von Clarmann, and N. Kämpfer, Trend analysis of the 20-year time series of stratospheric ozone profiles observed by the GROMOS microwave radiometer at Bern, *Atmos. Chem. Phys.*, *15*, 10,999-11,009, doi:10.5194/acp-15-10999-2015, 2015.

Morgenstern, O., H. Akiyoshi, S. Bekki, P. Braesicke, N. Butchart, M.P. Chipperfield, D. Cugnet, M. Deushi, S.S. Dhomse, R.R. Garcia, A. Gettel-

man, N.P. Gillett, S.C. Hardiman, J. Jumelet, D.E. Kinnison, J.-F. Lamarque, F. Lott, M. Marchand, M. Michou, T. Nakamura, D. Olivié, T. Peter, D. Plummer, J.A. Pyle, E. Rozanov, D. Saint-Martin, J.F. Scinocca, K. Shibata, M. Sigmond, D. Smale, H. Teyssèdre, W. Tian, A. Voldoire, Y. Yamashita, Anthropogenic forcing of the Northern Annular Mode in CCMVal-2 models, *J. Geophys. Res.*, *115* (D3), doi:10.1029/2009JD013347, 2010.

Morgenstern, O., M.I. Hegglin, E. Rozanov, F.M. O'Connor, N.L. Abraham, H. Akiyoshi, A.T. Archibald, S. Bekki, N. Butchart, M.P. Chipperfield, M. Deushi, S.S. Dhomse, R.R. Garcia, S.C. Hardiman, L.W. Horowitz, P. Jöckel, B. Josse, D. Kinnison, M. Lin, E. Mancini, M.E. Manyin, M. Marchand, V. Marécal, M. Michou, L.D. Oman, G. Pitari, D.A. Plummer, L.E. Revell, D. Saint-Martin, R. Schofield, A. Stenke, K. Stone, K. Sudo, T.Y. Tanaka, S. Tilmes, Y. Yamashita, K. Yoshida, and G. Zeng, Review of the global models used within phase 1 of the Chemistry–Climate Model Initiative (CCMI-1), *Geosci. Model Dev.*, *10*, 639–671, doi:10.5194/gmd-10-639-2017, 2017.

Morgenstern, O., K.A. Stone, R. Schofield, H. Akiyoshi, Y. Yamashita, D.E. Kinnison, R.R. Garcia, K. Sudo, D.A. Plummer, J. Scinocca, L.D. Oman, M.E. Manyin, G. Zeng, E. Rozanov, A. Stenke, L.E. Revell, G. Pitari, E. Mancini, G. Di Genova, D. Visioni, S.S. Dhomse, and M.P. Chipperfield, Ozone sensitivity to varying greenhouse gases and ozone-depleting substances in CCMI-1 simulations, *Atmos. Chem. Phys.*, *18*, 1091–1114, doi:10.5194/acp-18-1091-2018, 2018.

Muthers S., F. Arfeuille, C.C. Raible, and E. Rozanov, The impacts of volcanic aerosol on stratospheric ozone and the Northern Hemisphere polar vortex: Separating radiative-dynamical changes from direct effects due to enhanced aerosol heterogeneous chemistry, *Atmos. Chem. Phys.*, *15*, 11,461–11,476, doi:10.5194/acp-15-11461-2015, 2015.

Naik, V., A.Voulgarakis, A.M. Fiore, L.W. Horowitz, J.-F. Lamarque, M. Lin, M.J. Prather, P.J. Young, D. Bergmann, P.J. Cameron-Smith, I. Cionni, W.J. Collins, S.B. Dalsøren, R. Doherty, V. Eyring, G. Faluvegi, G.A. Folberth, B. Josse, Y.H. Lee, I.A. MacKenzie, T. Nagashima, T.P.C. van Noije, D.A. Plummer, M. Righi, S.T. Rumbold, R. Skeie, D.T. Shindell, D.S. Stevenson, S. Strode, K. Sudo, S. Szopa, and G. Zeng, Preindustrial to present-day changes in tropospheric hydroxyl radical and methane lifetime from the Atmospheric Chemistry and Climate Model Intercomparison Project (ACCMIP), *Atmos. Chem. Phys.*, *13*, 5277–5298, doi:10.5194/acp-13-5277-2013, 2013.

Nair, P. J., L. Froidevaux, J. Kuttippurath, J. M. Zawodny, J. M. Russell III, W. Steinbrecht, H. Claude, T. Leblanc, J.A.E. van Gijsel, B. Johnson, D.P.J. Swart, A. Thomas, R. Querel, R. Wang, and J. Anderson, Subtropical and midlatitude ozone trends in the stratosphere: Implications for recovery. *J. Geophys. Res. Atmos.*, *120*, 7247–7257, doi:10.1002/2014JD022371, 2015.

Naoe, H., M. Deushi, K. Yoshida, and K. Shibata, Future changes in the ozone quasi-biennial oscillation with increasing GHGs and ozone recovery in CCMI simulations, *J. Clim.*, *30*, 6977–6997, doi:10.1175/JCLI-D-16-0464.1, 2017.

Nédélec, P., R. Blot, D. Boulanger, G. Athier, J.-M. Cousin, B. Gautron, A. Petzold, A.Volz-Thomas, and V. Thouret, Instrumentation on commercial aircraft for monitoring the atmospheric composition on a global scale: The IAGOS system, technical overview of ozone and carbon monoxide measurements, *Tellus B: Chem. Phys. Meteorol.*, *67* (1), doi:10.3402/tellusb.v67.27791, 2015.

Nedoluha, G.E., I.S. Boyd, A. Parrish, R.M. Gomez, D.R. Allen, L. Froidevaux, B.J. Connor, and R.R Querel, Unusual stratospheric ozone anomalies observed in 22 years of measurements from Lauder, New Zealand, *Atmos. Chem. Phys.*, *15*, 6817–6826, doi:10.5194/acp-15-6817-2015, 2015, 2015a.

Nedoluha, G.E., D.E. Siskind, A. Lambert, and C. Boone, The decrease in mid-stratospheric tropical ozone since 1991, *Atmos. Chem. Phys.*, *15* (8), 4215–4224, doi:10.5194/acp-15-4215-2015, 2015b.

Neu, J.L., T. Flury, G.L. Manney, M.L. Santee, N.J. Livesey, and J. Worden, Tropospheric ozone variations governed by changes in stratospheric circulation, *Nat. Geosci.*, *7*, 340–344, doi:10.1038/ngeo2138, 2014.

Newman, P.A., E.R. Nash, and J.E. Rosenfield, What controls the temperature of the Arctic stratosphere during the spring?, *J. Geophys. Res.*, 106 (D17), 19,999–20,010, doi:10.1029/2000JD000061, 2001.

Newman, P.A., J.S. Daniel, D.W. Waugh, and E.R. Nash, A new formulation of equivalent effective

stratospheric chlorine (EESC), *Atmos. Chem. Phys.*, *7*, 4537–4552, doi:10.5194/acp-7-4537-2007, 2007.

Newman, P., L. Coy, S. Pawson, and L. Lait, The anomalous change in the QBO in 2015–2016, *Geophys. Res. Lett.*, *43*, 8791–8797, doi:10.1002/2016GL070373, 2016.

Nowack, P.J., N.L. Abraham, P. Braesicke, and J.A. Pyle., Stratospheric ozone changes under solar geoengineering: Implications for UV exposure and air quality, *Atmos. Chem. Phys.*, *16*, 4191–4203, doi:10.5194/acp-16-4191-2016, 2016.

Oberländer-Hayn, S., S. Meul, U. Langematz, J. Abalichin, and F. Haenel, A chemistry-climate model study of past changes in the Brewer-Dobson circulation, *J. Geophys. Res. Atmos.*, *120*, 6742–6757, doi:10.1002/2014JD022843, 2015.

Olsen, M.A., K. Wargan, and S. Pawson, Tropospheric column ozone response to ENSO in GEOS-5 assimilation of OMI and MLS ozone data, *Atmos. Chem. Phys.*, *16*, 7091–7103, doi:10.5194/acp-16-7091-2016, 2016.

Oman, L.D., A.R. Douglass, J.R. Ziemke, J.M. Rodriguez, D.W. Waugh, and J.E. Nielsen, The ozone response to ENSO in Aura satellite measurements and a chemistry-climate simulation, *J. Geophys. Res.*, *118*, 965–976, doi:10.1029/2012JD018546, 2013.

Oman, L.D., A.R. Douglass, R.J., Salawitch, T.P. Canty, J.R. Ziemke, and M. Manyin, The effect of representing bromine from VSLS on the simulation and evolution of Antarctic ozone, *Geophys. Res. Lett.*, *43*, 9869–9876, doi:10.1002/2016GL070471, 2016.

Oram, D.E., M.J Ashfold, J.C. Laube, L.J. Gooch, S. Humphrey, W.T. Sturges, E. Leedham-Elvidge, G.L. Forster, N.R.P. Harris, M.I. Mead, A.A. Samah, S.M. Phang, C.-F. Ou-Yang, N.-H. Lin, J.-L. Wang, A.K. Baker, C.A.M. Brenninkmeijer, and D. Sherry, A growing threat to the ozone layer from short-lived anthropogenic chlorocarbons, *Atmos. Chem. Phys.*, *17*, 11,929–11,941, doi:10.5194/acp-17-11929-2017, 2017.

Osprey, S.M., N. Butchart, J.R. Knight, A.A. Scaife, K. Hamilton, J.A. Anstey, V. Schenzinger, and C. Zhang, An unexpected disruption of the atmospheric quasi-biennial oscillation, *Science*, *353*, 1424–1427, doi:10.1126/science.aah4156, 2016.

Parrish, A., B.J. Connor, J.J. Tsou, I.S. Mcdermid, and W.P. Chu, Ground-based microwave monitoring of stratospheric ozone, *J. Geophys. Res.*, *97*, 2541–2546, doi:10.1029/91JD02914, 1992.

Petropavlovskikh, I., P.K. Bhartia, and J. DeLuisi, New Umkehr ozone profileretrieval algorithm optimized for climatological studies, *Geophys. Res. Lett.*, *32* (16), L16808, doi:10.1029/2005GL023323, 2005.

Petropavlovskikh, I., R. Evans, G. Mcconville, K. Miyagawa, S. Oltmans, Effect of the out-of-band stray light on the retrieval of the Umkehr Dobson ozone profiles, *Int. J. Remote Sens.*, *30* (24), 6461–6482, doi:10.1080/01431160902865806, 2009.

Petropavlovskikh, I., R. Evans, G. McConville, S. Oltmans, D. Quincy, K. Lantz, P. Disterhoft, M. Stanek, and L. Flynn, Sensitivity of Dobson and Brewer Umkehr ozone profile retrievals to ozone cross-sections and stray light effects, *Atmos. Meas. Tech.*, *4*, 1841–1853, doi:10.5194/amt-4-1841-2011, 2011.

Petropavlovskikh, I., R. Evans, G. McConville, G.L. Manney, and H.E. Rieder, The influence of the North Atlantic Oscillation and El Niño–Southern Oscillation on mean and extreme values of column ozone over the United States, *Atmos. Chem. Phys.*, *15*, 1585–1598, doi:10.5194/acp-15-1585-2015, 2015.

Pitari, G., V. Aquila, B. Kravitz, A. Robock, S. Watanabe, N.D. Luca, G.D. Genova, E. Mancini, S. Tilmes, and I. Cionni, Stratospheric ozone response to sulfate geoengineering: Results from the Geoengineering Model Intercomparison Project (GeoMIP), *J. Geophys. Res.*, *119*, 2629–2653, doi:10.1002/2013JD020566, 2014.

Polvani, L.M., L. Wang, V. Aquila, D.W. Waugh, The impact of ozone-depleting substances on tropical upwelling, as revealed by the absence of lower-stratospheric cooling since the late 1990s, *J. Clim.*, *30*, 2523–2534, doi:10.1175/JCLI-D-16-0532.1, 2017.

Rahpoe, N., M. Weber, A.V. Rozanov, K. Weigel, H. Bovensmann, J.P. Burrows, A. Laeng, G. Stiller, T. von Clarmann, E. Kyrölä, V.F. Sofieva, J. Tamminen, K. Walker, D. Degenstein, A.E. Bourassa, R. Hargreaves, P. Bernath, J. Urban, and D.P. Murtagh, Relative drifts and biases between six ozone limb satellite measurements from the last decade, *Atmos. Meas. Tech.*, *8*, 4369–4381,

doi:10.5194/amt-8-4369-2015, 2015.

Randel, W.J., and F. Wu, Isolation of the Ozone QBO in SAGE II Data by Singular-Value Decomposition, *J. Atmos. Sci.*, *53*, 2546–2559, doi:10.1175/1520-0469, 1996.

Randel, W.J., K.P. Shine, J. Austin, J. Barnett, C. Claud, N.P. Gillett, P. Keckhut, U. Langematz, R. Lin, C. Long, C. Mears, A. Miller, J. Nash, D.J. Seidel, D.W.J. Thompson, F. Wu, and S. Yoden, An update of observed stratospheric temperature trends, *J. Geophys. Res.*, *114* (D2), D010421, doi:10.1029/2008JD010421, 2009.

Randel, W.J., A.K. Smith, F. Wu, C. Zou, and H. Qian, Stratospheric Temperature Trends over 1979–2015 Derived from Combined SSU, MLS, and SABER Satellite Observations, *J. Climate*, *29*, 4843–4859, doi:10.1175/JCLI-D-15-0629.1, 2016.

Remsberg, E.E., Decadal-scale responses in middle and upper stratospheric ozone from SAGE II version 7 data, *Atmos. Chem. Phys.*, *14*, 1039–1053, doi:10.5194/acp-14-1039-2014, 2014.

Revell, L.E., G.E. Bodeker, P.E. Huck, B.E. Williamson, and E. Rozanov, The sensitivity of stratospheric ozone changes through the 21st century to N_2O and CH_4, *Atmos. Chem. Phys.*, *12*, 11,309–11,317, doi:10.5194/acp-12-11309-2012, 2012.

Revell, L.E., F. Tummon, R.J. Salawitch, A. Stenke, and T. Peter, The changing ozone depletion potential of N_2O in a future climate, *Geophys. Res. Lett.*, *42*, 10,047–10,055, doi:10.1002/2015GL065702, 2015.

Revell, L.E., A. Stenke, B. Luo, S. Kremser, E. Rozanov, T. Sukhodolov, and T. Peter, Impacts of Mt Pinatubo volcanic aerosol on the tropical stratosphere in chemistry–climate model simulations using CCMI and CMIP6 stratospheric aerosol data, *Atmos. Chem. Phys.*, *17*, 13,139–13,150, doi:10.5194/acp-17-13139-2017, 2017.

Richter, J.H., S. Tilmes, A. Glanville, B. Kravitz, D.G. MacMartin, M.J. Mills, I.R. Simpson, F. Vitt, J.J. Tribbia, J.-F. Lamarque, Stratospheric response in the first geoengineering simulation meeting multiple surface climate objectives, *J. Geophys. Res. Atmos.*, *123*, 5762–5782, doi:10.1029/2018JD028285, 2018.

Rieder, H.E., L. Frossard, M. Ribatet, J. Staehelin, J.A. Maeder, S. Di Rocco, A.C. Davison, T. Peter, P. Weihs, and F. Holawe, On the relationship between total ozone and atmospheric dynamics and chemistry at mid-latitudes – Part 2: The effects of the El Niño/Southern Oscillation, volcanic eruptions and contributions of atmospheric dynamics and chemistry to long-term total ozone changes, *Atmos. Chem. Phys.*, *13*, 165–179, doi:10.5194/acp-13-165-2013, 2013.

Salawitch, R.J., D.K. Weisenstein, L.J. Kovalenko, C.E. Sioris, P.O. Wennberg, K. Chance, M.K.W. Ko, and C.A. McLinden, Sensitivity of ozone to bromine in the lower stratosphere, *Geophys. Res. Lett.*, *32*, L05811, doi:10.1029/2004GL021504, 2005.

Scaife, A.A., R. Comer, N. Dunstone, D. Fereday, C. Folland, E. Good, M. Gordon, L. Hermanson, S. Ineson, A. Karpechko, J. Knight, C. MacLachlan, A. Maidens, K.A. Peterson, D. Smith, J. Slingo, and B. Walker, Predictability of European winter 2015/2016, *Atmos. Sci. Lett.*, *18*, 38–44, doi:10.1002/asl.721, 2017.

Sekiya, T., and K. Sudo, Roles of transport and chemistry processes in global ozone change on interannual and multidecadal time scales, *J. Geophys. Res. Atmos.*, *119*, 4903–4921, doi:10.1002/2013JD020838, 2014.

Sheese, P.E., C.D. Boone, and K.A. Walker, Detecting physically unrealistic outliers in ACE-FTS atmospheric measurements, *Atmos. Meas. Tech.*, *8*, 741–750, doi:10.5194/amt-8-741-2015, 2015.

Shepherd, T.G., D.A. Plummer, J.F. Scinocca, M.I. Hegglin, V.E. Fioletov, M.C. Reader, E. Remsberg, T. von Clarmann, and H. J. Wang, Reconciliation of halogen-induced ozone loss with the total-column ozone record, *Nat. Geosci.*, *7*, 443–449, doi:10.1038/ngeo2155, 2014.

Sinnhuber, B.-M., N. Sheode, M. Sinnhuber, M.P. Chipperfield, and W. Feng, The contribution of anthropogenic bromine emissions to past stratospheric ozone trends: A modelling study, *Atmos. Chem. Phys.*, *9*, 2863–2871, doi:10.5194/acp-9-2863-2009, 2009.

Sinnhuber, B.-M., and S. Meul, Simulating the impact of emissions of brominated very short-lived substances on past stratospheric ozone trends, *Geophys. Res. Lett.*, 42 (7), 2449–2456, doi:10.1002/2014GL062975, 2015.

Sioris, C.E., C.A. McLinden, V.E. Fioletov, C. Adams, J.M. Zawodny, A.E. Bourassa, C.Z. Roth, and D.A. Degenstein, Trend and variability in ozone in the tropical lower stratosphere over 2.5 solar cycles observed by SAGE II and OSIRIS, *Atmos. Chem.*

Phys., *14*, 3479–3496, doi:10.5194/acp-14-3479-2014, 2014.

Smit, H.G.J., W. Straeter, B. Johnson, S. Oltmans, J. Davies, D.W. Tarasick, B. Hoegger, R. Stubi, F. Schmidlin, T. Northam, A. Thompson, J. Witte, I. Boyd, F. Posny, Assessment of the performance of ECC-ozonesondes under quasi-flight conditions in the environmental simulation chamber: Insights from the Jülich Ozone Sonde Intercomparison Experiment (JOSIE), *J. Geophys. Res.*, *112*, D19306, doi:10.1029/2006JD007308, 2007.

Sofieva, V.F., E. Kyrölä, M. Laine, J. Tamminen, D. Degenstein, A. Bourassa, C. Roth, D. Zawada, M. Weber, A. Rozanov, N. Rahpoe, G. Stiller, A. Laeng, T. von Clarmann, K.A. Walker, P. Sheese, D. Hubert, M. van Roozendael, C. Zehner, R. Damadeo, J. Zawodny, N. Kramarova, and P.K. Bhartia, Merged SAGE II, Ozone_cci and OMPS ozone profile dataset and evaluation of ozone trends in the stratosphere, *Atmos. Chem. Phys.*, *17*, 12,533–12,552, doi:10.5194/acp-17-12533-2017, 2017.

Solomon, S., R.W. Portmann, R.R. Garcia, L.W. Thomason, L.R. Poole, and M.P. McCormick, The role of aerosol variations in anthropogenic ozone depletion at northern midlatitudes, *J. Geophys. Res.*, *101* (D3), 6713–6727, doi:10.1029/95JD03353, 1996.

Solomon, S., D. Kinnison, R. Garcia, J. Bandoro, M. Mills, C. Wilka, R. Neely III, A. Schmidt, J.E. Barnes, J.-P. Vernier, and M. Höpfner, Monsoon circulations and tropical heterogeneous chlorine chemistry in the stratosphere, *Geophys. Res. Lett.*, *43*, 12,624–12,633, doi:10.1002/2016GL071778, 2016a.

Solomon, S., D.J. Ivy, D. Kinnison, M.J. Mills, R.R. Neely III, and A.Schmidt, Emergence of healing in the Antarctic ozone layer, *Science*, *353*, 269–274, doi:10.1126/science.aae0061, 2016b.

Soukharev, B.E., and L.L. Hood, Solar cycle variation of stratospheric ozone: Multiple regression analysis of long-term satellite datasets and comparisons with models, *J. Geophys. Res.*, *111* (D20), D20314, doi:10.1029/2006JD007107, 2006.

SPARC (Stratospheric Processes And their Role in Climate), *SPARC Assessment of Stratospheric Aerosol Properties (ASAP)*, edited by L. Thomason and T. Peter, *SPARC Report No. 4*, WCRP-124, WMO/TD No. 1295, available at: www.sparc-climate.org/publications/sparc-reports/, 2006.

SPARC (Stratospheric Processes And their Role in Climate), *SPARC CCMVal Report on Evaluation Chemistry -Climate Models*, edited by V. Eyring, T. Shepherd, and D. Waugh, *SPARC Report No. 5*, WCRP-30/2010, WMO/TD-No. 40, available at: https://www.sparc-climate.org/publications/sparc-reports/, 2010.

SPARC (Stratopshere-troposphere Processes And their Role in Climate), *SPARC Report on the Lifetimes of Stratospheric Ozone-Depleting Substances, Their Replacements, and Related Species*, edited by M.K.W. Ko, P.A. Newman, S. Reimann, and S.E. Strahan, *SPARC Report No. 6*, WCRP-15/2013, available at: https://www.sparc-climate.org/publications/sparc-reports/sparc-report-no-6/, 2013.

Steinbrecht, W., L. Froidevaux, R. Fuller, R. Wang, J. Anderson, C. Roth, A. Bourassa, D. Degenstein, R. Damadeo, J. Zawodny, S. Frith, R. McPeters, P. Bhartia, J. Wild, C. Long, S. Davis, K. Rosenlof, V. Sofieva, K. Walker, N. Rahpoe, A. Rozanov, M. Weber, A. Laeng, T. von Clarmann, G. Stiller, N. Kramarova, S. Godin-Beekmann, T. Leblanc, R. Querel, D. Swart, I. Boyd, K. Hocke, N. Kämpfer, E. Maillard Barras, L. Moreira, G. Nedoluha, C. Vigouroux, T. Blumenstock, M. Schneider, O. García, N. Jones, E. Mahieu, D. Smale, M. Kotkamp, J. Robinson, I. Petropavlovskikh, N. Harris, B. Hassler, D. Hubert, and F. Tummon, An update on ozone profile trends for the period 2000 to 2016, *Atmos. Chem. Phys.*, *17*, 10,675–10,690, doi:10.5194/acp-17-10675-2017, 2017.

Sterling, C.W., B.J. Johnson, S.J. Oltmans, H.G.J. Smit, A.F. Jordan, P.D. Cullis, E.G. Hall, A.M. Thompson, and J.C. Witte, Homogenizing and estimating the uncertainty in NOAA's long- term vertical ozone profile records measured with the electrochemical concentration cell ozonesonde, *Atmos. Meas. Tech.*, *11*, 3661–3687, doi:10.5194/amt-11-3661-2018, 2018.

Stiller, G.P., F. Fierli, F. Ploeger, C. Cagnazzo, B. Funke, F.J. Haenel, T. Reddmann, M. Riese, and T. von Clarmann, Shift of subtropical transport barriers explains observed hemispheric asymmetry of decadal trends of age of air, *Atmos. Chem. Phys.*, *17*, 11,177–11,192, doi:10.5194/acp-17-11177-2017, 2017.

Stolarski, R.S., and S.M. Frith, Search for evidence of trend slow-down in the long-term TOMS/SBUV

total ozone data record: The importance of instrument drift uncertainty, *Atmos. Chem. Phys.*, *6*, 4057–4065, doi:10.5194/acp-6-4057-2006, 2006.

Stolarski R.S., A.R. Douglass, L.D. Oman, and D.W. Waugh, Impact of future nitrous oxide and carbon dioxide emissions on the stratospheric ozone layer, *Environ. Res. Lett.*, *10*, doi:10.1088/1748-9326/10/3/034011, 2015.

Stone, K.A., S. Solomon, and D.E. Kinnison, On the Identification of Ozone Recovery, *Geophys. Res. Lett.*, 45 (10), 5158–5165, doi:10.1029/2018GL077955, 2018.

Strahan, S.E., A.R. Douglass, and S.D. Steenrod, Chemical and dynamical impacts of stratospheric sudden warmings on Arctic ozone variability, *J. Geophys. Res. Atmos.*, *121*, 11,836–11,851, doi:10.1002/2016JD025128, 2016.

Studer, S., K. Hocke, M. Pastel, S. Godin-Beekmann, and N. Kämpfer, Intercomparison of stratospheric ozone profiles for the assessment of the upgraded GROMOS radiometer at Bern, *Atmos. Meas. Tech.*, *6*, 6097–6146, doi:10.5194/amtd-6-6097-2013, 2013.

Tang, M.J., P.J. Telford, F.D. Pope, L. Rkiouak, N.L. Abraham, A.T. Archibald, P. Braesicke, J.A. Pyle, J. McGregor, I.M. Watson, R.A. Cox, and M. Kalberer, Heterogeneous reaction of N_2O_5 with airborne TiO_2 particles and its implication for stratospheric particle injection, *Atmos. Chem. Phys.*, *14*, 6035–6048, doi:10.5194/acp-14-6035-2014, 2014.

Tang, M., J. Keeble, P.J. Telford, F.D. Pope, P. Braesicke, P.T. Griffiths, N.L. Abraham, J. McGregor, I.M. Watson, R.A. Cox, J.A. Pyle, and M. Kalberer, Heterogeneous reaction of $ClONO_2$ with TiO_2 and SiO_2 aerosol particles: Implications for stratospheric particle injection for climate engineering, *Atmos. Chem. Phys.*, *16*, 15,397–15,412, doi:10.5194/acp-16-15397-2016, 2016.

Tarasick, D.W., J. Davies, H.G.J. Smit, S.J. Oltmans, A re-evaluated Canadian ozonesonde record: Measurements of the vertical distribution of ozone over Canada from 1966 to 2013, *Atmos. Meas. Tech.*, *9*, 195–214, doi:10.5194/amt-9-195-2016, 2016.

Tegtmeier, S., M.I. Hegglin, J. Anderson, A. Bourassa, S. Brohede, D. Degenstein, L. Froidevaux, R. Fuller, B. Funke, J. Gille, A. Jones, Y. Kasai, K. Krüger, E. Kyrölä, G. Lingenfelser, J. Lumpe, B. Nardi, J. Neu, D. Pendlebury, E. Remsberg, A. Rozanov, L. Smith, M. Toohey, J. Urban, T. von Clarmann, K.A. Walker, R.H.J. Wang, SPARC Data Initiative: A comparison of ozone climatologies from international satellite limb sounders, *J. Geophys. Res. Atmos.*, *118*, 12,229–12,247, doi:10.1002/2013JD019877, 2013.

Thomason, L.W., S.P. Burton, B.-P. Luo, and T. Peter, SAGE II measurements of stratospheric aerosol properties at non-volcanic levels, *Atmos. Chem. Phys.*, *8*, 983–995, doi:10.5194/acp-8-983-2008, 2008.

Thomason, L.W., N. Ernest, L. Millán, L. Rieger, A. Bourassa, J.-P. Vernier, G. Manney, B. Luo, F. Arfeuille, and T. Peter, A global space-based stratospheric aerosol climatology: 1979–2016, *Earth Syst. Sci. Data*, *10*, 469–492, doi:10.5194/essd-10-469-2018, 2018.

Thompson, A.M., J.C. Witte, C. Sterling, A. Jordan, B.J. Johnson, S.J. Oltmans, M. Fujiwara, H. Vömel, M. Allaart, A. Piters, G.J.R. Coetzee, F. Posny, E. Corrales, J.A. Diaz, C.F.N. Komala, N. Lai, H.T.A. Nguyen, M. Maata, F. Mani, Z. Zainal, S-Y. Ogino, F. Paredes, T.L.B. Penha, F. Raimundo da Silva, S. Sallons-Mitro, H.B. Selkirk, F.J. Schmidlin, R. Stübi, K. Thiongo, First reprocessing of Southern Hemisphere Additional Ozonesondes (SHADOZ) ozone profiles (1998–2016): 2. Comparisons with satellites and ground-based instruments, *J. Geophys. Res. Atmos.*, *122*, 13,000–13,025, doi:10.1002/2017JD027406, 2017.

Thouret, V., A. Marenco, J.A. Logan, P. Nédélec, and C. Grouhel, Comparisons of ozone measurements from the MOZAIC airborne program and the ozone sounding network at eight locations, *J. Geophys. Res.*, *103* (D19), 25,695–25,720, doi:10.1029/98JD02243, 1998.

Tilmes, S., J.H. Richter, M.J. Mills, B. Kravitz, D.G. Macmartin, R.R. Garcia, D.E. Kinnison, J.-F. Lamarque, J. Tribbia, F. Vitt, Effects of different stratospheric SO_2 injection altitudes on stratospheric chemistry and dynamics, *J. of Geophys. Res. Atmos.*, *123*, 4654–4673, doi:10.1002/2017JD028146, 2018.

Tummon, F., B. Hassler, N.R.P. Harris, J. Staehelin, W. Steinbrecht, J. Anderson, G.E. Bodeker, A. Bourassa, S.M. Davis, D. Degenstein, S.M. Frith, L. Froidevaux, E. Kyrölä, M. Laine, C. Long, A.A. Penckwitt, C.E. Sioris, K.H. Rosenlof, C. Roth,

H.-J. Wang, and J. Wild, Intercomparison of vertically resolved merged satellite ozone datasets: Interannual variability and long-term trends, *Atmos. Chem. Phys.*, *15*, 3021–3043, doi:10.5194/acp-15-3021-2015, 2015.

Tweedy, O.V., N.A. Kramarova, S.E. Strahan, P.A. Newman, L. Coy, W.J. Randel, M. Park, D.W. Waugh, and S.M. Frith, Response of trace gases to the disrupted 2015–2016 quasi-biennial oscillation, *Atmos. Chem. Phys.*, *17*, 6813–6823, doi:10.5194/acp-17-6813-2017, 2017.

van der A, R.J., M.A.F. Allaart, and H.J. Eskes, Multi sensor reanalysis of total ozone, *Atmos. Chem. Phys.*, *10* (22), 11,277–11,294, doi:10.5194/acp-10-11277-2010, 2010.

van der A, R.J., M.A.F. Allaart, and H.J. Eskes, Extended and refined multi sensor reanalysis of total ozone for the period 1970–2012, *Atmos. Meas. Tech.*, *8*, 3021–3035, doi:10.5194/amt-8-3021-2015, 2015.

Van Malderen, R., M.A.F. Allaart, H. De Backer, H.G.J. Smit, D. De Muer, On instrumental errors and related correction strategies of ozonesondes: Possible effect on calculated ozone trends for the nearby sites Uccle and De Bilt, *Atmos. Meas. Tech.*, *9*, 3793–3816, doi:10.5194/amt-9-3793-2016, 2016.

Vernier, J.-P., L.W. Thomason, J.-P. Pommereau, A. Bourassa, J. Pelon, A. Garnier, A. Hauchecorne, L. Blanot, C. Trepte, D. Degenstein, F. Vargas, Major influence of tropical volcanic eruptions on the stratospheric aerosol layer during the last decade, *Geophys. Res. Lett.*, *38* (12), L12807, doi:10.1029/2011GL047563, 2011.

Vernier, J.-P., T.D. Fairlie, M. Natarajan, F.G. Wienhold, J. Bian, B.G. Martinsson, S. Crumeyrolle, L.W. Thomason, and K.M. Bedka, Increase in upper tropospheric and lower stratospheric aerosol levels and its potential connection with Asian pollution, *J. of Geophys. Res. Atmos.*, *120* (4), 1608–1619, doi.org/10.1002/2014JD022372, 2015.

Vigouroux, C., T. Blumenstock, M. Coffey, Q. Errera, O. García, N.B. Jones, J.W. Hannigan, F. Hase, B. Liley, E. Mahieu, J. Mellqvist, J. Notholt, M. Palm, G. Persson, M. Schneider, C. Servais, D. Smale, L. Thölix, and M. De Mazière, Trends of ozone total columns and vertical distribution from FTIR observations at eight NDACC stations around the globe, *Atmos. Chem. Phys.*, *15*, 2915–2933, doi:10.5194/acp-15-2915-2015, 2015.

Visioni, D., G. Pitari, and V. Aquila, Sulfate geoengineering: A review of the factors controlling the needed injection of sulfur dioxide, *Atmos. Chem. Phys.*, *17*, 3879–3889, doi:10.5194/acp-17-3879-2017, 2017.

Wallace, J.M., R.L. Panetta, and J. Estberg, Representation of the equatorial stratospheric quasi-biennial oscillation in EOF phase space, *J. Atmos. Sci.*, *50*, 1751–1762, doi: 10.1175/1520-0469(1993)050<1751:ROTESQ>2.0.CO;2, 1993.

Wargan, K., G. Labow, S. Frith, S. Pawson, N. Livesey, and G. Partyka, Evaluation of the Ozone Fields in NASA's MERRA-2 Reanalysis, *J. Clim.*, *30*, 2961–2988, doi:10.1175/JCLI-D-16-0699.1, 2017.

Wargan, K., C. Orbe, S. Pawson, J.R. Ziemke, L.D. Oman, M.A. Olsen, L. Coy, K.E. Knowland, Recent decline in extratropical lower stratospheric ozone attributed to circulation changes. *Geophys. Res. Lett.*, *45*, 5166–5176, doi:10.1029/2018GL077406, 2018.

Weatherhead, E.C., J. Harder, E.A. Araujo-Pradere, G. Bodeker, J.M. English, L.E. Flynn, S.M. Frith, J.K. Lazo, P. Pilewskie, M. Weber, and T.N. Woods, How long do satellites need to overlap? Evaluation of climate data stability from overlapping satellite records, *Atmos. Chem. Phys.*, *17*, 15,069–15,093, doi:10.5194/acp-17-15069-2017, 2017.

Weber, M., L.N. Lamsal, M. Coldewey-Egbers, K. Bramstedt, and J.P. Burrows, Pole-to-pole validation of GOME WFDOAS total ozone with ground-based data, *Atmos. Chem. Phys.*, *5*, 1341–1355, doi:10.5194/acp-5-1341-2005, 2005.

Weber, M., S. Dikty, J.P. Burrows, H. Garny, M. Dameris, A. Kubin, J. Abalichin, and U. Langematz, The Brewer-Dobson circulation and total ozone from seasonal to decadal time scales, *Atmos. Chem. Phys.*, *11*, 11,221–11,235, doi:10.5194/acp-11-11221-2011, 2011.

Weber, M., W. Steinbrecht, C. Roth, M. Coldewey-Egbers, D. Degenstein, Y.E. Fioletov, S.M. Frith, L. Froidevaux, J. de Laat, C.S. Long, D. Loyola, and J.D. Wild, [Global Climate] Stratospheric ozone [in "State of the Climate in 2015"], *Bull. Am. Meteorol. Soc.*, *97* (8), S49–S51, doi:10.1175/2016BAMSStateoftheClimate.1, 2016.

Weber, M., W. Steinbrecht, S.M. Frith, O. Tweedy, M.

Coldewey-Egbers, S. Davis, D. Degenstein, V.E. Fioletov, L. Froidevaux, J. de Laat, C.S. Long, D. Loyola, C. Roth, and J.D. Wild, [Global Climate] Stratospheric ozone [in "State of the Climate in 2016"], *Bull. Amer. Meteorol. Soc.*, 98, S49–S51, doi:10.1175/2017BAMSStateoftheClimate.1, 2017.

Weber, M., M. Coldewey-Egbers, V.E. Fioletov, S.M. Frith, J.D. Wild, J.P. Burrows, C.S. Long, and D. Loyola, Total ozone trends from 1979 to 2016 derived from five merged observational datasets – the emergence into ozone recovery, *Atmos. Chem. Phys.*, *18*, 2097–2117, doi:10.5194/acp-18-2097-2018, 2018.

Weisenstein, D.K., D.W. Keith, and J.A. Dykema, Solar geoengineering using solid aerosol in the stratosphere, *Atmos. Chem. Phys.*, *15*, 11,835–11,859, doi:10.5194/acp-15-11835-2015, 2015.

Weiss, A.K., J. Staehelin, C. Appenzeller, and N.R.P. Harris, Chemical and dynamical contributions to ozone profile trends of the Payerne (Switzerland) balloon soundings, *J. Geophys. Res.*, *106* (D19), 22,685–22,694, doi:10.1029/2000JD000106, 2001.

Wespes, C., D. Hurtmans, L.K. Emmons, S. Safieddine, C. Clerbaux, D.P. Edwards, and P.-F. Coheur, Ozone variability in the troposphere and the stratosphere from the first 6 years of IASI observations (2008–2013), *Atmos. Chem. Phys.*, *16*, 5721–5743, doi:10.5194/acp-16-5721–2016, 2016.

Wespes, C., D. Hurtmans, C. Clerbaux, A. Boynard, and P.-F. Coheur, Decrease in tropospheric O_3 levels in the Northern Hemisphere observed by IASI, *Atmos. Chem. Phys.*, *18*, 6867–6885, doi:10.5194/acp-18-6867-2018, 2018.

Wild, J.D., S.-K. Yang, and C.S. Long, Ozone Profile Trends: An SBUV/2 Perspective, in Proceedings of the Quadrennial Ozone Symposium, International Ozone Commission, Edinburgh, Scottland, QOS2016-133, 2016.

Witte, J.C., A.M. Thompson, H.G.J. Smit, M. Fujiwara, F. Posny, G.J.R. Coetzee, E.T. Northam, B.J. Johnson, C.W. Sterling, M. Mohamad, S.-Y. Ogino, A. Jordan, F.R. da Silva, First reprocessing of Southern Hemisphere ADditional OZonesondes (SHADOZ) profile records (1998–2015): 1. Methodology and evaluation, *J. Geophys. Res. Atmos.*, *122*, 6611–6636, doi:10.1002/2016JD026403, 2017.

WMO (World Meteorological Organization), *Scientific Assessment of Ozone Depletion: 2006*, Global Ozone Research and Monitoring Project - Report No. 50, 572 pp., Geneva, Switzerland, 2007.

WMO (World Meteorological Organization), *Scientific Assessment of Ozone Depletion: 2010*, Global Ozone Research and Monitoring Project-Report No. 52, 516 pp., Geneva, Switzerland, 2011.

WMO (World Meteorological Organization), *Scientific Assessment of Ozone Depletion: 2014*, World Meteorological Organization, Global Ozone Research and Monitoring Project-Report No. 55, 416 pp., Geneva, Switzerland, 2014.

Wolter, K., MultiMultivariate ENSO Index (MEI), available at: www.esrl.noaa.gov/psd/enso/mei/table.html (last access: 10 May 2013), 2013.

Xia, L., P.J. Nowack, S. Tilmes, and A. Robock, Impacts of stratospheric sulfate geoengineering on tropospheric ozone, *Atmos. Chem. Phys.*, *17*, 11,913–11,928, doi:10.5194/acp-17-11913-2017, 2017.

Young, P.J., A.T. Archibald, K.W. Bowman, J.-F. Lamarque, V. Naik, D.S. Stevenson, S. Tilmes, A. Voulgarakis, O. Wild, D. Bergmann, P. Cameron-Smith, I. Cionni, W.J. Collins, S.B. Dalsøren, R.M. Doherty, V. Eyring, G. Faluvegi, L.W. Horowitz, B. Josse, Y.H. Lee, I.A. MacKenzie, T. Nagashima, D.A. Plummer, M. Righi, S.T. Rumbold, R.B. Skeie, D.T. Shindell, S.A. Strode, K. Sudo, S. Szopa, and G. Zeng, Pre-industrial to end 21st century projections of tropospheric ozone from the Atmospheric Chemistry and Climate Model Intercomparison Project (ACCMIP), *Atmos. Chem. Phys.*, *13*, 2063–2090, doi:10.5194/acp-13-2063-2013, 2013.

Zawada, D.J., L.A. Rieger, A.E. Bourassa, and D.A. Degenstein, Tomographic retrievals of ozone with the OMPS Limb Profiler: Algorithm description and preliminary results, *Atmos. Meas. Tech.*, *11*, 2375–2393, doi:10.5194/amt-11-2375-2018, 2018.

Zeng, G., and J.A. Pyle, Changes in tropospheric ozone between 2000 and 2100 modeled in a chemistry-climate model, *Geophys. Res. Lett.*, *30* (7), doi:10.1029/2002GL016708, 2003.

Zhang, L., D.J. Jacob, X. Yue, N.V. Downey, D.A. Wood, and D. Blewitt, Sources contributing to background surface ozone in the US Intermountain West, *Atmos. Chem. Phys.*, *14*, 5295–5309,

doi:10.5194/acp-14-5295-2014, 2014.

Ziemke, J.R., S. Chandra, B.N. Duncan, L. Froidevaux, P.K. Bhartia, P.F. Levelt, and J.W. Waters, Tropospheric ozone determined from Aura OMI and MLS: Evaluation of measurements and comparison with the Global Modeling Initiative's Chemical Transport Model, *J. Geophys. Res.*, *111* (D19), D19303, doi:10.1029/2006JD007089, 2006.

Appendix 3A

Data Sources

3A.1 Ground-based Measurements

Ground-based instruments at numerous stations around the globe monitor changes in total column and profile ozone amounts at local to regional scales (WMO, 2014; Hassler et al., 2014). These instruments include:

- **remote-sensing instruments** such as Dobson and Brewer spectrophotometers (Fioletov et al., 2002, 2008; Petropavlovskikh et al., 2005, 2009, 2011), SAOZ spectrometers (Hendrick et al., 2011), filter ozonometers (Bojkov et al., 1994), FTIR spectrometers (Hase et al., 1999; Vigouroux et al., 2015), lidars (Claude et al., 1988; Godin et al., 1989; McDermid et al., 1990), and microwave radiometers (MWR; Parrish et al., 1992; McDermid et al., 1998a,b; McPeters et al., 1999; Calisesi et al, 2003; Studer et al., 2013; Nedoluha et al., 2015); and
- **in situ instruments** such as balloon-borne ozonesondes (Komhyr, 1969; Smit et al., 2007; Deshler et al., 2008, 2017) and aircraft-mounted sensors (Thouret et al., 1998; Nédélec et al., 2015).

Since the last Assessment, most ground-based data records were merely extended in time. However, several station records were revised to address inhomogeneities in time (changes in measurement process at the site) or in space (differences in measurement process between sites in the network). Such revisions were done for 2 MWR stations and for about 30 ozonesonde sites. The Bern microwave instrument was upgraded and the entire time series was referenced to the current spectrometer (Moreira et al., 2015). The Payerne microwave data changed as a result of improvements in the retrieval method and in the integration of the measurements (private communications with PI Maillard-Barras). Both revised MWR records were used for this Assessment. Over the past few years, the ozonesonde community has put considerable effort into reducing uncertainties in the measurements to 5–10%. Biases between different types of ozonesonde instrumentation have been characterized, correction schemes developed, and the ozone profile records of 30 stations in the NDACC, GAW, and SHADOZ networks reprocessed accordingly (Tarasick et al., 2016; Van Malderen et al., 2016; Deshler et al., 2017; Witte et al., 2017; Sterling et al., 2018). Further efforts to assess the outcome of this homogenization activity are ongoing. At the time of this Assessment, not all reprocessed sonde data were available.

The profile trends assessed here are based on observations at the sites listed in **Table 3A-1**, most of which have operated continuously for at least 20 years. Zonally averaged, ground-based data records, one for each measurement technique, were computed from deseasonalized anomaly time series at each site in a given latitude band (Fioletov et al., 2002, 2008; WMO, 2014; Steinbrecht et al., 2017; LOTUS, 2018). Such an approach reduces the impact of station-dependent instrument biases, temporal coverage, and sampling.

The **WOUDC** ground-based total column dataset is based on available Dobson, Brewer, SAOZ, and filter ozonometer data that have been averaged monthly and zonally (using a TOMS v7 climatology to translate deviations in ozone at a single point into zonal mean deviations) and then binned in 5-degree intervals (Fioletov et al., 2002). Time series based on these relatively sparse ground-based measurements may not always reproduce monthly zonal fluctuations well, particularly in the tropics and Southern Hemisphere. However, seasonal (and longer) averages can be estimated with a precision comparable with satellite-based datasets (~1%) (Chiou et al., 2014).

3A.2 Space-Based Ozone Profiles

Space-based observations of stratospheric ozone are performed in nadir-, limb-, or occultation-viewing geometry in different wavelength ranges using different measurement techniques (Chiou et al., 2014; Hassler et al., 2014;

Table 3A-1. Overview of the sources of ozone profile observations by ground-based techniques used for the monthly zonal mean data considered in this Assessment. Stations are sorted by instrument type and chronologically by the starting year of the record. Those with an asterisk are located outside the attributed latitude zones.

Instruments and Data Archives	Stations (Start of Data Record)		
	35°–60°S	20°S–20°N	35°–60°N
Ozonesonde (0– 30 km) http://www.ndsc.ncep.noaa.gov/data, http://www.woudc.org/data/explore.php?lang=en, https://tropo.gsfc.nasa.gov/shadoz/Archive.html	Lauder (1986), Macquarie Island (1994), Broadmeadows (1999)	Hilo (1982), Ascension Island (1998), Kuala Lumpur (1998), Nairobi (1998), Natal (1998), Pago Pago (1998), Suva (1998), Hong Kong Observatory* (2000)	Goose Bay (1963), Uccle (1965), Hohenpeißenberg (1966), Payerne (1968), Edmonton (1970), Wallops Island (1970), Lindenberg (1975), Legionowo (1979), Praha (1979), Boulder (1991), De Bilt (1992), Valentia (1994), Huntsville* (1999)
Lidar (15–50 km) http://www.ndsc.ncep.noaa.gov/data	Lauder (1994)	Mauna Loa (1993)	OHP (1986), Hohenpeißenberg (1987), Table Mountain (1988)
Microwave (MWR) (20–70 km) http://www.ndsc.ncep.noaa.gov/data	Lauder (1992)	Mauna Loa (1995)	Bern (1994), Payerne (2000)
FTIR (0–50 km) http://www.ndsc.ncep.noaa.gov/data	Wollongong (1996), Lauder (2001)	Izaña* (1999)	Jungfraujoch (1995)
Dobson/Brewer Umkehr (0–50 km) ftp://aftp.cmdl.noaa.gov/data/ozwv/DobsonUmkehr/Stray%20light%20corrected/monthlymean	Perth (1984), Lauder (1987)	Mauna Loa (1984)	Arosa (1956), Boulder (1984), OHP (1984), Fairbanks (1994)

Table 3A-2. Merged satellite vertical ozone profile datasets used in this Assessment (monthly zonal mean data).

Merged Data Set	Instruments and Data Version	Ozone Representation	Latitude Coverage and Sampling	Altitude Coverage and Sampling	Temporal Coverage
SBUV-NASA MOD v8.6 (release 6)	Nimbus 4 BUV v8.6 Nimbus 7 SBUV v8.6 NOAA 11 SBUV/2 v 8.6 NOAA 14 SBUV/2 v8.6 NOAA 16 SBUV/2 v8.6 NOAA 17 SBUV/2 v8.6 NOAA 18 SBUV/2 v8.6 NOAA 19 SBUV/2 v8.6	Partial columns over pressure layers	80°N–80°S 5 deg	50–0.5 hPa, 9 layers (~6–15 km thick)	1970–2016
SBUV-NOAA COH v8.6	Nimbus 4 BUV v8.6 Nimbus 7 SBUV v8.6 NOAA 11 SBUV/2 v 8.6 NOAA 14 SBUV/2 v8.6 NOAA 16 SBUV/2 v8.6 NOAA 17 SBUV/2 v8.6 NOAA 18 SBUV/2 v8.6 NOAA 19 SBUV/2 v8.6	Partial columns over pressure layers	80°N–80°S 5 deg	50–0.5 hPa, 13 layers (~6–15 km thick)	1978–2016
GOZCARDS v2.20	SAGE I v5.9_rev, SAGE II v7.0, HALOE v19, Aura MLS v4.2	Mixing ratio at pressure levels	90°S–90°N, 10 deg	215–0.2 hPa	1979–2016
SWOOSH v2.60	SAGE II v7.0, HALOE v19, UARS MLS v5, SAGE III v4, Aura MLS v4.2	Mixing ratio at pressure levels	90°S–90°N, 10 deg (also 5 and 2.5 deg)	316–1 hPa, ~3 km	1984–2016
SAGE II-OSIRIS- OMPS	SAGE II v7.0, OSIRIS v5.10, OMPS USask-2D v1.0.2	Number density (anomaly) at altitude levels	60°S–60°N, 10 deg	0–50 km, 1 km	1984–2016
SAGE II-CCI-OMPS	SAGE II v7.0, OSIRIS v5.10, GOMOS ALGOM2s v1, MIPAS IMK/IAA v7, SCIAMACHY UBr v3.5, ACE-FTS v3.5/3.6, OMPS USask-2D v1.0.2	Number density (anomaly) at altitude levels	90°S–90°N, 10 deg	10–50 km, 1 km	1984–2016
SAGE II-MIPAS- OMPS	SAGE II v7.0, MIPAS IMK/IAA v7, OMPS NASA v2.0	Deseasonalized ozone anomalies at altitude levels	60°S–60°N, 10 deg	10–50 km, 1 km	1984–2017

Table 3A-3. Merged total ozone column datasets used in this Assessment (annual zonal mean data).

Merged dataset	Instruments	Record length	Reference	URL
WOUDC	Dobson, Brewer, SAOZ, Filter ozonometer	1964–2016	Fioletov et al. (2002, 2008)	http://woudc.org/archive/Projects-Campaigns/ZonalMeans
SBUV NASA MOD v8.6 (release 6)	Nimbus 4 BUV Nimbus 7 SBUV NOAA 11 SBUV/2 NOAA 14 SBUV/2 NOAA 16 SBUV/2 NOAA 17 SBUV/2 NOAA 18 SBUV/2 NOAA 19 SBUV/2	1970–2016	Frith et al. (2014)	http://acdb-ext.gsfc.nasa.gov/Data_services/merged
SBUV NOAA COH v8.6	Nimbus 4 BUV Nimbus 7 SBUV NOAA 11 SBUV/2 NOAA 14 SBUV/2 NOAA 16 SBUV/2 NOAA 17 SBUV/2 NOAA 18 SBUV/2 NOAA 19 SBUV/2	1978–2016	Wild et al. (2016)	ftp://ftp.cpc.ncep.noaa.gov/SBUV_CDR
GTO	GOME, SCIAMACHY, GOME-2A, OMI	1995–2016	Coldewey-Egbers et al. (2015)	http://www.esa-ozone-cci.org/?q=node/163
GSG	GOME, SCIAMACHY, GOME-2A	1995–2016	Weber et al. (2011, 2016)	http://www.iup.uni-bremen.de/gome/wfdoas

Weber et al., 2017; Garane et al., 2018). Revised datasets have been released for most instruments in recent years: (nadir) GOME, SCIAMACHY, GOME-2, OMI (Wever et al., 2017; Garane et al., 2018); (limb) OSIRIS v5.10 (Bourassa et al., 2018), SCIAMACHY IUP v3.5 (Jia et al., 2015), Aura MLS v4.2 (Livesey et al., 2018); (occultation) SAGE II v7.0 (Damadeo et al., 2013, 2014), GOMOS ALGOM2s v1 (Sofieva et al., 2017), and ACE-FTS v3.6 (Boone et al., 2013; Sheese et al.; 2015). Revisions include modification of calibration and altitude-registration data as well as updates to radiative transfer models, retrieval and screening algorithms, and meteorological datasets used to convert retrieved ozone values to different units. The largest improvements in stability of the data record were achieved for OSIRIS (altitude registration), MIPAS (calibration data), SCIAMACHY (retrieval algorithm), and SAGE II (meteorological data).

The records of two additional instruments have now reached sufficient length and maturity to be used in trend assessments: The Ozone Mapping and Profiler Suite (OMPS), onboard the Suomi-NPP platform launched in 2011, provides total column data (nadir) in addition to profile data in nadir and limb geometry (Jaross et al., 2014; Kramarova et al., 2014, 2018; Arosio et al., 2018; Zawada et al., 2018). The Infrared Atmospheric Sounding Interferometer (IASI), on the MetOp-A platform launched in 2006, provides nadir ozone profiles (Clerbaux et al., 2009; Dufour et al., 2012; Boynard et al., 2016; Wespes et al., 2016, 2018).

Merged, space- and time-gridded profile records can be categorized in a number of ways, depending on the type of instruments used (nadir versus limb), the profile representation (altitude/pressure, partial columns/volume mixing ratio/number density), the adjustment procedure (single versus multiple references) and the averaging

method (absolute versus anomaly-based, weighted versus unweighted). The following families of merged profile records are used in **Chapter 3** (see **Table 3A-2**):

SBUV MOD and SBUV COH. These records are based on the series of SBUV/2 v8.6 data. Since the last Assessment, NOAA-19 data were added, but only minor changes were made to the merging algorithms of the Merged Ozone Data (MOD) release 6 (Frith et al., 2017) and Cohesive data record (COH; Wild et al., 2016). The approach used for the MOD dataset is to average data from different records during overlap periods; the approach used for COH is to adjust and chain contiguous records sequentially. SBUV COH also incorporates some corrections to individual satellite profiles and excludes measurements from some SBUV instruments (e.g., the NOAA-9 ascending node data).

GOZCARDS and SWOOSH. A second family of merged datasets is built around SAGE II and Aura MLS: GOZCARDS v2.20 and SWOOSH v2.6 (Froidevaux et al., 2015; Davis et al., 2016). Both records use SAGE II as an absolute reference, but differences are expected from their use of different instruments, adjustment procedures, and averaging methods. For GOZCARDS, each record is weighted equally in the average after adjusting derived monthly zonal mean data during the overlap period. For SWOOSH, space–time collocated profile pairs are used for the adjustments, and weighting is done according to the number of observations. Current versions of GOZCARDS and SWOOSH differ considerably from those used in the previous Assessment; these differences are largely a result of revisions in the input data records and/or a different selection of instruments.

SOO, SCO, and SMO. The last family comprises records constructed from SAGE II and two (or more) other instruments: SAGE-OSIRIS-OMPS (SOO), SAGE-CCI-OMPS (SCO), SAGE-MIPAS-OMPS (SMO) (Bourassa et al., 2014, 2018; Sofieva et al., 2017). All of these were constructed by 1) adjusting deseasonalized anomalies of individual records to those of SAGE II and then 2) either computing an unweighted (SOO) or weighted (SMO) average or the median (SCO). The latter exploits the larger ensemble of up to five instruments in the 2002–2012 period. The MIPAS-based record requires using ACE-FTS as a transfer standard between MIPAS and OMPS, which leads to larger uncertainties in the adjustments. This 3-member family can be considered new to the WMO Assessment. Besides the addition of OMPS data, the previously used SAGE-GOMOS and SAGE-OSIRIS records were based on older and less stable versions of GOMOS and OSIRIS data.

3A.3 Space-Based Total Ozone Columns

Zonal and global total ozone time series are regularly updated and reported; e.g., in the annual State of the Climate reports published in the Bulletin of the American Meteorological Society (BAMS) (Weber et al., 2016, 2017). They are based on ground-based measurements, as well as merged data from multiple satellite instruments. The following total ozone datasets are used in this report (**Table 3A-3**; see Weber et al., 2018 for details).

SBUV MOD and **SBUV COH**. Both datasets are based on integrated vertical ozone profiles from the SBUV MOD and SBUV COH datasets described in **Section 3A.2** (Bhartia et al., 2013).

GTO. The GOME-type Total Ozone Essential Climate Variable (GTO-ECV) data record (Coldewey-Egbers et al., 2015) is based on GOME, SCIAMACHY, OMI, and GOME-2A measurements. The total ozone columns were retrieved using the GOME-type Direct FITting (GODFIT) version 3 algorithm (Lerot et al., 2014). Adjustments to OMI measurements were used to merge data from different instruments into one record in order to correct for small remaining inter-sensor biases and temporal drifts. The record was validated using ground-based measurements (Coldewey-Egbers et al., 2015; Koukouli et al., 2015; Garane et al., 2018).

GSG. The merged GOME-SCIAMACHY-GOME-2A (GSG) total ozone time series (Kiesewetter et al., 2010; Weber et al., 2011, 2016) consists of total ozone data that were retrieved using the University of Bremen Weighting Function DOAS algorithm (Coldewey-Egbers et al., 2005; Weber et al., 2005). The SCIAMACHY and GOME-2A observations were successively adjusted for apparent offsets to be continuous with the original

GOME data. These offsets were determined as a function of latitude in steps of 1 degree using monthly zonal means and then smoothed over 10-degree latitude bands (Weber et al., 2018).

Thus, similar to the SBUV MOD and COH datasets, GTO and GSG are not independent and are in fact based on almost the same measurements by GOME, SCIAMACHY, and GOME-2A, although GTO also uses OMI data. The main difference is in the processing algorithms and/or how the data from different satellites were merged together.